UNIVERSITY OF CALIFORNIA

Los Angeles

Proteomic Analysis of Cancer Cell Metabolism

A thesis submitted in partial satisfaction

of the requirements of the degree Master of Science

in Oral Biology

by

Yang Chai

2013

ABSTRACT OF THESIS

Proteomic Analysis of Cancer Cell Metabolism

by

Yang Chai

Master of Science in Oral Biology

University of California, Los Angeles, 2013

Professor Shen Hu, Chair

Tumor cells can adopt alternative metabolic pathways during oncogenesis. This is an event characterized by an enhanced utilization of glucose for rapid synthesis of macromolecules such as nucleotides, lipids and proteins. This phenomenon was also known as the 'Warburg effect', distinguished by a shift from oxidative phosphorylation to increased aerobic glycolysis in many types of cancer cells. Increased aerobic glycolysis was also indicated with enhanced lactate production and glutamine consumption, and has been suggested to confer growth advantage for proliferating cells during oncogenic transformation. Development of a tracer-based

methodology to determine de novo protein synthesis by tracing metabolic pathways from nutrient utilization may certainly enhance current understanding of nutrient gene interaction in cancer cells. We hypothesized that the metabolic phenotype of cancer cells as characterized by nutrient utilization for protein synthesis is significantly altered during oncogenesis, and ^{13}C stable isotope tracers may incorporate ^{13}C into non-essential amino acids of protein peptides during de novo protein synthesis to reflect the underlying mechanisms in cancer cell metabolism.

OBJECTIVE: The aims of this study are: 1) To examine the effects of using siRNA to knockdown metabolic enzymes, transketolase (TKT) and adenylate kinase 2 (AK2) of glycolysis and pentose phosphate pathway (PPP) in oral cancer cells. 2) To develop a ^{13}C stable isotope tracer-based approach for studying de novo protein synthesis in oral squamous cell carcinoma. 3) To develop a ^{13}C stable isotope tracer-based approach to investigate ^{13}C labeled proteins in TKT siRNA and control scrambled siRNA transfected oral cancer cells. 4) To develop a ^{13}C stable isotope tracer-based approach to determine differential ^{13}C labeled proteins in normal human pancreatic duct epithelial (HPDE) cells and human pancreatic ductal adenocarcinoma (PDAC) cells via *in-vitro* and *in-vivo*.

METHODS: Knockdown of TKT or AK2 was achieved by transfecting oral cancer cells with small interfering RNA for TKT or AK2. ^{13}C labeling of proteins was achieved by infusing cells *in-vitro* and *in-vivo* with [U -$^{13}C_6$]-glucose. Protein samples were analyzed using proteomic approach based on liquid chromatography mass spectrometry (LC-MS/MS). Protein identification was performed by MASCOT database search. Protein clustering and functional annotation was performed using Database for Annotation, Visualization and Integrated Discovery (DAVID) software.

RESULTS: Knockdown of TKT or AK2 in oral cancer cells inhibited cell proliferation and displayed enhanced glucose, glutamine consumption, and lactate production. Knockdown of TKT in oral cancer cells displayed a decrease in ^{13}C labeled protein peptides for TKT compared to control. Overall, knockdown of TKT displayed lower frequency of ^{13}C labeled protein peptides compared to control, but comparison of the same ^{13}C labeled peptide displayed no significant difference in peptide mass isotopomer distribution. Enzymes involved in glycolysis including glyceraldehyde 3 phosphates, enolase, and phosphoglycerate mutase also displayed enhanced ^{13}C labeling compared to control. ^{13}C labeled proteins among HPDE cells, PDAC cells, and PDAC mouse tumor tissue displayed differential labeling frequency primarily in vimentin, β-tubulin and cytoskeletal keratin proteins. Peptide mass isotopomer distribution displayed mass shift in ^{13}C labeled peptides compared to unlabeled (natural ^{12}C) peptide mass isotopomer distribution. Overall, ^{13}C enrichment of proteins achieved greater yield in cell lines compared to mouse tumor tissue. Structural proteins and metabolic enzymes involved in glycolysis, cell cycle, and apoptosis signaling pathways were predominately found labeled.

CONCLUSION: This study, we have developed a novel methodology based on ^{13}C labeling of de novo synthesized proteins to study cancer cell metabolism. ^{13}C labeling of cancer cells with truncated PPP due to knock down of TKT suggested robust metabolic adaptation for glucose utilization. Differential expression of ^{13}C labeled proteins between HPDE cells and PDAC cells, suggested alteration in nutrient gene interaction and metabolic pathways for de novo synthesis during oncogenesis. Our findings demonstrated that ^{13}C stable isotope may serve as a valuable tracer-based tool for studying metabolic regulation of de novo protein synthesis in cancer cells.

The Thesis of Yang Chai is approved.

Robert H. Chiu

Diana V. Messadi

Shen Hu, Committee Chair

University of California, Los Angeles

2013

DEDICATION

This work is dedicated to

Dr. Shen Hu for all his guidance

and my family and friends

who have supported me throughout my life.

TABLE OF CONTENTS

Chapter 2

Chapter 3

LIST OF FIGURES

LIST OF TABLES

ACKNOWLEDGEMENTS

First and foremost, I would like to thank my parents, Mr. Kai Xu and Ms. Huiyan Wu, for their constant sacrifice, love and support throughout my life.

I would like to express my sincere gratitude to my mentor, Dr. Shen Hu, for his tremendous support and encouragement throughout my course of study. My research could not have been possible without his empowering guidance and expertise.

I would like to acknowledge my colleagues, Dr. Jeremy Barrett, Dr. Chuck Carlson, Dr. Kaori Misuno, Dr. Xiaojun Liu, Dr. Min Zhang, Dr. Shize Feng, Dr. Naseim Elzakraand, Dr. Gregory Czerwieniec, Dr. Melissa Sondej, Dr. Jiye Ai, Dr. Yan Yang, Dr. Junewei Huang, Jeffery Brumbaugh, Martha Arellano, Prashant Charugundla, Ramin Rabii, and Grace Ji for their help and support throughout my research.

I would like to give my sincere appreciation to the faculties and staffs of UCLA School of Dentistry, and particular thanks to the faculties and staffs in the Division of Oral Biology for their excellence in teaching, research, and mentorship.

Last but not least, I would like to thank my committee members, Dr. Robert H Chiu and Dr. Diana V. Messadi for their admirable teaching in and outside of the classrooms, as well as their precious time and support for my research project.

INTRODUCTION

A. Cancer Cell Metabolism

Altered cellular metabolic regulation has been intrinsically linked with oncogenic progression [1]. Tumor cells require rapid synthesis of macromolecules such as nucleotides, lipids and proteins for growth. One of the first identified biochemical hallmarks of tumor cells was the "Warburg effect," a shift in the glucose metabolism from oxidative phosphorylation to increased aerobic glycolysis, even in the presence of sufficient oxygen [2]. This phenomenon was a unique characteristic of many cancer cells and proliferating cells, and was also coupled with enhanced glucose, glutamine uptake, and lactate production. Since Otto Warburg's discovery in 1930s, many questions have been raised about how to identify unique aspects of metabolic pathways responsible for oncogenesis. Current understanding of nutrient utilization and biosynthetic pathways regulating cancer cells remain elusive; partly due to the seeming paradox that glucose catabolism by glycolysis compared to mitochondrial oxidative phosphorylation is a less efficient pathway to maximize adenosine 5'-triphosphate (ATP) production [4]. Theories of cancers adaptation to hypoxic environment and hypoxia-dependent mitochondrial mutations suggested that alteration in receptor-initiated signaling pathways may have contributed to the shift to a glycolytic phenotype favorable for cancer cell survival [1]. Recent evidence also revealed that oncogenes and tumor suppressors can respectively promote and inhibit the glycolytic switch. These findings suggest that metabolic reprogramming is intrinsically linked with oncogenic transformation [1, 4, 5]. However, this metabolic reprogramming phenomenon is also associated with non-transformed proliferating cells. Therefore, distinguishing a specific metabolic feature unique to oncogenesis is critical to enhancing current understanding of metabolic reprogrammings interplay with oncogenesis.

B. Glucose Metabolism

Glucose metabolism is essential for a wide variety of cellular processes such as nucleotides synthesis, non-essential amino acid synthesis, and fatty acid synthesis, which are all critical for cellular function and cell survival. Cells can breakdown glucose ($C_6H_{12}O_6$) through glycolysis to form pyruvate ($C_3H_3O_3$) in the cytoplasm [6]. One molecule of glucose yields two molecules of pyruvate, and the resultant free energies released is captured in the form of ATP and nicotinamide adenine dinucleotide (NADH). In the absence of oxygen, pyruvate is converted into lactate and gets secreted out of the cell as waste product. In the presence of oxygen, decarboxylation of pyruvate occurs in the mitochondrial matrix. Pyruvate dehydrogenase converts pyruvate into acetyl-CoA, which can then enter the tricarboxylic acid (TCA) cycle where carbon atoms are oxidized to release CO_2, and energy captured by NADH. Intermediates of the TCA cycle can transport out of the mitochondria for synthesis of non-essential amino acids and fatty acids, which are the building blocks of proteins and lipids. In the case of lipid synthesis, citrate in the TCA can transport out of the mitochondria and into the cytoplasm, citrate is then broken down into acetyl-CoA for fatty acid synthesis (**Figure 1**). NADH's primary role in the TCA cycle is to funnel energy into the electron transport chain (ETC) of the inner mitochondrial membrane via oxidative phosphorylation [6]. This event fuels the proton gradient, allowing the cell to generate abounding amount of ATP, the cells primary energy currency.

An alternative pathway to glycolysis for synthesis of nucleotide and cellular reductive power in the form of nicotinamide adenine dinucleotide phosphate (NADPH) via glucose oxidation is pentose phosphate pathway (PPP). PPP occurs in the cytoplasm and is fundamentally an anabolic process [7]. PPP entailed two distinctive branches: oxidative branch

and non-oxidative branch. The oxidative phase of PPP involves NADPH production for maintenance of cellular reductive power. The non-oxidative phase of PPP involves ribose 5-phosphate (R5P) and erythrose-4-phosphate (E4P) generation for synthesis of nucleotide, nucleic acids (DNA and RNA), and aromatic amino acids [8]. In addition to glucose oxidation, glutamine utilization may also contribute to these metabolic pathways for macromolecule synthesis. In cancer cells and proliferating cells, glucose nutrient pathways are considerably more complex. In fact, cancer cells can adopt alternative metabolic pathways for glucose catabolism by favoring increased glycolysis as their primary pathways to generate ATP (**Figure 1**).

C. Aerobic Glycolysis in Cancer Cells

Cancer cells display enhanced glucose uptake and lactate production. This is partly due to increased aerobic glycolysis in cancer cells, by which glucose can be broken down into pyruvate under normoxic conditions. In normal cells, glycolysis is an inefficient process to generate ATP in comparison with oxidative phosphorylation. Cancer cells have adopted aerobic glycolysis as an improvident yet favorable mechanism to process glucose. However, aerobic glycolysis is not exclusively observed in cancer cells, it was also observed in proliferating cells under normoxia conditions [9]. Increase in glycolytic rate was demonstrated by previous studies to serve as a mechanism to support increasing anabolic requirements for precursor metabolites in proliferating cells [10]. Thus, modification of cancer cells metabolism by metabolic pathways favorable of aerobic glycolytic phenotypes allow cancer cells and proliferating cells to confer selective growth advantages through glycolysis. In addition, the interplay between aerobic glycolysis and PPP also facilitates an acidic environment through the production of R5P, NADPH and lactate, which also have shown to confer growth and survival advantage for tumor cells.

D. Metabolic Check Points and Signaling Pathways of Glucose Metabolism

Cells sense glucose and amino acid in the environment through metabolic sensing molecules. When glucose is scarce, intracellular AMP is elevated, cells sense elevated intracellular AMP by activating 5' adenosine monophosphate-activated protein kinase (AMPK). In turn, AMPK can inhibit rapamycin kinase (mTOR) and activate p53 tumor suppressor [12]. Activation of this check point seeks to promote cell survival by enhancing damage repair pathways including, autophagy, ER stress-UPR, and fatty acid oxidation. In contrast, glucose catabolism and anabolic processes such as protein synthesis and DNA synthesis are limited as well. Dysfunction in master metabolic checkpoints such as p53, AMPK, or mTOR can mediate programmed cell death via death receptor mediated pathways (extrinsic, cytokine and caspases) or mitochondria mediated pathways (intrinsic, Bcl-2 and BH-3only proteins).

In cancer cells, mutation or loss of p53, AMPK, or mTOR has been associated with cancer cells aggressive phenotype for enhanced glucose consumption (**Figure 2**). This is depicted by activation of oncogenes to enhance glucose uptake in an uncontrolled manner via aerobic glycolysis [11]. p53 is a tumor suppressor protein, also known as the 'guardian of the genome', which can regulate cell cycle, DNA repair, and apoptosis [13,14]. Inactivation of p53 is commonly detected in many tumor cells, loss of p53 can promote glycolysis by several means including transcriptional regulation of TP53-induced glycolysis and apoptosis regulator, or synthesis of SCO_2 for cytochrome c oxidase complex of the ETC [1,15,16]. Tumor cells lacking p53 often cannot undergo the proper metabolic checkpoints during glucose scarce situations, as a result, cellular metabolic stress is elevated and can cause cells to die. AMPK is a master metabolic stress sensing protein upstream of p53 that functions to promote cell survival by controlling the balance between cellular catabolism and anabolism. In many tumor cells,

serine/threonine kinase 11 (STK11), an important upstream activator of AMPK is absent. Loss of STK11 limit cells ability to process metabolic stress during glucose deprivation conditions. Thus, cells cannot properly sense and react to metabolic stress [1, 17, 48]. mTOR is a master regulator of protein translation and cellular proliferation. Hyperactivation of mTOR in context of oncogenesis can disrupt cellular sensing signals by terminating anabolic pathways during nutrient deprivation in cancer cells, which can lead to mTOR mediated cell death [1, 18].

Growth factor mediated signals such as activation of the Ras gene can transduce proliferating signals [1]. In cancer cell, mutation in Ras is linked to Ras hyperactivation, which can activate down-stream effectors of phosphoinositide 3-kinase (PI3K)/ protein kinase B (Akt)/mTOR pathway [1, 19-21]. PI3K activation in cancer cells is partly due to phosphatase and tensin homolog (PTEN) loss, as a result, PI3K can induce serine-threonine kinase (Akt) activation; a master switch for many downstream cellular signaling pathways. Akt can induce glycolysis by promoting membrane localization of glucose transporter GLUT1, and can also stimulate phosphofructokinase activity and the association of hexokinases I and II with the mitochondria [1, 22-25]. mTOR can promote glycolytic activity by up-regulating pyruvate kinase M2 (PKM2) via transcription factor Hypoxia-Inducible Factor (HIF)-1 α through direct binding to PKM2 [1, 25-26]. PKM2 is one of four isoforms of pyruvate kinase, a profoundly regulated enzyme of glycolysis pathway that converts phosphoenolpyruvate (PEP) into pyruvate + ATP. In the case of low pyruvate kinase (PK) activity, pyruvate production in cancer cells can take route in a PK-independent pathway that evades ATPs inhibitory effect on upstream glycolytic intermediates. PK-independent pathway can transfer a phosphate group from PEP to upstream glycolytic enzymes such as phosphoglycerate mutase 1 (PGAM1), which can increase

the mutase activity, therefore, disconnecting the link between ATP production and anabolic processes that are required for rapid cell division [1, 28].

Myc oncogene can promote aerobic glycolysis similar to Akt by enhancing membrane localization of GLUT1 [29]. In addition, Myc can also enhances lactate dehydrogenase (LDH-A) by converting pyruvate into lactate [29]. The over-expression of LDH-A can facilitate rapid cytoplasmic oxidization of NADH to NAD+, and increase the glycolytic flux though amino acids- primarily glutamine and asparagine to mitigate the flux [6]. LDH-A overexpression has also correlated with enhanced lactate production, and further confers with the Warburg effect [1, 29].

As mentioned previously, nutrient utilization for anabolic and catabolic pathways are intricately monitored by cellular metabolic checkpoints and signaling transduction pathways to enhance cell survival. Glucose utilization and metabolic regulation are intrinsically related to oncogenic progression. Cancer cells can reprogram its metabolic phenotype to enhance anabolic process. Exactly how cancer cells can reprogram their metabolic machinery is currently not well understood, therefore the need to develop an approach to trace nutrient utilization for biosynthesis of macromolecules at the molecular level may be a useful intervention to enhance current understanding of cancer cell metabolism.

E. Proteomics and Mass Spectrometry

Proteomics is the study of total proteins expressed in a biological system using technologies for large-scale protein separation and identification. It is a powerful approach for biomedical research because it aims for a comprehensive, quantitative analysis of protein expression changes under biological perturbations such as disease or drug treatment. [30-32, 49] As proteomics tools evolve, quantitative analysis or profiling of proteins in a defined biological system or disease sample (quantitative proteomics) has grown to be the central application for proteomics. Such analysis often encompasses 2-D gel electrophoresis and mass spectrometry (2-DE/MS) or tandem mass spectrometry [30-32, 49].

Mass spectrometry (MS) is the primary tool used for protein identification; for many reasons due to rapid processing, high throughput, highly sensitive and selective approach to quantify protein peptides with minimal samples required. 'Bottom up' approach is a common proteomic approach to analyze proteins by first breaking down proteins into smaller peptides through proteolytic cleavage using proteases. The advantage of this approach is that smaller sized tryptic peptides can be ionized more efficiently than the whole protein, allowing greater sensitivity for separation and detection. To reduce the mass spectra complexity for sensitive detection of small molecules such as metabolites (<1500 Da) or low abundant proteins, MS separation often encompasses interplay between MS instrument with liquid chromatography (LC) or gas chromatography (GC) separation to separate out molecules prior to analysis [35,36,49]. MS technique involves an ionization source (electrospray ionization, ESI), which ionizes the sample. Ionized sample is then accelerated by voltage through ionization chamber. Ions are deflected by electromagnetic field to generate mass-to-charge (m/z) ratio with respective peak intensities represented by mass spectrum based on molecular weight. The peptide list can

then be analyzed by peptide mass fingerprinting through vast and growing array of genome and protein database such as MASCOT, or by de novo sequencing through MS/MS peptide fragment analysis to determine peptide amino acid sequences [33-36, 49].

F. Global Metabolomics and Tracer-Based Metabolomics

The metabolome refers to the complete set of small molecules (metabolites), which are the end products of gene expressions in a biological system. Metabolomics is the "comprehensive characterization and systematic determination of unique small molecule chemical fingerprints in a biological system". While mRNA gene expression and proteomic analyses do not tell the whole story of what is happening in a cell, metabolic profiling can give an instantaneous snapshot of the integrated cellular physiology of the cell [39-40]. Metabolomics analysis uses a global profiling tool to measure the concentration of the metabolites; the subsequent data is interrogated by multivariate statistics and data processing tools. In addition, pattern recognition tools through supervised and unsupervised classification techniques are used to derive the metabolic profiles [35, 37, 38]. Currently, flux measurements has proven effective for simple model organisms, but has proven challenging in complex organisms, because acquiring samples at multiple time points and appropriate temporal intervals for many sample types is difficult (e.g., clinical samples) [41].

The goal of global metabolomics is to link cellular biochemistry to systems biology by tracking alterations in small molecule fluxes to determine cellular dynamics with respect to dysregulation of metabolic flux as a function of time [41]. Therefore, it is important to compare results from large numbers of studies and harness the statistical power from thousands of studies via meta-analysis; a strategy to delineate metabolic cause and effects perturbations. By examining the combination of untargeted metabolomics data from multiple pairwise comparison

studies, the association between specific changes in small molecules to unique phenotypic alterations can be drawn [41].

Currently, Mass spectrometry (MS) and nuclear magnetic resonance (NMR) spectroscopy are by far the two leading technologies for studying metabolomics. Tracer-based metabolomics is a subset of metabolomics that focuses on metabolite distribution and flux determination using tracers [42, 43]. Meanwhile, the advancement of MS, NMR, and stable isotope tracers (e.g., [U-^{13}C]-glucose) has essentially replaced the original radioactive tracer for metabolomics analysis. When a ^{13}C-labeled substrate is introduced into a biological system, ^{13}C can incorporate itself either through exchange or by direct synthesis into a wide range of metabolites and proteins [44]. The incorporation of a stable isotope carbon molecule into a metabolic product generates a mass signature (a difference in molecular weight from the naturally existing molecule ^{12}C) that can be detected by MS. The distribution and destination of a labeled carbon can reflect the intracellular metabolic pathways that it traverses [45]. Therefore, the tracer distribution within individual compounds can represent the metabolic functions of the cell and define its metabolic phenotype. The enrichment of ^{13}C among metabolic intermediates is a measure of flux distribution from the labeled precursor to its various products [46], and the distribution of ^{13}C within a protein molecule can provide estimation about its contribution to synthesis.

The purpose of this study is to analyze cancer cell metabolism by tracer-based proteomic and metabolomics approach. We hypothesized that cancer cells metabolism is a highly robust system, and the metabolic phenotype of cancer cells as characterized by nutrient utilization for biosynthesis is significantly altered during oncogenesis. In this study, we have investigated the effects of down-regulating metabolic enzymes, transketolase (TKT) or adenylate kinase 2 (AK2) that are involved in glycolysis and PPP of oral cancer cells. In addition, we aim to develop a

tracer-based metabolomics methodology based on ^{13}C stable isotope tracers from [$U^{13}C_6$]-glucose to test in *in-vitro* (cell line model) and *in-vivo* (xenograft mouse model). Our focus is to investigate the incorporation of ^{13}C labels into amino acids of proteins peptides in oral squamous cell carcinoma (OSCC) cells, pancreatic ductal adenocarcinoma (PDAC) cells, and human pancreatic ductal epithelial (HPDE) cells. Profiling of ^{13}C labeled proteins in TKT siRNA transfected OSCC cells will be compared with scrambled control siRNA transfected OSCC cells to reveal distinct changes in metabolic phenotypes and biosynthetic pathways in cancer cells.

References

1. Munoz-Pinedo, C., N. El Mjiyad, and J.E. Ricci, Cancer metabolism: current perspectives and future directions. Cell Death Dis. 3(1): p. e248.

2. Kim, J.W. and C.V. Dang, Cancer's molecular sweet tooth and the Warburg effect. Cancer Res, 2006. 66(18): p. 8927-30.

3. Vander Heiden, M.G., L.C. Cantley, and C.B. Thompson, Understanding the Warburg effect: the metabolic requirements of cell proliferation. Science, 2009. 324(5930): p. 1029-33.

4. Jones RG, Thompson CB. Tumor suppressors and cell metabolism: a recipe for cancer growth.Genes Dev. 2009;23:537–548.

5. DeBerardinis RJ, Sayed N, Ditsworth D, Thompson CB. Brick by brick: metabolism and tumor cell growth. Curr Opin Genetics Dev. 2008;18:54.

6. Wendisch, V.F., Amino Acid Biosynthesis: Pathways, Regulation, and Metabolic Engineering. 2007, Springer: London.

7. Smolke, C.D., The Metabolic Pathway Engineering Handbook: Tools and Applications. 2009, CRC Press. p. 1259.

8. Kruger NJ, von Schaewen ., The oxidative pentose phosphate pathway: structure and organisation". Curr. Opin. Plant Biol. 6 (3): 236–46.

9. Zu, X.L. and M. Guppy, *Cancer metabolism: facts, fantasy, and fiction.* Biochem Biophys Res Commun, 2004. 313(3): p. 459-65.

10. Vander Heiden, M.G., L.C. Cantley, and C.B. Thompson, *Understanding the Warburg effect: the metabolic requirements of cell proliferation.* Science, 2009. 324(5930): p. 1029-33.

11. Griffin, J.L. and R.A. Kauppinen, *A metabolomics perspective of human brain tumours.* FEBS J, 2007. 274(5): p. 1132-9.

12. Luo, Z., M. Zang, and W. Guo, *AMPK as a metabolic tumor suppressor: control of metabolism and cell growth.* Future Oncol. 6(3): p. 457-70.

13. Read, A. P.; Strachan, T.. *Human molecular genetics 2*. New York: Wiley; 1999. Chapter 18: Cancer Genetics

14. Sermeus A, Michiels C. Reciprocal influence of the p53 and the hypoxic pathways. Cell Death Dis.2011;2:e164.

15. Bensaad K, Tsuruta A, Selak MA, Vidal MN, Nakano K, Bartrons R, et al. TIGAR, a p53-inducible regulator of glycolysis and apoptosis. Cell. 2006;126:107–120.

16. Matoba S, Kang J-G, Patino WD, Wragg A, Boehm M, Gavrilova O, et al. p53 Regulates Mitochondrial Respiration. Science. 2006;312:1650–1653.

17. Shaw RJ, Kosmatka M, Bardeesy N, Hurley RL, Witters LA, DePinho RA, et al. The tumor suppressor LKB1 kinase directly activates AMP-activated kinase and regulates apoptosis in response to energy stress. Proc Natl Acad Sci USA. 2004;101:3329–3335.

18. Choo AY, Kim SG, Vander Heiden MG, Mahoney SJ, Vu H, Yoon S-O, et al. Glucose addiction of TSC null cells is caused by failed mTORC1-dependent balancing of metabolic demand with supply. Molecular Cell. 2010;38:487.

19. lberola-Ila J, Hernandez-Hoyos G. The Ras/MAPK cascade and the control of positive selection. Immunol Rev. 2003;191:79–96.

20. Ramjaun AR, Downward J. Ras and phosphoinositide 3-kinase: partners in development and tumorigenesis. Cell Cycle. 2007;6:2902–2905.

21. Ahmad I, Patel R, Liu Y, Singh LB, Taketo MM, Wu XR, et al. Ras mutation cooperates with beta-catenin activation to drive bladder tumourigenesis. Cell Death Dis. 2011;2:e124.

22. Barthel A, Okino ST, Liao J, Nakatani K, Li J, Whitlock JP, Jr, et al. Regulation of GLUT1 gene transcription by the serine/threonine kinase Akt1. J Biol Chem. 1999;274:20281–20286.

23. Robey RB, Hay N. Mitochondrial hexokinases, novel mediators of the antiapoptotic effects of growth factors and Akt. Oncogene. 2006;25:4683–4696.

24. Rathmell JC, Fox CJ, Plas DR, Hammerman PS, Cinalli RM, Thompson CB. Akt-Directed Glucose Metabolism Can Prevent Bax Conformation Change and Promote Growth Factor-Independent Survival. Mol Cell Biol. 2003;23:7315–7328.

25. Gottlob K, Majewski N, Kennedy S, Kandel E, Robey RB, Hay N. Inhibition of early apoptotic events by Akt/PKB is dependent on the first committed step of glycolysis and mitochondrial hexokinase. Genes Dev. 2001;15:1406–1418.

26. Sun Q, Chen X, Ma J, Peng H, Wang F, Zha X, et al. Mammalian target of rapamycin up-regulation of pyruvate kinase isoenzyme type M2 is critical for aerobic glycolysis and tumor growth. Proc Natl Acad Sci USA. 2011;108:4129–4134.

27. Luo W, Hu H, Chang R, Zhong J, Knabel M, O′meally R, et al. Pyruvate Kinase M2 Is a PHD3-Stimulated Coactivator for Hypoxia-Inducible Factor 1. Cell. 2011;145:732–744.

28. Vander Heiden MG, Locasale JW, Swanson KD, Sharfi H, Heffron GJ, Amador-Noguez D, et al. Evidence for an Alternative Glycolytic Pathway in Rapidly Proliferating Cells. Science.2010;329:1492–1499.

29. Dang CV, Le A, Gao P. MYC-induced cancer cell energy metabolism and therapeutic opportunities. Clin Cancer Res. 2009;15:6479–6483.

30. Tao WA, Aebersold R. 2003. *Advances in quantitative proteomics via stable isotope tagging and mass spectrometry*. Curr Opin Biotechnol. 14:110-8.

31. Goo YA, Yi EC, Baliga NS, Tao WA, Pan M, Aebersold R, Goodlett DR, Hood L,Ng WV. 2003. *Proteomic analysis of an extreme halophilic archaeon, Halobacterium sp. NRC-1*. Mol Cell Proteomics. 2:506-24.

32. Tao, W.A. and R. Aebersold, *Advances in quantitative proteomics via stable isotope tagging and mass spectrometry.* Curr Opin Biotechnol, 2003. 14(1): p. 110-8.

33. American Society for Mass Spectrometry - What is MS. http://www.asms.org/whatisms/p4.html.

34. Mass Spectrometry in the Postgenomic Era Annual Review of Biochemistry Vol. 80: 239-246 (Volume publication date July 2011) DOI: 10.1146/annurev-biochem-110810-095744.

35. Griffin, J.L. and R.A. Kauppinen, *A metabolomics perspective of human brain tumours.* FEBS J, 2007. 274(5): p. 1132-9.

36. Jellum E, Bjornson I, Nesbakken R, Johansson E & Wold S (1981) Classification of human cancer cells by means of capillary gas chromatography and pattern recognition analysis. J Chromatogr 217, 231–237.

37. Hagberg G (1998) From magnetic resonance spectroscopy to classification of tumors. A review of pattern recognition methods. NMR Biomed 11, 148–156.

38. El-Deredy W, Ashmore SM, Branston NM, Darling JL, Williams SR & Thomas DG (1997) Pretreatment prediction of the chemotherapeutic response of human glioma cell cultures using nuclear magnetic resonance spectroscopy and artificial neural networks. Cancer Res 57, 4196–4199.

39. Daviss, Bennett (April 2005). "Growing pains for metabolomics". *The Scientist* 19 (8): 25–28.

40. Jordan KW, Nordenstam J, Lauwers GY, Rothenberger DA, Alavi K, Garwood M, Cheng LL (March 2009). "Metabolomic characterization of human rectal adenocarcinoma with intact tissue magnetic resonance spectroscopy". *Diseases of the Colon & Rectum* 52 (3): 520–5.

41. Patti, G.J., et al., *Meta-analysis of global metabolomics and proteomics data to link alterations with phenotype.* Spectroscopy. 26(3): p. 151-154.

42. Lee, W.N. and V.L. Go, *Nutrient-gene interaction: tracer-based metabolomics.* J Nutr, 2005. 135(12 Suppl): p. 3027S-3032S.

43. Boros, L.G., M. Cascante, and W.N. Lee, *Metabolic profiling of cell growth and death in cancer: applications in drug discovery.* Drug Discov Today, 2002. 7(6): p. 364-72.

44. Xiao, G.G., et al., *Determination of protein synthesis in vivo using labeling from deuterated water and analysis of MALDI-TOF spectrum.* J Appl Physiol, 2008. 104(3): p. 828-36.

45. Paul Lee, W.N., et al., *Tracer-based metabolomics: concepts and practices.* Clin Biochem. 43(16-17): p. 1269-77.

46. Wai-Nang Paul Lee, L.G.B.a.V.-L.W.G., *Metabolic Pathways as Targets for Drug Screening*. p. 195-210.

47. Cairns, P., et al., *Frequent inactivation of PTEN/MMAC1 in primary prostate cancer.* Cancer Res, 1997. 57(22): p. 4997-5000.

48. Browne, G.J., S.G. Finn, and C.G. Proud, *Stimulation of the AMP-activated protein kinase leads to activation of eukaryotic elongation factor 2 kinase and to its phosphorylation at a novel site, serine 398.* J Biol Chem, 2004. 279(13): p. 12220-31.

49. Wysocki, V.H., et al., *Mass spectrometry of peptides and proteins.* Methods, 2005. 35(3):p. 211-22.

Hypothesis and Specific Aims

Cancer cells require rapid synthesis of biomolecules such as proteins to maintain their potential for fast and uncontrolled proliferation. The purpose of this study is to investigate cancer cells metabolism via tracer-based proteomic and metabolomics approach. We hypothesize that cancer cells metabolism is a highly robust system and the metabolic phenotypes as characterized by glucose utilization for biosynthesis are significantly altered during oncogenesis. Therefore, the transformation of ^{13}C from [U-$^{13}C_6$]-glucose nutrient into non-essential amino acids of de novo synthesized proteins would reflect this metabolic adaptation in cancer cells.

Working Hypothesis # 1: Cancer cells exhibit highly robust metabolic system that can undergo metabolic reprogramming to overcome single enzymatic defect introduced to the pathways involved in regulating glucose metabolism.

Specific Aim # 1: To examine the effects of siRNA knockdown of metabolic enzymes, transketolase (TKT) or adenylate kinase 2 (AK2), on the glycolysis and pentose phosphate pathway (PPP) in oral cancer cells.

OSCC cell lines were treated with small interfering RNA (siRNA) for TKT or AK2. The effects of siRNA inhibition of TKT and AK2 on glucose, glutamine uptake and lactate production were investigated.

Working Hypothesis # 2 and # 3: The metabolic phenotype of oral cancer cells as characterized by nutrient utilization for protein synthesis is significantly altered during oncogenesis, and the transformation of ^{13}C from [U-$^{13}C_6$]-glucose into non-essential amino acids of proteins would reflect this metabolic adaptation in oral squamous cell carcinoma.

Specific Aim # 2: To develop a novel ^{13}C stable isotope tracer-based methodology for studying de novo protein synthesis and metabolic regulation in cancer cells.

OSCC cell line was cultured with 4.5g/L [U-$^{13}C_6$]-glucose (99%) for 5 days. Cellular proteins were lysed and separated by 2-DE based on charge and size. Protein spots were stained, exercised, trypsin digested, and analyzed with LC-MS/MS and protein database search. Mass spectrums of ^{13}C labeled protein peptides were compared with unlabeled (^{12}C) protein peptides.

Specific Aim # 3: To develop a novel ^{13}C stable isotope tracer-based methodology for studying de novo protein synthesis, and to identify differential ^{13}C labeled protein expression in siTKT and siCTRL transfected oral cancer cells.

OSCC cell line was transfected with siTKT and control siRNA, and cultured with 4.5g/L [U-$^{13}C_6$]-glucose (99%) for 5 days. Cellular proteins were lysed, trypsin digested in-solution, and analyzed with LC-MS/MS and protein database search. Mass spectrums of ^{13}C labeled peptides for siTKT transfected cells were compared with control siRNA transfected cells.

Working Hypothesis # 4: We hypothesize that the metabolic phenotype of PDAC cells as characterized by nutrient utilization for protein synthesis is significantly altered during oncogenesis, and the transformation of ^{13}C from [U-$^{13}C_6$]-glucose nutrients into non-essential amino acids of proteins would reflect this metabolic adaptation in PDAC cells.

Specific Aim # 4: To develop a novel ^{13}C stable isotope tracer-based methodology for studying de novo protein synthesis, and to determine differential ^{13}C labeled protein expression in normal human pancreatic duct epithelial cells (HPDE) and human pancreatic ductal adenocarcinoma cells (PDAC) through *in vitro* and *in vivo*.

In vitro model: HPDE and PDAC cell lines were cultured with 4.5g/L [U-$^{13}C_6$]-glucose (99%) for 5 days. Cellular proteins were lysed and separated by 2-DE based on charge and size. Protein spots were stained, exercised, trypsin digested, and analyzed with LC-MS/MS and protein database search. Mass spectrums of ^{13}C labeled protein peptides for HPDE cells were compared with ^{13}C labeled protein peptides of PDAC cells.

In vivo model: Xenograft mouse PDAC tumor was transplanted by injection of MIA PaCa-2 cells into mouse pancreas. [U-$^{13}C_6$]-glucose (99%) was pumped into tumor site via transplanted pump held at constant flow for 24hrs. Mouse tumor tissue was dissected and lysed. Cellular proteins were separated by 2-DE based on charge and size. Protein spots were stained, exercised, trypsin digested, and analyzed with LC-MS/MS and protein database search. Mass spectrums of ^{13}C labeled protein peptides were compared with unlabeled (^{12}C) protein peptides.

CHAPTER 1: Highly Robust Metabolisms of Oral Cancer Cells: siRNA Silencing of Transketolase or Adenylate Kinase 2 in Oral Cancer Cells Inhibits Cell Proliferation and Activates Alternative Modes of Metabolism

INTRODUCTION

The pentose phosphate pathway (PPP) is a biological process that mainly functions to produce ribose-5-phosphate for nucleic acid synthesis. There are two distinct branches of this pathway: oxidative and non-oxidative phase. The oxidative PPP converts glucose-6-phosphate into pentose phosphate sugars, and the non-oxidative PPP recycles pentose phosphates sugars back into glycolytic intermediates or generates de novo ribose-5-phosphate from glycolytic intermediates (**Figure 1-2**).

Metabolic control analysis has indicated that glucose-6-phosphate dehydrogenase (G6PDH) and transketolase (TKT) are the rate-limiting enzymes in the PPP [1,2]. Together with transaldolase, TKT converts D-pentose (xylulose and ribose) 5-phosphate into D-glyceraldehyde 3-phosphate and D-fructose 6-phosphate. In addition, TKT utilizes these glycolytic intermediates for de novo synthesis of ribose-5-phosphate in the non-oxidative phase of PPP. In cancer cells, the PPP catalyzed by TKT plays an important role in utilizing glucose for ribose-5-phosphate synthesis. As shown in **Figure 1-2**, ribose-5-phosphate can be synthesized from the glycolytic intermediates, fructose-6-phosphate and glyceraldehyde-3-phosphate, via the non-oxidative branch of PPP or from glucose-6-phosphate via the oxidative branch of PPP. Several studies have underlined the importance of TKT for tumor cell metabolism, by demonstrating that enhancement of TKT activity supports tumor cell survival and proliferation, suggesting that TKT inhibition dramatically suppresses tumor proliferation [3,5]. Furthermore, two small-molecule

inhibitors of human TKT have also been identified to suppress proliferation of cancer cell lines [6].

Likewise, the enzyme adenylate kinase 2 (AK2) plays a significant role in tumor cell metabolism. Adenylate kinases (ADKs) represent a set of enzymes that regulate phosphorylation of intracellular adenine nucleotides, catalyzing the phosphoryl exchange reaction 2ADP ↔ ATP + AMP, which are critical and universal in cellular life [7]. AK2, a specific isozyme of ADK, functions in the mitochondria and is the only ADK to localize into the mitochondrial intermembrane space [8,9]. Two other major isozymes of ADK include AK1 and AK3, which vary from AK2 and from each other in their intracellular distribution and kinetic properties [7]. AK1 is localized in the cytosol, while AK3 exists only in the mitochondrial matrix. Each isoform has its own substrate specificity, binding affinity, and kinetics [7,8]. The linear localization of these isozymes provides the ability to form a bidirectional relay through phosphoryl transfer, linking sites of ATP-generation with sites of ATP-utilization [7]. AK2 is a crucial component of this ADK relay mechanism, unique in its localization, and its functions to maintain low cytosolic AMP concentration as its primary role to utilize and sequester AMP [7]. During periods of metabolic stress, cytosolic AMP concentration rises, AK2 can compensate for the rise in AMP:ATP ratio by binding to AMP, and in turn activate activates downstream ATP-sensing mechanisms – such as AMP-activated protein kinase (AMPK) – to regulate cellular metabolism (**Figure 1-2**). While AK2 is a significant component of cellular metabolism and adaption, it has not yet been linked to oral cancer. Previous studies have demonstrated a biochemical difference of AK2 in lung tumors, but evidence of its role in other types of cancers remains limited [10,11].

Proteomic analysis and identification of membrane and membrane-associated proteins in UM1 (high metastatic phenotype) and UM2 (low metastatic phenotype) oral cancer cells using

liquid chromatography mass spectrometry (LC-MS/MS) showed TKT and AK2 are present in both cell lines (**Figure 1-1**). To segue our finding to cancer cell metabolism, the purpose of our present study is to test if oral cancer cells can overcome defects introduced by siRNA knock down of important metabolic enzymes (TKT or AK2). Our aim is to study the effects of down-regulating TKT or AK2 may have on the proliferation and metabolic changes of oral cancer cells. Small interfering RNAs (siRNA) were used to knockdown the expression levels of the two enzymes, and the effects of their inhibition on the uptake of glucose, glutamine, and lactate production were investigated.

MATERIALS AND METHODS

A. Cell Line and Cell Culture

Normal human oral keratinocytes (NHOKs were kindly provided by Wilshire Park Dental Institute, Los Angeles, CA) were maintained in EpiLife media supplemented with human keratinocyte growth supplement (Invitrogen, Carlsbad, CA, USA). Oral and head/neck cancer cell lines UM1 (high invasive) and UM2 (low invasive) were cultured in Dulbecco's modified eagle medium (DMEM) plus 10% fetal bovine serum, penicillin (100 units/mL), and streptomycin (100 μg/mL). The cells were maintained at 37 °C in a humidified 5% CO_2-95% O2 incubator. Cells were passaged and harvested at 90-95% confluence.

B. siRNA Knockdown of TKT or AK2

UM1 and UM2 cells were transfected with siRNA in 96-well or 6-well plates using the Hilymax transfection regent (HilyMax, Rockville, MD, USA) according to the manufacturer's instruction. Validated double-stranded siRNAs of TKT, AK2 or non-target control scrambled siRNAs (Santa Cruz Biotech, Santa Cruz, CA, USA) were separately mixed with transfection

reagent and added to the cell culture. After 24-hour treatment, the siRNAs were removed and the cells were maintained in fresh culture media for 48 hours.

C. Cell Proliferation Assay

Cell proliferation assay was performed at 72 hours post-transfection using the CellTiter 96® aqueous non-radioactive MTT cell proliferation kits (Promega, Madison, WI, USA). Briefly, 20ul of the MTT/PMS mix was added to each well of the 96-well plate and incubated at 37ºC in CO_2 incubator for 60 min. The absorbance was read at 490 nm with a 96-well plate reader (BioTek Instruments, Winooski, VT, USA).

D. Glucose Assay

Prior to glucose assay, UM1 and UM2 cells were transfected with TKT siRNA (siTKT), AK2 siRNA (siAK2) or control siRNA (siCTRL). At 72 hours post-transfection, the transfected cells were incubated with complete culture media, and the concentration of the remaining glucose in the culture media was measured with a glucose assay kit (BioVision, Mountain View, CA, USA). Culture media was de-proteinized with a 10-KDa ultracentrifuge filter unit (Millipore, Billerica, MA, USA). The media were then diluted with phosphate buffer saline and subjected to enzymatic reactions at 37ºC for 30 min in the dark. The absorbance was read at 570 nm with the 96-well plate reader (BioTek).

E. Lactate Assay

Similar to glucose assay mentioned above, the culture media of post siRNA-transfected cells were harvested for lactate assay. The lactate in the culture media was measured with a colorimetric lactate assay kit (BioVision). The reactions were incubated at 37ºC for 30 min in the dark. The absorbance was read at 570 nm with the 96-well plate reader.

F. Glutamine Assay

Remaining glutamine in culture media from post siRNA- transfection was measured with a glutamine assay kit (BioAssay Systems, Hayward, CA, USA). The culture media were first de-proteinized with a 10-KDa ultracentrifuge filter unit, and then incubated with the enzyme mix at room temperature for 40 min in the dark. The absorbance was read at 565 nm with the 96-well plate reader.

G. NADPH/NADP Assay

UM1 cells were transfected with TKT siRNA and control siRNA in 6-well plate. At 72 hours post-transfection. The transfected cells were harvested for NADPH/NADP assays using a NADPH/NADP assay kit (BioVision). The enzymatic reactions were incubated at room temperature for 60 min in the dark. Absorbance was read at 450nm with the 96-well plate reader to determine the ratio of intracellular NADPH to NADP.

RESULTS

A. Knockdown of TKT and AK2 Expression in UM1 and UM2 Oral Cancer Cells

To investigate if TKT is abnormally expressed in oral cancer cells, we compared the endogenous expression levels of TKT between NHOKs and oral/head and neck cancer cell lines. Western blot analysis indicated that TKT expression was not dramatically altered in the cancer cells when compared to NHOKs (**Figure 1-3A**). In order to assess the effects of TKT down-regulation on cell proliferation and metabolism, we used siRNA to knock down TKT expression in UM1 and UM2 oral cancer cells. As shown in **Figure 1-3**, siTKT transfection led to a significant decline in the expression of TKT in both UM1 and UM2 cells.

Similarly, AK2 was not aberrantly expressed in oral/head and neck cancer cell lines when compared to NHOKs. However, low invasive UM2 cells expressed a higher amount of AK2 than highly invasive UM1 cells (**Figure 1-4A**). As shown in **Figure 1-4B**, siAK2 transfection led to significant decline in the expression of AK2 in both UM1 and UM2 cells. It was also demonstrated that knockdown of TKT did not affect AK2 expression, and conversely knockdown of AK2 did not impact the expression of TKT. However, knockdown of ASCT2, which is a glutamine transporter, suppressed the expression of AK2 in UM1 cells (**Figure 1-4C**).

B. Effect of TKT or AK2 Knockdown on the Proliferation of UM1 and UM2 Cells

To study the effect of TKT or AK2 down-regulation on cell proliferation, UM1 and UM2 cells were transfected with either siTKT (or siAK2) or scrambled siCTRL. The cells were harvested at 72 hours post-transfection for cell proliferation assays. As shown in **Figure 1-5**, the siTKT-transfected UM1 cells displayed a 49% reduction in cell proliferation compared to the cells transfected with siCTRL ($p=0.003$). similarly, the siTKT transfected UM2 cells exhibited a 23% reduction in proliferation ($p=0.003$) compared to siCTRL. As for cell viability assays, a reduction of 44% was observed in siTKT-transfected UM1 cells ($p=0.004$) and a reduction of 53% was observed in siTKT-transfected UM2 cells ($p=0.02$).

The proliferation of UM1 and UM2 cells was also significantly inhibited when the cells were transfected with siAK2. When compared to siCTRL-transfected cells, siAK2-transfected UM1 cells exhibited a 31% decrease in cell proliferation ($p=0.01$), and siAK2-transfected UM2 cells displayed a 24% decrease in cell proliferation ($p=0.003$) (**Figure 1-6**). Similarly, significant reductions in cell viability were also observed in siAK2-transfected UM1 (42%, $p=0.02$) and UM2 cells (33%, $p=0.03$).

C. Effect of TKT Knockdown on Glucose Uptake and Lactate Production in UM1/UM2 Cells

To investigate the effect of TKT or AK2 knockdown on the glucose uptake in UM1 and UM2 cells, The cells were transfected with siRNA for TKT, AK2 or scrambled CTRL. The cells were cultured in complete growth media. Afterwards, the remaining culture media were collected for glucose and lactate assays to determine the glucose uptake as well as the lactate production.

As shown in **Figure 1-7**, siTKT-transfected UM1 cells consumed 1.24-fold greater amount of glucose (p=0.01) than siCTRL-transfected UM1 cells. siTKT-transfected UM2 cells utilized 1.39-fold greater amount of glucose (p=0.003) compared to siCTRL-transfected UM1 cells. Meanwhile, siTKT-transfected UM1 cells produced 1.54-fold more lactate (p=0.0006) compared to siCTRL-transfected UM1 cells, whereas siTKT-transfected UM2 cells produced 1.44-fold more lactate (p=0.0001) compared to siCTRL-transfected UM2 cells. These findings corroborates with the observed increased in glucose uptake by siTKT-transfected cells.

D. Effect of AK2 Knockdown on Glucose Uptake and Lactate Production in UM1/UM2 Cells

Glucose depletion assays were also performed to determine the glucose uptake by siAK2-transfected UM1 and UM2 cells (**Figure 1-8**). The siAK2-transfected UM1 cells utilized 1.44-fold more glucose (p=0.002) than siCTRL-transfected UM1 cells, and the siAK2-transfected UM2 cells consumed 1.26-fold more glucose (p=0.03) than siCTRL-transfected UM2 cells. Similar to the TKT-transfected UM1 cells, the AK2-transfected UM1 cells secreted a 1.25-fold greater amount of lactate (p=0.02), which corroborates with the increased uptake of glucose by the cells. However, only a slight increase of 1.13-fold in lactate production was observed in siAK2-transfected UM2 cells (p=0.09).

E. Effect of TKT or AK2 Knockdown on Glutamine Uptake by UM1 and UM2 Cells

As shown in **Figure 1-9**, the siTKT-transfected UM1 cells utilized 2.23-fold greater amount of glutamine (p=0.01) than the siCTRL-transfected UM1 cells, while the siTKT-transfected UM2 cells utilized 1.7-fold greater amount of glutamine (p=0.02) than the siCTRL-transfected UM2 cells. Similarly, the siAK2-transfected UM1 cells consumed 1.99-fold more glutamine (p=0.02) than the siCTRL-transfected UM1 cells, whereas the siAK2-transfected UM2 cells consumed 1.25-fold more glutamine (p=0.03) than the siCTRL transfected UM2 cells.

F. Effect of TKT Knockdown on NADPH/NADP Production in UM1 Cells

Cellular reducing power of the PPP is contributed by elevation in NADPH production. The ratio of NADPH/NADP can indicate the conversion of G6P into 6-phosphoglucono-σ-lactone, catalyzed by G6P dehydrogenase, or conversion of 6-phosphogluconate into ribulose-5-phosphate of PPP. To investigate the effect of TKT knockdown on NADPH production, siTKT and siCTRL transfected UM1 cells were compared. As shown in **Figure 1-10**, siTKT-transfected UM1 cells produced 1.5-fold more NADPH than siCTRL transfected UM1 cells, which corroborates with the observed increase in glucose uptake. This finding suggests that glucose may be redirected through alternative pathways to couple production of NADPH.

DISCUSSION

Tumor cell proliferation requires rapid synthesis of biomolecules such as nucleotides, proteins and lipids. The metabolism for tumor cells deviates from the norm; re-programmed to facilitate the uptake of nutrients such as glucose and glutamine for de novo synthesis of biomolecules. TKT, a critical metabolic enzyme in the non-oxidative branch of PPP, catalyzes reactions that enable oxygen-independent glucose degradation and plays a crucial role in the

biosynthesis of ribose-5-phosphate in tumor cells. Our study demonstrated that siRNA knockdown of endogenous TKT expression significantly impairs the proliferation of the UM1 and UM2 oral cancer cells. The resultant limitation of UM1 and UM2 growth stems from the severe defects in the PPP caused by silencing TKT, affecting the biosynthesis of ribose-5-phosphate, nucleotides and possibly precursors for other biomolecules. Due to siRNA silencing of TKT in these cells, ribose-5-phosphate may have to be mainly synthesized from the glycolytic intermediate glucose-6-phosphate via the oxidative branch of PPP. However, this pathway alone is less efficient in the synthesis of ribose-5-phosphate, contributing to a reduced proliferation rate of the cells. Meanwhile, PPP involves the biosynthesis of glycolytic intermediates such as fructose-6-phosphate and glyceraldehyde-3- phosphate, which are normally recycled by glycolytic process. Silencing of TKT in the cancer cells obviously abolish the cross-talk between PPP and glycolysis, causing deficiency in utilizing glycolytic metabolites for down-stream biosynthesis and energy production in the cells.

When compared to the cells transfected with scrambled control siRNA, the cells transfected with siTKT also displayed an increased in glucose uptake. The high level of glycolysis is required to confer metabolic adaption when facing defects in the PPP; providing not only ATP for the tumor cells high bioenergetics demands, but also increasing the precursors for biomolecule synthesis. Consistent with the results of increased glucose uptake and glycolysis, higher levels of lactate production were observed in the TKT knock-downed cells. When endogenous TKT expression is inhibited by siRNA, UM1 and UM2 cells also uptake a markedly higher amount of glutamine. Glutamine and its degradation products, glutamate and aspartate, are precursors for de novo synthesis of nucleotides and proteins. Our study suggests that, survival from TKT silencing, UM1 and UM2 cells increasingly utilize glucose and glutamine to

rescue the production of ribose-5-phosphate, nucleotides and other biomolecules. In addition to composing the structural units of nucleic acids, nucleotides play a central role in metabolism by serving as sources for biochemical energy, such as ATP and GTP. Thus, it is possible that an increase in the uptake and metabolism of glucose and glutamine contributes greatly to maintaining the chemical energy in cancer cells.

Comparable to the results obtained with the TKT knockdown study, the siRNA knockdown of AK2 also impaired the proliferation of UM1 and UM2. Due to AK2's unique localization in the mitochondrial intermembrane space, the crucial function of AK2 in maintaining AMP: ATP ratios cannot be compensated by other ADK isozymes. Because AK2 primarily utilizes AMP to produce ADP and eventually ATP, AK2 knock-down will inhibit the ability for the cell to generate ATP, resulting in an increased AMP: ATP ratio. Consequently, AMPK, a kinase sensitive to AMP: ATP ratios, is activated to regulate cellular energetics and restore energy homeostasis through the phosphorylation of many downstream targets [13, 14].The overall effect of AMPK activation results in the reduced proliferation of UM1 and UM2, as it is well established that AMPK deters cell growth and down-regulates anabolic pathways, such as protein and lipid synthesis, in order to conserve ATP [15].

While AMPK acts to conserve ATP through a reduction in cell growth and proliferation, its activation can also results in the up-regulation of energy producing catabolic pathways, such as glycolysis [13, 15]. The UM1 and UM2 cells transfected with siAK2 displayed elevated consumption of glucose and glutamine, both essential for the production of cellular energy. AMPK has been referred to as a "master switch" of metabolism and glycolysis, and it has been indicated in studies of tumor cells that AMPK highly regulates cellular glycolytic flux [13, 16]. The increased levels of lactate production may serve as an indicator for the increased level of

glycolysis, and it has been noted that greater concentrations of lactate can further stimulate AMPK activity [16]. While AMPK has an established and well-studied role in cancer, it has not been previously linked with AK2 in this context, and recently investigated functions of AK2 in tumorgenesis and tumor cell survival are still emerging [17].

CONCLUSION

In this study, we have demonstrated that the knockdown of TKT or AK2 expression significantly inhibits the proliferation of oral cancer cells. Due to deficiencies in the PPP caused by siRNA silencing of TKT, UM1 and UM2 cells displayed an increase in uptake of glucose and glutamine, and subsequently produce a higher amount of lactate. These findings suggest that the partial inactivation of the PPP due to siRNA silencing of TKT was compensated by the activation of the alternative modes of metabolism, including glycolysis and possibly oxidative PPP. The siRNA silencing of AK2 may have contributed to the depletion of ATP and an increase in the AMP: ATP ratio to activate AMPK as a master regulatory metabolic control, both down-regulating anabolic pathways to preserve ATP and up-regulating catabolic mechanisms to generate ATP. Thus, the defects in the ATP-producing capacity and phosphoryl relay mechanism of AK2 may be compensated by alternative metabolic pathways initiated by AMPK. Previous studies have shown that cancer cells can overcome single chemotherapeutic strategies through different metabolic network adaptations, demonstrating the robustness of cancer cell metabolism [18, 19]. Our study corroborates with these earlier findings and indicates that cancer cells, as a system, can activate alternative pathways for biosynthesis when one of the biosynthetic pathways is truncated or suppressed. The highly robust nature of cancer cell metabolism can logically complicate cancer treatment since therapeutic intervention targeting one of the metabolic pathways cannot prevent cancer cells from utilizing other pathways for biosynthesis and

proliferation. As such, a more comprehensive, systematic medical approach targeting multiple metabolic pathways may be needed to accomplish the continued improvement in cancer treatment.

References

1. J. Boren, A. R. Montoya, P. de Atauri, B. Comin-Anduix, A. Cortes, J. J. Centelles, W. M. Frederiks, C. J. F. Van Noorden and M. Cascante, Molecular Biology Reports, 2002, 29, 7-12-12.

2. M. Cascante, L. G. Boros, B. Comin-Anduix, P. de Atauri, J. J. Centelles and P. W. N. Lee, Nat Biotech, 2002, 20, 243-249.

3. L. G. Boros, J. Puigjaner, M. Cascante, W.-N. P. Lee, J. L. Brandes, S. Bassilian, F. I. Yusuf, R. D. Williams, P. Muscarella, W. S. Melvin and W. J. Schirmer, Cancer Research, 1997, 57, 4242-4248.

4. C. J. Cascante M, Veech RL, Lee WN, Boros LG., Nutr Cancer, 2000, 36, 150-154.

5. B. Rais, B. Comin, J. Puigjaner, J. L. Brandes, E. Creppy, D. Saboureau, R. Ennamany, W.-N. Paul Lee, L. G. Boros and M. Cascante, FEBS Letters, 1999, 456, 113-118.

6. M. X. Du, J. Sim, L. Fang, Z. Yin, S. Koh, J. Stratton, J. Pons, J. J.-X. Wang and B. Carte, Journal of Biomolecular Screening, 2004, 9, 427-433.

7. P. Dzeja and A. Terzic, Adenylate kinase and AMP Signaling Networks: Metabolic Monitoring , Signal Communication and Body Energy Sensing. International Journal of Molecular Sciences, 2009, 10, 1729-1772.

8. G. A. Bruns and V. M. Regina, Biochem Genet, 1977, 15, 477-486.

9. C. Köhler, A. Gahm, T. Noma, A. Nakazawa, S. Orrenius and B. Zhivotovsky, FEBS Letters, 1999, 447, 10-12.

10. O. Greengard, J. F. Head and S. L. Goldberg, Cancer Res, 1980, 40, 2295-2299.

11. B. D. Nelson and F. Kabir, Biochimica et Biophysica Acta (BBA) - General Subjects, 1985, 841, 195-200.

12. S. Nakayama, A. Sasaki, H. Mese, R. E. Alcalde and T. Matsumura, Invasion and Metastasis, 1998, 18, 219-228.

13. W. Wang and K. L. Guan, Acta Physiologica, 2009, 196, 55-63.

14. D. Carling, F. V. Mayer, M. J. Sanders and S. J. Gamblin, Nat Chem Biol, 2011, 7, 512-518.

15. D. Carling, C. Thornton, A. Woods and M. J. Sanders, Biochemical Journal, 2012, 445, 11-27.

16. M. G. P. Erin E Mendoza, Xiangul Kong, Dennis B Leeper, Jaime Caro, Kirsten H Limesand, Randy Burd, Translational Oncology, 2012, 5, 208-216.

17. S.-M. Jeon, N. S. Chandel and N. Hay, Nature, 2012, 485, 661-665.

18. Ramos-Montoya, W.-N. P. Lee, S. Bassilian, S. Lim, R. V. Trebukhina, M. V. Kazhyna, C. J. Ciudad, V. Noé, J. J. Centelles and M. Cascante, International Journal of Cancer, 2006, 119, 2733-2741.

19. P. Vizán, G. Alcarraz-Vizán, S. Díaz-Moralli, O. N. Solovjeva, W. M. Frederiks and M. Cascante, International Journal of Cancer, 2009, 124, 2789-2796.

CHAPTER 2: Development of a Novel ^{13}C Stable Isotope Tracer-Based Methodology for Studying De Novo Protein Synthesis in Oral Cancer Cells

INTRODUCTION

Oral cancer, predominantly oral squamous cell carcinoma (OSCC) is the sixth most common human cancer worldwide. The disease accounts for nearly 3% of the total cancer burdens and results in 128,000 annual deaths globally [1, 2]. Patients with OSCC often present symptoms at a late stage of the disease, and post-treatment recurrence rate remain high, especially in metastatic patients [3]. Despite clinical and treatment advances, the overall 5-year survival rates for oral cancer have remained low and relatively unchanged during the past few decades [4, 5].

Uncontrolled proliferating cells such as tumor cells exhibit an enhanced utilization of glucose for rapid synthesis of macromolecules such as nucleotides, lipids and proteins. In many cancer cells, this is characterized by a shift in glucose metabolism from oxidative phosphorylation to increased aerobic glycolysis [6]. Tumor cells voracity for glucose have revealed many connections about mitogenic signaling pathways with nutrient status of the environment. In addition, many oncogenes and tumor suppressor genes also contributes to the regulation of cellular metabolism. For instance, p53 expression can control metabolic genes and alter glucose utilization mechanisms. Expression of TIGAR (TP53-induced glycolysis and apoptosis regulator), a gene induced by p53, can cause inhibition of phosphofructokinase, and direct glucose toward the pentose phosphate shunt to upregulate NADPH production [7]. Many tyrosine kinase oncogene signaling pathways have also been associated with cellular proliferation and regulation of glucose metabolism. Activation of tyrosine kinase oncogene signals can direct the flow of glucose towards anabolic pathways as opposed to complete

catabolic pathways for ATP production. In principle, the metabolic dependencies of cancer cells can be exploited for therapeutic interventions [8-10]. Understanding the roles by which dietary supplements contributes to glucose regulation may serve as adjuncts to cancer treatment [11].

Cancer cells are known to thrive in hypoxic environment better than normal adjacent cells. The distinctive feature of this adaptation is increased lactate production without increased oxygen consumption (anaerobic glycolysis). This event is associated with the transcriptional activation of metabolic enzymes controlled by the activation of hypoxic inducible factor (HIF). HIF is a transcriptional factor that regulates glycolysis and oxygen dependent enzymes, and in turn, gets regulated by substrates of the TCA cycle [12-18]. Oxidative phosphorylation either through β-oxidation of fatty acids or through actions of pyruvate dehydrogenase can cause TCA cycle intermediate to hydroxylase proline in HIF; inhibiting the function of HIF. The regulation of the TCA cycle is an important component to HIF regulation and is closely linked with cancer cells phenotype to thrive in hypoxic environment [12-18].

Traditionally, radioactive tracers were used to determine protein synthesis and turnover. Meanwhile, the advancement in Mass Spectrometry (MS) technologies have provided highly sensitive and precise detection methods through stable isotope tracers, and have essentially replaced the traditional radioactive based methods. Stable isotope labeling of non-essential amino acids can be used to determine protein synthesis in cancer cells. ^{13}C labeling (heavy) to replace natural ^{12}C (light) can elucidate mass difference in protein peptides, and link de novo protein synthesis process to nutrient metabolic pathways to enhance current understanding of nutrient-gene interaction. Cells can breakdown [U-$^{13}C_6$]-glucose for anabolic processes and trap ^{13}C into the carbon backbones of intracellular amino acids during protein synthesis. The mass difference of ^{13}C labeled peptide can then be readily detected by MS as a distribution of mass

isotopomers. This distribution patterns can reflect respective metabolic fluxes, because the amino acid isotopomers carry information regarding the paths they have traversed, and the final distribution can reflect the relative contribution from these individual pathways [19]. Quantitation of the isotopic peak intensities from the labeled and the unlabeled peaks can generate a synthesis-to-degradation ratio to represent the relative dynamics in protein turnover [20]. In addition, comparing the ^{13}C labeled and ^{12}C unlabeled ion fragments can identify peptide amino acid sequences to depict carbon flow from glucose, and to map out protein synthesis pathways and alterations in nutrient-gene interactions between cancer and normal cells.

In previous study, small interfering RNA down-regulated transketolase (TKT) metabolic enzymes of pentose phosphate pathways (PPP) in oral cancer cells. UM1 oral cancer cells displayed increased glucose, glutamine uptake, and lactate production compared to scrambled control siRNA transfected UM1 cells. This observation suggested that cancer cells can overcome single defect in the metabolic pathway by reprogramming their metabolic system to turn on alternative metabolic pathways for enhanced utilization of glucose.

The purpose of this study aims to develop a novel ^{13}C stable isotope tracer-based methodology for studying de novo protein synthesis in oral cancer cells. We also aim to apply ^{13}C stable isotope tracer-based methodology to investigate differential ^{13}C labeling patterns in oral cancer cells transfected with small interfering RNA for TKT compared to control siRNA transfected oral cancer cells. Since TKT is an important metabolic enzyme that regulates PPP for nucleotide synthesis and NADPH production, we expect to identify unique ^{13}C labeling signatures that are distinctive to siTKT transfected cells.

MATERIALS AND METHODS

A. Cell Culture

Oral squamous cell carcinoma UM-SCC-1 cell line was obtained from Japanese Research Resources Bank (JCRB) and was cultured with glucose-free DMEM (GIBCO) supplemented with 4.5g/L [U-$^{13}C_{6,}$ 99%] D-glucose (Cambridage Isotope Laboratories, Inc.), 10% fetal bovine serum, 100units/mL penicillin and 100µg/mL streptomycin. The cell line was maintained at 5% CO2-95% O_2 and 37°C. Fresh culture media was replaced every 24 hour for 5 days. When UM1 cells reached 80-90% confluence, the cells were washed with PBS three times and harvested with cell lysis buffer (RB buffer) containing 62.5 mM Tris-HCL (pH=6.8), 2% SDS (w/v), 10% Glycerol and 0.2 mM DTT.

B. siRNA Knockdown of TKT

UM1 cells were transfected with siRNA in 6-well plates using the Hilymax transfection regent (HilyMax, Rockville, MD, USA) according to the manufacturer's instruction. Validated double-stranded siRNAs of TKT and non-target control scrambled siRNAs (Santa Cruz Biotech, Santa Cruz, CA, USA) were separately mixed with transfection reagent and added to the cell culture. After 24-hour treatment, the siRNAs were removed and the cells were maintained in fresh 4.5g/L [U-$^{13}C_{6,}$ 99%] D-glucose (Cambridage Isotope Laboratories, Inc.) supplemented culture media for 48 hours.

C. Sample Preparation

Harvested proteins from UM1 cells were precipitated with cold acetone (9:1 acetone: sample volume) and stored in -20°C freezer for 24 hours. Precipitated proteins were centrifuged at 4°C and 16,000g for 15 min. The above-mentioned steps were then repeated twice, and cold acetone was carefully removed. Afterwards, the precipitated protein pellet was re-suspended in

RB buffer. 1% Ampholyte (Bio-Lyte 3/10, Bio-Rad) was added to 100µg of protein and vortex for 30s prior to loading sample onto PROTEAN IEF focusing tray (PROTEAN IEF Cell System, Bio-Rad) for active rehydration via immobilized pH gradient (IPG) strip (Ready Strip, Bio-Rad).

D. 2-Dimensional Gel Electrophoresis

Cellular proteins of UM1 were mapped out using 2-dimensional gel electrophoresis, with isoelectric focusing (IEF) in the first-dimension of separation and SDS-PAGE in the second-dimension of separation. Bio-Lyte 3/10 1% Ampholyte (Bio-Rad) was added to 100µg of UM1 proteins and vortex for 30s prior to loading onto PROTEAN IEF focusing tray. IPG gel strips were laid onto the protein samples and mineral oil (Bio-Rad) was added to IEF focusing tray for active rehydration for 16 h at 50V. Hydrated IPG Strips were then transferred to a new IEF focusing tray and samples were run under the following IEF program setting: 250 V (linear), 1 h; 500 V (rapid), 2 h; 3,000 V (linear), 1 h; 3,000 V (rapid), 3h; 8,000 V (linear), 3 h; 8,000 V (rapid), 10 h; and 250 V (rapid), 99 h. IPG strips were then transferred to a new tray and incubated with 2% DTT and 2.5% iodoacetic acid solutions separately at room temperature for 10 mins each. Prior to second-dimension protein separation by 7.5% Criterion TGX precast gel (Bio-Rad), IPG strips were briefly washed with 1x TGS running buffer. 7.5% Criterion TGX precast gels were run at 200V for 50 min in Criterion Dodeca Cell (Bio-Rad). Finally 7.5% Criterion TGX precast gels were washed with fix/destain (7% acetic acid–10% methanol) solution prior to and after fluorescent Sypro-Ruby staining (Molecular Probes) to visualize the protein spots. Bio-Rad GS 800 imager and PDQuest program were used to scan the stained Criterion gels, and gel images were analyzed using Progenesis SameSpot software (Nonlinear dynamics). A matched set of stained proteins were created for D-glucose (U-$^{13}C_{6,}$ 99%) treated UM1 cells and DMEM treated control UM1 cells. Afterwards, matched gel spots were exercised

using ProPic II Spot Cutter (DIGILAB Genomics Solutions), and spots were collected into 96 well plates for in-gel tryptic digestion.

E. In-Gel Trypsin Digestion

Protein spots of interest were repeatedly washed and dried with 50 mM NH_4HCO_3 50% CH_3CN solution and 100% CH_3CN solution. To reduce protein disulfide bonds, protein gel spots were incubated in 10 mM dithiothreitol (DTT) for 1 h. The supernatants were discarded and 50 mM iodoacetic acid (IAA) alkylating agent was added to protein gel spots and incubated for 1h in the dark to prevent re-formation of disulfide bonds. Protein gel spots were digested with 10-ng/μL enzyme-grade trypsin (Promega, Madison, WI) in 100 mM NH_4HCO_3 at 37°C incubation for 24 hours. After proteolytic cleavage, all samples were dried and re-constituted with 5% acetonitrile/ 0.1% formic acid (v/v) for subsequent LC-MS/MS analysis.

F. In-Solution Trypsin Digestion

siTKT and control siRNA transfected UM1 cells were lysed with 8M urea. Cell lysates containing 25ug of total proteins were treated with 100mM dithiothreitol (DTT) for 1hr to reduce protein disulfide bonds, and then treated with 150 mM iodoacetic acid (IAA) alkylating agent in 200mM NH_4HCO_3 for 1hr in the dark to prevent re-formation of disulfide bonds. Protein samples were digested with 10 ng/μL enzyme-grade trypsin (Promega, Madison, WI) in 200 mM NH_4HCO_3 at 37°C incubation for 24 hours. After proteolytic cleavage, samples were spun down at 14000g. The supernatant was transferred and dried. The peptide samples were dissolved in 0.1% formic acid and transferred to sample injection vials.

G. LC-MS/MS and Database Search

Liquid Chromatography (LC) with tandem MS (LC-MS/MS) of peptides was performed using an Eksigent NanoLC-2D HPLC system with Thermo LTQ Orbitrap XL Mass

Spectrometer. Aliquots (5µL) of peptide digest derived from each gel spot were injected using an auto-sampler at a flow rate of 3.5µL/min. The peptides were concentrated and desalted on a C_{18} Integral Frit Nano-Precolumn (New Objective, Woburn, MA) for 10 min, then eluted and resolved using a C_{18} reversed- phase capillary column (New Objective). LC separation was performed at 400nL/min with the following mobile phases: A, 5% acetonitrile/0.1% formic acid (v/v); B, 95% acetonitrile/0.1% formic acid (v/v). The chosen LC gradient was: from 5% to 15% B in 1 min, from 15% to 100% B in 40 min, and then maintained at 100% B for 15 min [21]. In-solution digested protein samples were run at 170 min gradient. The eluent was introduced directly to the LTQ mass spectrometer via electrospray using a PicoTip emitter (tip inner diameter, 10 µm). Each full MS scan is followed by 5 data-dependent MS/MS scans on the most intense ions at 35% normalized collision energy. Database search was performed using Mascot database search engine against the SwissProt protein sequence database. The search criteria were set with a mass tolerance of 0.5 Da for precursor and product ions, semi-style cleavage by trypsin, and one missed tryptic cleavages were allowed. Varied modification accounted for cysteine carbamidomethylation, methionine oxidation, and serine, threonine and tyrosine phosphorylation. The MS/MS spectra for each peptide were manually examined to verify the identification [22].

H. Data Analysis of ^{13}C Incorporated Peptides

Xcalibur 2.1 software (Thermo Scientific) was used to manually examine the MS/MS spectra of ^{13}C incorporated peptides within 300-1600 m/z range. Peptide fragment ions, ‘b’ ions and ‘y’ ions were matched against SwissProt protein sequence database to identify the incorporated ^{13}C mass difference corresponding to ^{13}C labeled protein peptides. Database for

Annotation Visualization and Integrated Discovery (DAVID) software v6.7 was used to perform functional annotation and classification of ^{13}C labeled proteins and their unique labeled peptides.

RESULTS

A. Identification of ^{13}C Labeling in UM1 Cells

The purpose of this study was to develop a novel ^{13}C stable isotope tracer-based methodology for studying metabolic regulation of protein synthesis in cancer cells. OSCC-UM1 cell line of metastatic phenotype was derived from tongue origin of a 47 year-old Japanese male. Cellular proteins from UM1 cells were isolated and resolved with 2-dimensional gel electrophoresis. Protein gel slices were proteolytically cleaved and the remaining protein peptides were analyzed with LC-MS/MS. Protein identification was conducted by searching MASCOT database against raw MS spectra data. In total, we identified 100 proteins with at least two unique peptide hits and with peptide sequence match scores over 40. Peptide mass isotopomer distribution pattern from MS1 full scan (300-1600 m/z) were manually processed by matching the observed mass-to-charge (m/z) value from the 1st isotopic peak (Monoisotopic-base peak, M0, ^{12}C) and the 2nd isotopic peak (^{13}C labeled peak, M1, ^{13}C or ^{12}C+^{13}C) of the labeled peptide (displaying mass shift of +1 Da; M0, M1, M2, M3…) to known peptide sequences from MASCOT peptide mass fingerprinting database. In total, 38% (38 proteins) of identified proteins displayed some form of ^{13}C incorporation into amino-acids of protein peptides; many of which are metabolic enzymes (**Tables 2-1, 2-2, 2-3**). The low percentage yield achieved in ^{13}C labeled proteins may be due to complexity of ^{13}C labeled isotopic peak patterns generated by multiple mass shifts, which led to confusion by MS to correctly select out the monoisotopic peak for fragmentation used in protein identification. As shown in **Figure 2-4 B&C**, ^{13}C labeled peptide for 78k Da glucose-related protein displays triple isotopic envelop indicated by high intensities

(relative abundance) in peaks M0, M3, and M6 proceeded by declining intensities in the isotopic peaks. In addition, the low percentage yield in ^{13}C labeled proteins may also indicate precise synthesis of end products from [U-$^{13}C_6$]-glucose, and reflect the ratio of protein synthesis to degradation in the cell. In the case of zeta/delta subunit of 14-3-3 protein, the peptide labeling was characterized by extended isotopic tailing pattern shown in **Figure 2-1 B&C**. A greater quantity of ^{13}C labeled peptides was identified in zeta/delta subunit in comparison with other subunits (sigma, epsilon, and beta/alpha) of 14-3-3 protein family. Zeta/delta of 14-3-3 protein is an adaptor protein implicated in the regulation of a large spectrum of specialized signaling pathways. Zeta/delta of 14-3-3 protein can interact with TP53 to enhance p53 transcriptional activity. In turn, p53 activation can activate TIGAR (TP53-induced glycolysis and apoptosis regulator) to inhibit phosphofructokinase and direct glucose toward the pentose phosphate shunt for enhanced NADPH production [7]. The labeling difference observed in particular subunits/subfamily of proteins could potentially suggest regulated flow of ^{13}C from glucose, which may reflect the metabolic status of UM1 cells as well as the phenotype and functional relation to glucose metabolism.

B. Analysis of ^{13}C Labeled Peptide Isotopomers in UM1 Cells

LC-MS analysis of peptide isotopomers from 14-3-3 protein zeta/delta is shown in **Figure 2-1**. **Figure 2-1 A** shows peptide isotopomer patterns of natural unlabeled ^{12}C peptide for 14-3-3 protein zeta/delta. Unlabeled peptide (m/z=774.86, z=+2) displayed rapid isotopic decay pattern within 4 peaks (M0, M1, M2, M3). **Figure 2-1 B&C** shows ^{13}C labeling for the same peptide displaying extended isotopic decay pattern consisting of 14 consecutive isotopic peaks. The monoisotopic peak was fragmented to determine the sequence of ^{13}C labeled peptide. MS/MS fragmentation of the monoisotopic peak (m/z=774.86) into respective ‘b’ and ‘y’ ions,

matched 20/146 fragments from the most intense peaks and determined peptide sequence SVTEQGAELSNEER (underlined amino acids sequence correspond to matched 'y' ions). The 2nd isotopic peak (m/z=775.36) fragments revealed similar sequence match, differing by 0.984 Da (~1 Da) at the N (asparagine) position, SVTEQGAELSNEER (**Figure 2-1B**). This finding depicted post-translational modification deamidation reaction, converting asparagine to aspartate by replacing the amide in asparagine side chain with carboxylate group. Since deamidation modification was only depicted on the 2nd isotopic peak (^{13}C) and not the 1st isotopic peak (^{12}C), the mass difference was initially thought to represent ^{13}C incorporation into asparagine by replacing one of the ^{12}C with ^{13}C. However, inconsistency in deamidation between the 1st and 2nd isotopic peak of ^{12}C unlabeled and ^{13}C labeled peptides were also observed in other proteins, thus, complicates the process for determining specific amino acid with ^{13}C enrichment and the pathway in which ^{13}C transverses.

Similar isotopic decay pattern was also observed in 78k Da glucose-related protein shown in **Figure 2-3 B&C**. Enrichment of ^{13}C into peptides generated a double envelop pattern. This envelop pattern is represented by a relatively high peak intensity at the M3 position of K.TFAPEEISAMVLTK.M peptide sequence. The mass shift from the first isotopic peak (M0) to the fourth isotopic peak (M3) displayed a mass shift of 3 Dalton, which could suggest labeling of a three carbon amino acid, such as alanine, since alanine can be directly synthesized from pyruvate. Similarly, the peptide isotopomers of triosephosphate isomerase, a critical enzyme of glycolysis for interconversion of dihyroxyacetone phosphate to glyceraldehyde 3-phosphate displayed a triple envelop pattern (**Figure 2-5**). The mass shift from the 1st isotopic peak to the 4th and 7th isotopic peak (M0, M3, and M6) displayed +3 and +6 Da shift. The high intensity at the M3 and M6 position may also potentially correspond to labeling of three carbon amino acid

alanine presented in the peptide (K.SNVSDAVAQSTR.I). This type of pattern was consistently identified in many other protein peptides, which suggests that patterns of mass shift and envelop may potentially indicate ^{13}C enrichment for specific amino acids in a peptide. The complexity in ^{13}C labeled peptide isotopomer distribution can complicate automated detection by MS, because high intensity in isotopic envelop base peaks may sometime mimic the intensity of the monoisotopic peak for fragmentation. This creates an issue in the downstream identification step during protein database search, in which, monoisotopic peak from ^{13}C labeled peptide may not get selected for identification. To overcome these obstacles, manual inclusion parameters to fragment all isotope peaks (M_0, M_1, M_2, M_3, M_4, M_5…) within a ^{13}C labeled peptide may be necessary to help overcome the limitation for determining specific position of amino acids that are labeled with ^{13}C. In conjunction, the error of overlooked isotopic peaks may be reduced and specificity of MS fragmentation may be enhanced to determine peptide labeling sequences.

C. ^{13}C Labeled Proteins and Related Pathways in UM1 Cells

^{13}C labeled proteins with matched peptides were analyzed with Database for Annotation, Visualization and Integrated Discovery (DAVID) software v6.7 according to UNIGENE protein code converted from UniProtKB/Swiss-Prot protein accession number (**Table 2-2**). ^{13}C labeled proteins were categorized based on their related cellular pathways (**Table 2-3**). In relative with total ^{13}C labeled proteins, 31% of ^{13}C labeled proteins were involved in glycolysis/gluconeogenesis pathways, 14% were involved in cell cycle, and 10% were involved in RNA degradation (**Figure 2-6**). MAPK signaling, p53 signaling, glutathione metabolism and PPP were reflected by relatively small percentages. These findings suggest that glycolysis and cell cycle pathways may be the primary modes by which the end products of [U-$^{13}C_6$]-glucose are directed to, reflecting the metabolic and physiological status of UM1 oral cancer cells.

D. Identification of ^{13}C labeling in siTKT and siCTRL transfected UM1 Cells

UM1 cells were transfected with small interfering RNA for TKT or control scrambled siRNA in 4.5g/L of [U-$^{13}C_6$]-glucose for 5 days. In-solution tryptic digestion of siTKT-transfected UM1cells and siCTRL-transfected UM1 cells were analyzed by LC-MS/MS and MASCOT protein database search. In total, we identified 564 proteins (labeled and unlabeled) in siCTRL-transfected UM1 cells and 515 proteins (labeled and unlabeled) in siTKT-transfected UM1 cells (**Figure 2-8**). The lower yield in total number of identified proteins in siTKT-transfected UM1cells compared to siCTRL-transfected UM1 cells corresponds with inhibition of cell proliferation by siTKT. In total, both groups had 438 proteins in common (**Figure 2-8**). There were 77 unique proteins identified in siTKT-transfected UM1 cells and 126 unique proteins in siCTRL-transfected UM1 cells (**Table 2-4**). The difference in unique proteins identified in both groups may be due to intrinsic changes introduced by knockdown of TKT or random sampling of peptide ions by MS.

E. Analysis of ^{13}C Labeled Peptide Isotopomers in siTKT and siCTRL UM1 Cells

siTKT-transfected UM1 cells displayed lower expression in abundance and ^{13}C labeling for TKT protein compared to siCTRL-transfected UM1 cells. Similarly, lower ^{13}C labeling expression was also observed in other enzymes involved in glycolysis including triosephosphate isomerase and pyruvate kinase isozyme M1/M2. Enzymes glyceraldehyde 3 phosphate dehydrogenase, enolase (gamma, beta), and phosphoglycerate mutase displayed greater ^{13}C labeling expression in siTKT-transfected UM1 cells compared to siCTRL-transfected UM1 cells. Same ^{13}C labeled peptide isotopomer distribution of glyceraldehyde-3-phosphate dehydrogenase enzyme of glycolysis pathway and cytoplasmic β-actin protein of siTKT-transfected UM1 cells and siCTRL-transfected UM1 cells were compared. Shown in **Figure 2-7**, we identified different

sequences of ^{13}C labeled peptides for the same protein, but mass isotopomer distribution for the same peptide showed no significant difference in precursor ions between siTKT-transfected UM1 cells and siCTRL-transfected UM1 cells. **Figure 2-7A-C** shows the peptide isotopomer distribution of ^{13}C labeled peptide for glyceraldehyde 3-phosphate dehydrogenase in siTKT-transfected UM1 cells and siCTRL-transfected UM1 cells. There were no significant difference in the intensity of isotopic peaks and mass shift of isotopic peaks between siTKT UM1 and siCTRL UM1 cells (**Figure 2-7C**). Three isotopic envelops (mass shift M0, M3, M6) were also observed, a common case seen in peptides with presence of three carbon amino acids, which suggest labeling of cysteine, alanine, or serine. Similarly, highly abundant β-actin protein also showed no significant difference in the intensity of isotopic peaks and mass shift of isotopic peaks between siTKT UM1 and siCTRL UM1 cells (**Figure 2-7D-F**). These findings suggests that carbon flow and carbon integration from [U-$^{13}C_{6]}$-glucose into protein peptides are highly specific and regulated process. The specificity of ^{13}C flow and quantity of ^{13}C labeled proteins may reveal insight about nutrient-gene interaction and metabolic pathways regulating de novo synthesis in cancer cells.

DISCUSSION

Protein expression and relative abundance within individual cells and species are controlled by a variety of factors including transcription, translation, post-translational modification, and degradation [28]. Therefore, protein abundance level alone cannot serve to characterize the activity of various regulatory processes involved. Determination of both the protein synthesis and degradation is required [28]. Measuring protein synthesis through tracers depends on the precursor/product relationship [27]. For example, determination of protein synthesis via radioactive labeled amino acids require determination of the specific activity of the

radioactive amino acid in the cell as well as the specific activity of the same amino acid in the protein of interest [27]. The incorporation of stable isotopes (^{13}C) into amino acids is an alternative method that can be used to determine protein synthesis. The following will discuss attempts by which stable isotope labeling has been used to determine protein synthesis and turnover.

To understand the application of stable isotope labeling and protein synthesis relationship, we must first understand the principles of protein turnover and fractional synthesis rate (FSR). Protein turnover is a ratio expressed by the rate of protein synthesis over the rate of protein degradation. The term is usually expressed as the rate of protein synthesis (in moles/unit time; or weight/unit time) or its half-life (time required to achieve half of the maximum concentration of the protein) [20]. The rate of synthesis/degradation ratio reflects the balance between anabolic and catabolic status within the cell. These dynamic changes in the concentration of cellular proteins and the rate of protein turnover may indicate physiological status of the cell [20]. FSR is the fraction of a new protein at a certain time after the introduction of isotope labeling. It is a key parameter for characterizing protein turnover. FSR value can be estimated from tracer kinetics by first determining the isotope incorporation and isotope content of the amino acid precursor (acyl-tRNA bound) [27-28] via quantifying differences in the relative intensities of the labeled and unlabeled mass spectra [27]. When several FSRs are determined over time, the turnover rate of protein can be precisely calculated.

In principle, measuring protein turnover through stable isotope tracers (^{13}C) relies on the enrichment of ^{13}C in the labeling agent ([U-$^{13}C_6$]-glucose 99%) and the enrichment of ^{13}C in the protein [20]. The ratio of ^{13}C protein enrichment to ^{13}C enrichment of the labeling agent can determine the newly synthesized fraction, which can then be used to calculate protein synthesis

rate (PSR= [protein concentration] x [newly synthesized fraction]/ (unit time)) [20]. Enrichment of ^{13}C into amino acids of peptides will generate a heavier protein molecule than the natural ^{12}C unlabeled protein molecule. The mass difference will depend on the probability of ^{13}C enrichment into amino acids of proteins. In the case of peptides highly enriched with ^{13}C, the mass isotopomer distribution can reveal a larger mass shift than the unlabeled peptide. The differences in mass shifts and peak intensities can then be quantified to reflect the synthesis/degradation ratios that represent the relative protein turnover dynamics in the cell [20, 27, and 30].

Previously, Cargile et al. developed a method to determine protein synthesis without the effort of determining precursor enrichment [20, 27, and 30]. The study introduced [U-$^{13}C_6$]-glucose into bacteria, and ^{12}C was effectively replaced by ^{13}C during the process of protein synthesis [20, 23]. Amino acid synthesis in bacteria achieved >50% enrichment of ^{13}C labeling in newly synthesized amino acids. The intensities of the labeled and unlabeled peaks were quantified to calculate synthesis/degradation ratio to reflect the relative dynamics of protein turnover. This method was a valid approach for studying simple model organisms such as bacteria, because they can synthesize both essential and non-essential amino acids. In multicellular organisms that can only synthesize non-essential amino acids, this approach has limited application [20, 27].

Determining protein synthesis requires labeling on the precursor amino acids (acyl-tRNA bound) and the fraction of the specific proteins that was de novo synthesized during the labeling period [28]. However, ^{13}C labeling via [U-$^{13}C_6$]-glucose can generate complex labeling patterns that are difficult to link labeled pattern to its constituent amino acids [28]. Vogt et al. developed a method to estimate the FSR of de novo synthesized protein based on changes in average mass

of the protein; given that the amino acid sequences and the mass shifts of the peptides are known [27,31]. Plasma apolipoproteins or secretory proteins were proposed for measuring precursor labeling due their systems steady state to maintain constant flux and high turnover rate to achieve near 100% fractional synthesis [28, 32]. The average mass shift from the precursor amino acid (acyl-tRNA bound) can then be linked to the average mass shift of the labeled protein peptides and their fractional synthesis rate [28]. This interrelation in mass shift provided an approach to assess precursor labeling via plasma apolipoproteins or secretory protein (close to 100% FSR) comparison with protein peptide of interest to assess the fractional synthesis of their parent protein [28]. While this technique demonstrated the ability to quantify the relative synthesis rate in complex organisms, accurate estimation of isotope content of the biosynthetic precursor pool (acetyl-tRNA in cells or tissue) remain as an inherent issues that needs to be addressed [28].

Mass isotopomer distribution analysis (MIDA) is approach that can be combined with vogt et al. method for measuring precursor enrichment [25-26]. This technique involves quantifying relative abundance, difference in mass shift and isotopomer distribution of molecular polymers (peptide) via a combinatorial probability model to compare measured abundances (^{13}C-99% labeled peptide) to theoretical (^{12}C unlabeled or natural ^{13}C abundance) distributions predicted from the binomial or multinomial expansion [25-26]. MIDA was previously attempted by Papageorgopoulos et al. to determine protein synthesis in vivo by infusing rat with [5,5,5-$^{2}H_3$] leucine (99%) via the jugular catheter for 24h at a rate of 50 $mg \cdot kg^{-1} \cdot h^{-1}$ using a minipump [20,24]. ESI-MS analysis determined incorporation of [5,5,5-$^{2}H_3$] leucine into protein peptides, which resulted in a mass shift of +3, +6 Da [20, 25-26]. However, low protein turnover rate and low amount of the +3 or +6 isotopomers found, described MIDA to be non-practical for in-*vivo* and low enrichment studies [20, 24-26]; for combinatorial probabilities to be applicable, a

labeled precursor must combine with itself in the form of two or more repeating subunits [20, 25-26].

Our study demonstrated metabolic labeling via [$U^{13}C_6$]-glucose can generate complex peptide isotopomer patterns. This makes it difficult to link labeled peptide patterns to its constituent amino acids. High enrichment of ^{13}C label (99%) into peptides can contribute to high peak intensity in the 2nd isotopic peak (^{13}C), because the natural abundance of ^{13}C in nature is about 1.1%. Protein database search to match respective peptide sequences depends on the isotopic peaks selected for fragmentation into respective 'y' and 'b' ions; usually the highest peak or the monoisotopic peak (1st peak, ^{12}C) are selected for sequencing. In many cases, the 2nd peak is higher than the 1st peak which leads to selection for peptide sequencing via database search (**Figure 2-7D-F)**. Since ^{13}C labeling may be present in any of the peaks within the peptide isotopomer distribution. This complicates the process for determining specific amino acids that are labeled with ^{13}C. To overcome this limitation, fragmentation of all precursor peaks (parent ion) within the peptide isotopomer distribution may allow direct comparison of mass difference in daughter ions ('b' and 'y' ion) for all sequenced/fragmented peaks, and in turn, determine the specific amino acid that is labeled with ^{13}C.

Extreme pathways are mathematically derived vectors that can be used to characterize the phenotypic potential of a defined metabolic network [33-35], which represents the interconversion of metabolites to maintain cellular homeostasis [8]. ^{13}C Stable isotope tracers may distribute into metabolic intermediates in specific carbon positions according to the extreme pathways [8]. The mass isotopomers in labeled metabolites may represent individual extreme pathways from glucose carbon to the respective products [8]. Using [U ^{13}C]-glucose with specific ^{13}C labeled at different position of the glucose molecule (C_1, C_2, C_3, C_4, C_5, C_6), i.e.

[$U^{13}C_1$]-glucose, may allow different mass isotopomer distributions to be constructed. The isotopomer ratios can then be quantified to construct phenotypic phase planes through computational algorithms or isocline analysis to compare the difference between individual phenotypes on different phenotypic phase planes [8, 19, and 36].

Our methods demonstrated ^{13}C labeling of proteins in cancers cells via 2-dimensional gel electrophoresis and in-solution digestion method. Both methods have their pros and cons. 2-dimensional gel method showed useful application for analysis of single or multiple protein spots, but analysis of low abundant proteins is limited. In- solution method allows analysis of all proteins within the cell, but high quantity of protein peptides analyzed by MS generates complex mass spectra and large quantity of peptides may get masked by other peptides, which further complicates downstream analysis processing. Development of a method for studying ^{13}C labeling in a single protein may be a feasible method to overcome the current issues in ^{13}C labeling methods and peptide mass isotopomer analysis. In addition, investigation of ^{13}C labeling through *in-vivo* mouse models may also be of appealing interest to investigate physiological systems interaction with cellular gene interaction during glucose utilization to reveal underlying metabolic mechanisms in cancer cells.

All of these methods previously mentioned are promising means for studying de novo protein synthesis related to cancer cell metabolism. Stable isotope tracers have demonstrated its feasibility to investigate cellular dynamics for protein turnover and nutrient gene interaction. There's no doubt that the current field of metabolomics and cancer biology face many inherent and long standing challenges. Advancement in technology and bioinformatics data processing in the future may serve as valuable assets to reveal the underlying ontology of cancer cells.

CONCLUSION

In this study, we have demonstrated a novel tracer-based methodology to study the utilization of glucose for de novo protein synthesis in UM1 oral cancer cells. UM1 cells demonstrated the ability to consume [U-$^{13}C_6$]-glucose (99%) and incorporate ^{13}C into amino acids of protein peptides. Labeling of protein peptides by ^{13}C generated a difference in mass shift within the mass isotopomer distribution compared to natural ^{12}C unlabeled protein peptides. This difference was also characterized by spike in isotopic envelop peak intensities displaying a +3, +6 Da mass shift from the monoisotopic peak, which suggested potential ^{13}C labeling of a three carbon amino acid such as alanine cysteine, or serine. Many ^{13}C labeled proteins identified in UM1 cells were metabolic enzymes involved in glycolysis. Small interfering RNA knockdown of TKT in UM1 cells displayed differential expression in ^{13}C labeled peptides compared to siCTRL UM1 cells, but mass isotope distribution for the same ^{13}C labeled peptide in siTKT UM1 cells and siCTRL UM1 cells did not display any significant difference in mass shift or the isotopic peak intensities. These finds suggests that the directed flow of ^{13}C into proteins is highly regulated by cancer cells metabolic state. The specificity of carbon flow and the enrichment of ^{13}C into specific non-essential amino acids sequences may reflect nutrient-gene interaction and the metabolic pathways regulating de novo protein synthesis in oral cancer cells. The current method for labeling proteins in cancer cells may find valuable clinical applications when combined with mathematical algorithm of mass isotopomer distribution analysis to determine protein synthesis rate, and to quantify dynamics of protein turnover to reflect the regulation of protein expression and reveal underlying metabolic mechanisms in the cancer cells.

References

1. Jemal A, Bray F, Center MM, Ferlay J, Ward E, Forman D. Global cancer statistics. CA: A Cancer Journal for Clinicians 2011;61: 69-90.

2. Boring CC, Squires TS, Tong T, Montgomery S. Cancer statistics, 1994. CA: A Cancer Journal for Clinicians 1994;44: 7-26.

3. Day GL, Blot WJ. Second primary tumors in patients with oral cancer. Cancer 1992;70: 14-9.

4. Lippman SM, Hong WK. Molecular Markers of the Risk of Oral Cancer. New England Journal of Medicine 2001;344: 1323-6.

5. Park BJ, Chiosea SI, Grandis JR. Molecular changes in the multistage pathogenesis of head and neck cancer. Cancer Biomarkers 2011;9: 325-39.

6. Kim, J.W. and C.V. Dang, *Cancer's molecular sweet tooth and the Warburg effect.* Cancer Res, 2006. 66(18): p. 8927-30.

7. Bensaad, K., et al., *TIGAR, a p53-inducible regulator of glycolysis and apoptosis.* Cell, 2006. 126(1): p. 107-20.

8. Wai-Nang Paul Lee, Laszlo G. Boros and Vay-Liang W. Go (2012). Metabolic Pathways as Targets for Drug Screening, Metabolomics, Dr Ute Roessner (Ed.), ISBN: 978-953-51-0046-1.

9. Boros, L.s.G., M. Cascante, and W.-N. Paul Lee, *Metabolic profiling of cell growth and death in cancer: applications in drug discovery.* Drug Discovery Today, 2002. 7(6): p. 364-372.

10. Wu, A.H., et al., *Soy intake and breast cancer risk in Singapore Chinese Health Study.* Br J Cancer, 2008. 99(1): p. 196-200.

11. Lee, W.N. and V.L. Go, *Nutrient-gene interaction: tracer-based metabolomics.* J Nutr, 2005. 135(12 Suppl): p. 3027S-3032S.

12. Selak, M.A., et al., *Succinate links TCA cycle dysfunction to oncogenesis by inhibiting HIF-alpha prolyl hydroxylase.* Cancer Cell, 2005. 7(1): p. 77-85.

13. Bleeker, F.E., et al., *IDH1 mutations at residue p.R132 (IDH1(R132)) occur frequently in high-grade gliomas but not in other solid tumors.* Hum Mutat, 2009. 30(1): p. 7-11.

14. Bleeker FE, Lamba S, Zanon C, van Tilborg AA, Leenstra S, et al. (2009) Absence of*AKT1* Mutations in Glioblastoma. PLoS ONE 4(5): e5638. doi:10.1371/journal.pone.0005638

15. Yan, H., et al., *IDH1 and IDH2 mutations in gliomas.* N Engl J Med, 2009. 360(8): p. 765-73.

16. Robey, I.F., et al., *Hypoxia-inducible factor-1alpha and the glycolytic phenotype in tumors.* Neoplasia, 2005. 7(4): p. 324-30.

17. Hu, C.J., et al., *Differential roles of hypoxia-inducible factor 1alpha (HIF-1alpha) and HIF-2alpha in hypoxic gene regulation.* Mol Cell Biol, 2003. 23(24): p. 9361-74.

18. Ke, Q. and M. Costa, *Hypoxia-inducible factor-1 (HIF-1).* Mol Pharmacol, 2006. 70(5): p. 1469-80.

19. Paul Lee, W.N., et al., *Tracer-based metabolomics: concepts and practices.* Clin Biochem. 43(16-17): p. 1269-77.

20. Xiao, G.G., et al., *Determination of protein synthesis in vivo using labeling from deuterated water and analysis of MALDI-TOF spectrum.* J Appl Physiol, 2008. 104(3): p. 828-36.

21. Liu, X., et al., *Membrane proteomic analysis of pancreatic cancer cells.* J Biomed Sci. 17: p. 74.

22. Martha Arellano, Roger Li , Xiaojun Liu, Yongmin Xie, Xinmin Yan, Joseph Loo, Shen Hu. Identification of tetranectin as a potential biomarker for metastatic oral cancer. Int J Mol Sci. 2010, 11(9): 3106-21.

23. Cargile BJ, Bundy JL, Grunden AM, Stephenson JL Jr. Synthesis/degradation ratio mass spectrometry for measuring relative dynamic protein turnover. Anal Chem 76: 86–97, 2004.

24. Papageorgopoulos C, Caldwell K, Schweingrubber H, Neese RA, Shackleton CH, Hellerstein M. Measuring synthesis rates of muscle creatine kinase and myosin with stable isotopes and mass spectrometry. Anal Biochem 309: 1–10, 2002.

25. Hellerstein MK, Neese RA. Mass isotopomer distribution analysis at eight years: theoretical, analytic, and experimental considerations. Am J Physiol Endocrinol Metab 276: E1146–E1170, 1999.

26. Papageorgopoulos C, Caldwell K, Shackleton C, Schweingrubber H, Hellerstein MK. Measuring protein synthesis by mass isotopomer distribution analysis (MIDA). Anal Biochem 267: 1–16, 1999.

27. Zhao, Y., et al., *Quantitative proteomics: measuring protein synthesis using 15N amino acid labeling in pancreatic cancer cells.* Anal Chem, 2009. 81(2): p. 764-71.

28. Vogt, J.A., et al., *Determination of fractional synthesis rates of mouse hepatic proteins via metabolic 13C-labeling, MALDI-TOF MS and analysis of relative isotopologue abundances using average masses.* Anal Chem, 2005. 77(7): p. 2034-42.

29. Toffolo, G., D.M. Foster, and C. Cobelli, *Estimation of protein fractional synthetic rate from tracer data.* Am J Physiol, 1993. 264(1 Pt 1): p. E128-35.

30. Cargile, B. J.; Bundy, J. L.; Grunden, A. M.; Stephenson, J. L., Jr. Anal. Chem. 2004, 76, 86–97.

31. Vogt, J. A.; Schroer, K.; Holzer, K.; Hunzinger, C.; Klemm, M.; Biefang- Arndt, K.; Schillo, S.; Cahill, M. A.; Schrattenholz, A.; Matthies, H.; Stegmann, W. Rapid Commun. Mass Spectrom. 2003, 17, 1273–1282.

32. Reeds, P. J.; Hachey, D. L.; Patterson, B. W.; Motil, K. J.; Klein, P. D. J. Nutr. 1992, 122, 457-466.

33. Schilling CH, Schuster S, Palsson BO, Heinrich R. Metabolic pathway analysis: Basic concepts and scientific applications in the post-genomic era. Biotech Prog. 1999;15:296–303.

34. Schilling CH, Letscher D, Palsson BO. Theory for the systemic definition of metabolic pathways and their use in interpreting metabolic function from a pathway-oriented perspective. J Theor Biol. 2000; 203:229–248.

35. Papin, J.A., N.D. Price, and B.O. Palsson, Extreme pathway lengths and reaction participation in genome-scale metabolic networks. Genome Res, 2002. 12(12): p. 1889-900.

36. Edwards JS, Ramakrishna R, Palsson BO. Characterizing the Metabolic Phenotype: a Phenotype Phase Plane Analysis. Biotechnol Bioeng. 2002; 77:27-36.

CHAPTER 3: Development of a Novel ^{13}C Stable Isotope Tracer-Based Methodology for Studying De Novo Protein Synthesis in Pancreatic Cancer Cells: *In-Vitro* Cell Line Model and *In-Vivo* Xenograft Mouse Model

INTRODUCTION

Pancreatic cancer is a malignant neoplasm of the pancreas. Each year in the US, more than 40,000 individuals are diagnosed with pancreatic cancer (PC), and approximately 35,000 die from the disease [1]. Exocrine pancreatic cancers are more common than endocrine pancreatic cancers (islet cell carcinomas), which make up about 1% of total cases [2]. About 95% of exocrine pancreatic cancers are adenocarcinoma. The remaining 5% include adenosquamous carcinomas, squamous cell carcinomas, and giant cell carcinomas [1,2]. Potential risk factors for PC include cigarette smoking, obesity, aging, family history, and long-term inflammation of the pancreas (pancreatitis). Diet habit has also been linked to PC and the disease is more common in men than in women. Patients diagnosed with PC typically have poor prognosis mainly due to lack of symptoms early on, resulting in locally advanced or metastatic disease at time of diagnosis [3]. The median survival from diagnosis is around 3 to 6 months, and the 5-year survival is less than 5% [2]. PC is one of the few cancers for which survival rate has not improved substantially over the past 30 years. As a result, in 2003, PC surpassed prostate cancer as the 4th leading cause of cancer-related death in the US [4, 5]. Scientific understanding of PC in terms of its etiology, pathogenesis, detection, and treatment, lags far behind that of most other forms of cancer. Therefore, development of new tools to study PCs at the molecular level may elucidate better diagnostic and therapeutic interventions to target PC. It is an immediate task that needs to be addressed.

It is known that metabolic regulation represents an important component to cellular growth machinery in tumor cells. Many metabolic enzymes can directly contribute to carcinogenesis. For instance, germline mutations in the TCA cycle enzymes succinate dehydrogenase and fumarate hydratase have been identified in many forms of human cancers [6, 7]. One effect of this mutation is activation of HIF1α-mediated glucose utilization pathway [26]. Monoallelic mutation of the gene encoding for cytosolic isocitrate dehydrogenase–1 (IDH1) or (IDH2) is a common feature of more than 80% of gliomas [8, 9]. These two metabolic enzymes couple the inter-conversion of cytosolic isocitrate and α-ketoglutarate in an $NADP^+$/NADPH-dependent reaction. The ability to dynamically model truncated TCA cycle may yield valuable knowledge about metabolic regulation for uncontrolled growth in cancer cells, and allows for direct comparison of *in-vitro* cell line models with *in-vivo* mouse models. Therefore, developing a tracer-based metabolomics approach to study protein synthesis can have wide array of applications to enhance understanding of the metabolic regulations in cancer cells.

The purpose of this study aims to develop a novel ^{13}C stable isotope tracer-based methodology for studying de novo protein synthesis in PDAC cells. We predict that the metabolic phenotype of PDAC cells as characterized by enhanced glucose utilization for macromolecular synthesis is progressively altered during pancreatic oncogenesis, and that transformation of ^{13}C labeled glucose into non-essential amino acids of proteins would reflect this metabolic adaptation in PDAC cells. We also predict that the conversion of glucose to non-essential amino acids is a relatively rapid process, while synthesis of protein is a slow process occurring in hours (there are two metabolic phenotypes – one for the function of the TCA cycle and the other for protein synthesis). In this study, we have employed [U-$^{13}C_6$]-glucose, *in-vitro* (cell line model) and *in-vivo* (xenograft mouse model), to investigate the fundamental changes in

peptide isotopomers and compare the difference in ^{13}C labeled protein of pancreatic ductal adenocarcinoma (PDAC) cells, human pancreatic ductal epithelial (HPDE) cells, and mouse PDAC tumor tissues. The significance of the study aims to reveal differences in ^{13}C labeling between pancreatic cancer cells and normal cells, and in turn, may lead to new diagnostic and therapeutic interventions for pancreatic cancer.

MATERIALS AND METHODS

A. Cell Culture:

Pancreatic ductal adenocarcinoma cell lines BxPC-3 and MIA PaCa-2 were obtained from American Tissue Culture Collection (ATTCC, Rockville, MD), and were respectively cultured in glucose free RPMI 1640 (ATCC) or glucose free DMEM (GIBCO) supplemented with 4.5g/L [U-$^{13}C_{6,}$ 99%] D-glucose (Cambridage Isotope Laboratories, Inc.), 10% fetal bovine serum, 100units/mL penicillin and 100µg/mL streptomycin. Immortalized HPDE cell line was kindly provided by Dr. Stephen Pandol (Veteran's Administration Medical Center, Los Angeles, CA), the cells were cultured with glucose free, keratinocyte serum-free media supplemented with [U$^{13}C_6$]-glucose, epidermal growth factor, bovine pituitary extract (Life Technologies, Inc., Grand Island, NY), 100units/ml penicillin and 100µg/mL streptomycin. All cells were maintained at conditions of 5% CO2-95% O_2 and 37°C. Fresh [U$^{13}C_6$]-glucose was replaced every 24 hours and cells were harvested at 80-90% confluence. Cells were washed with PBS three times prior to administering cell lysis (RB buffer) containing 62.5 mM Tris-HCL (pH=6.8), 2% SDS (w/v), 10% Glycerol and 0.2 mM DTT.

B. Mouse Xenograft Model:

Mice studies were approved by the Chancellor's Animal Research Committee of the University of California, Los Angeles, in accordance with the National Institutes of Health's Guide for the Care and Use of Laboratory. Twelve mice were housed with controlled temperature at 20°C–22°C. Mouse xenograft model was prepared by subcutaneous injection of $3x10^6$ MIA PaCa-2 cells into the pancreas. Six mice were administered $[U^{13}C_6]$-glucose via transplanted osmotic pump (Alzet) to the pancreas of MIA PaCa-2 tumor region for 24 hours. Six control mice were administered D-glucose via transplanted pump to the pancreas MIA PaCa-2 tumor region for 24 hours as well. Afterwards, all xenograft mice were anesthetized and pancreatic tumor tissue was surgically removed. Tissue protein sample was prepared using tissue lysis buffer containing 50mM Tris-HCl pH 7.4, 150mM NaCl, 1mM EDTA, 1% Triton X-100, 0.1% SDS, 1% Sodium deozycholate and 1mM PMSF. The tissues were rigorously homogenized, vortexed, and centrifuged (27000g). The remaining supernatant was finally collected for subsequent experiments.

C. Sample Preparation

Protein samples from BxPC-3, MIA PaCa-2, HPDE cell lines and MIA PaCa-2 mouse tumor tissues were precipitated with cold acetone (9:1 acetone: sample volume) and stored in -20°C freezer for 24 hours. Precipitated proteins were centrifuged at 4°C and 16,000g for 15 min. The above-mentioned steps were then repeated twice, and cold acetone was carefully removed. Afterwards, the precipitated protein pellet was re-suspended in RB buffer, and 1% Ampholyte (Bio-Lyte 3/10, Bio-Rad) was added to 100µg of protein and vortex for 30s prior to loading sample onto PROTEAN IEF focusing tray (PROTEAN IEF Cell System, Bio-Rad) for active rehydration via immobilized pH gradient (IPG) strip (Ready Strip, Bio-Rad).

D. 2-Dimensional Gel Electrophoresis

Cellular proteins of BxPC-3, MIA PaCa-2, HPDE cell lines and MIA PaCa-2 mouse tumor tissues were mapped out using 2-dimensional electrophoresis, with isoelectric focusing (IEF) in the first-dimension of separation and SDS-PAGE in the second-dimension of separation. Bio-Lyte 3/10 1% Ampholyte (Bio-Rad) was added to 100µg of each BxPC-3, MIA PaCa-2, HPDE cell line and MIA PaCa-2 mouse tumor tissue proteins and vortex for 30s prior to loading onto PROTEAN IEF focusing tray. IPG gel strips were laid onto the protein samples and mineral oil (Bio-Rad) was added to IEF focusing tray for active rehydration for 16 h at 50V. Hydrated IPG Strips were then transferred to a new IEF focusing tray and samples were run under the following IEF program setting: 250 V (linear), 1 h; 500 V (rapid), 2 h; 3,000 V (linear), 1 h; 3,000 V (rapid), 3h; 8,000 V (linear), 3 h; 8,000 V (rapid), 10 h; and 250 V (rapid), 99 h. IPG strips were then transferred to a new tray and incubated with 2% DTT and 2.5% iodoacetic acid solutions separately at room temperature for 10 min each. Prior to second-dimension protein separation by 7.5% Criterion TGX precast gel (Bio-Rad), IPG strips were briefly washed with 1x TGS running buffer. 7.5% Criterion TGX precast gels were run at 200V for 50 min in Criterion Dodeca Cell (Bio-Rad). Finally 7.5% Criterion TGX precast gels were washed with fix/destain (7% acetic acid–10% methanol) solution prior to and after fluorescent Sypro-Ruby staining (Molecular Probes) to visualize the protein spots. Bio-Rad GS 800 imager and PDQuest program were used scan the stained Criterion gels, and gel images were analyzed using Progenesis SameSpot software (Nonlinear dynamics). A matched set of stained proteins were created for [U-$^{13}C_6$] D-glucose (99%) treated BxPC-3, MIA PaCa-2, HPDE cell lines and MIA PaCa-2 xenograft mouse tumor tissues, and DMEM treated control BxPC-3, MIA PaCa-2, HPDE cell lines and MIA PaCa-2 xenograft mouse tumor tissues. Afterwards, matched gel spots were

exercised using ProPic II Spot Cutter (DIGILAB Genomics Solutions), and spots were collected into 96 well plates for in-gel tryptic digestion.

E. In-Gel Trypsin Digestion

Protein spots of interest were repeatedly washed and dried with 50 mM NH_4HCO_3 50% CH_3CN solution and 100% CH_3CN solution. To reduce protein disulfide bonds, protein gel spots were incubated in 10 mM dithiothreitol (DTT) for 1 hour. The supernatant was discarded and 50 mM iodoacetic acid (IAA) alkylating agent was added to protein gel spots and incubated for 1 hour in the dark to prevent re-formation of disulfide bonds. Protein gel spots were digested with 10-ng/µL enzyme-grade trypsin (Promega, Madison, WI) in 100 mM NH_4HCO_3 at 37°C incubation for 24 hours. After proteolytic cleavage, all samples were dried and re-constituted with 5% acetonitrile/ 0.1% formic acid (v/v) for subsequent LC-MS/MS analysis.

F. LC-MS/MS and Database Search

Liquid Chromatography (LC) with tandem MS (LC-MS/MS) of peptides was performed using an Eksigent NanoLC-2D HPLC system with Thermo LTQ Orbitrap XL Mass Spectrometer. Aliquots (5µL) of peptide digest derived from each gel spots were injected using an auto-sampler at a flow rate of 3.5µL/min. The peptides were concentrated and desalted on a C_{18} Integral Frit Nano-Precolumn (New Objective, Woburn, MA) for 10 min, then eluted resolved using a C_{18} reversed- phase capillary column (New Objective). LC separation was performed at 400nL/min with the following mobile phases: A, 5% acetonitrile/0.1% formic acid (v/v); B, 95% acetonitrile/0.1% formic acid (v/v). The chosen LC gradient was: from 5% to 15% B in 1 min, from 15% to 100% B in 40 min, and then maintained at 100% B for 15 min [10]. The eluent was introduced directly into the LTQ mass spectrometer via electrospray using a PicoTip emitter (tip inner diameter, 10 µm). Each full MS scan was followed by 5 data-

dependent MS/MS scans on the most intense ions at 35% normalized collision energy. Database search was performed using Mascot database search engine against the SwissProt protein sequence database. The search criteria were set with a mass tolerance of 0.5 Da for precursor and product ions, semi-style cleavage by trypsin and one missed tryptic cleavage were allowed. Varied modification accounted for cysteine carbamidomethylation, methionine oxidation, and serine, threonine, tyrosine phosphorylation. The MS/MS spectra for each peptide were manually examined to verify the identification [11].

G. Data Analysis of ^{13}C Incorporated Peptides

Xcalibur 2.1 software (Thermo Scientific) was used to manually examine the MS/MS spectra of ^{13}C incorporated peptides within 300-1600 m/z range. Peptide fragment ions, 'b' ions and 'y' ions were matched against SwissProt protein sequence database to identify the incorporated ^{13}C mass difference corresponding to ^{13}C labeled amino acid. Database for Annotation Visualization and Integrated Discovery (DAVID) software v6.7 was performed for functional annotation and classification of ^{13}C labeled proteins and their unique labeled peptides.

RESULTS

A. Identification of ^{13}C Labeling in Human Pancreatic Duct Epithelial Cells and Pancreatic Adenocarcinoma Cells

The purpose of this study was to develop a novel ^{13}C stable isotope tracer-based methodology to study de novo protein synthesis in PDAC cells and HPDE cells through *in-vitro* and *in-vivo* models to determine difference in ^{13}C labeled proteins. Two PDAC cell lines, BxPC-3 and MIA PaCa-2, were used in this study for comparison with immortalized HPDE cell line. BxPC-3 is a primary PDAC cell line from a 62 year- old Caucasian female, whereas MIA PaCa-2 is a primary PDAC cell line from a 65 year-old Caucasian male. All cells were cultured in

4.5g/L [U-$^{13}C_6$]-glucose (99%) for 5 days. Cellular proteins were lysed and separated by 2-dimensional gel electrophoresis based on charge and size. Protein spots were stained, exercised, trypsin digested, and analyzed with LC-MS/MS and database search. Mass spectrums of ^{13}C labeled protein peptides for HPDE cells were compared with ^{13}C labeled protein peptides of PDAC cells [12-14]. In total, we identified 39 ^{13}C labeled proteins for BxPC-3 (2,631 ^{13}C labeled peptides), 70 ^{13}C labeled proteins for MIA PaCa-2 (2,945 ^{13}C labeled peptides), and 60 ^{13}C labeled proteins for HPDE (2,241 ^{13}C labeled peptides) based on at least 2 unique peptide match (**Tables 3-1, 3-2, 3-3**). On average, ^{13}C labeled proteins accounted for ~ 7% relative to the total number of unlabeled proteins identified for all three cell lines. The greater abundance of ^{13}C labeled peptides in PDAC cells compared to HPDE cells suggests that PDAC cells may direct [U-$^{13}C_6$]-glucose for do novo synthesis at a faster rate than HPDE cells for cell proliferation. In addition, the low percentage of ^{13}C labeling yield relative to all unlabeled proteins identified reflects the precise and regulated synthesis of end products from [U-$^{13}C_6$]-glucose, which can serve as a direct indicator for determining ratio of protein synthesis to degradation in the cells.

B. Analysis of ^{13}C Labeled Peptide Isotopomers in Human Pancreatic Duct Epithelial Cells and Pancreatic Adenocarcinoma Cells

The mass spectra of multiple ^{13}C labeled protein peptides for BxPC-3 are shown in **Figure 3-1**. ^{13}C labeled peptide isotopomer distribution displayed extended decay pattern with each isotopic peak shifted by 1 Da apart. We observed a rapid decay pattern tailing the monoisotopic peak in the natural ^{12}C unlabeled peptide isotopomer distribution. In **Figure 3-1C**, we observed ^{13}C labeling in peptide sequence SDLGPSYGGWQVLDATPQER of enzyme glutamine gamma-glutamyl transferase. ^{13}C labeling of this peptide is represented by a gradual decay pattern represented by 16 isotopic peaks (m/z=1088.50) with Δm/z of ~8 (total mass shift

~16Da). The extended labeling pattern suggests correlation with the probability of ^{13}C enrichment into amino acid because longer peptides may incorporate more ^{13}C. In **Figure 3-1C&D**, the M1 peak of tranketolase (m/z=943.47) and glutamine gamma-glutamyltransferase (m/z=1089.00) displayed greater peak intensity than M0's peak intensity. This indicates high level of ^{13}C labeling for these peptides since M1 peak reflects the relative abundance of ^{13}C isotope (2^{nd} isotope) present in the peptide.

^{13}C labeled peptides are generally noted by isotopic envelops. This is shown in **Figure 3-2A**, spike in the isotopic peak intensities were observed at the M3, M6, and M9 peak from the M0 peak to reflect 4 envelop pattern for peptide sequence GALQNIIPASTGAAK of glyceraldehyde 3-phosphate dehydrogenase enzyme in HPDE cells. The $\Delta m/z$ difference from the M0 peak to the M3 peak is 1.5, which represents 3 Da mass shifts. Consistent mass shift was also observed in the M3-M6 and M6-M9 isotopic peaks. The 3 Da mass shifts suggest potential labeling of a three carbon amino acid such as alanine or serine.

Relative all ^{13}C labeled peptides identified, ^{13}C peptide labeling frequency analysis showed 89% of ^{13}C labeled peptides occurred in cytoskeletal keratins of BxPC-3, whereas 60% in HPDE, 45% in MIAPaCa-2, and 67% in MIAPaCa-2 in xenograft mouse tumor tissues (**Figure 3-4**). Cytoskeletal keratin is an abundant intermediate filament forming proteins of epithelial cells and changes in keratin expression have been indicated in the involvement of cancer cell invasion and metastasis [15-16]. Interestingly, Both BxPC-3 and MIA PaCa-2 cells exhibited relatively greater frequency of ^{13}C labeled peptide for β-tubulin protein compared to HPDE cells. β-tubulin protein is a important component of microtubules/mitotic spindles in multiple cell types, upregulated expression of β-tubulin has been associated many types of breast and pancreatic cancers [17, 27]. Large quantities of ^{13}C labeled peptides for vimentin

protein were observed in MIA PaCa-2 cells and MIAPaCa-2 xenograft mouse tumor tissue. Vimentin is an abundant intermediate filament protein overexpressed in various epithelial cancer cells and was recognized as a marker for epithelial-mesenchymal transition [18]. **Figure 3-2C** illustrates high frequency of ^{13}C labeled peptides observed in MS1 spectra from m/z range 500-600. We notice multiple ^{13}C labeled peptides encoding for structural proteins including cytoskeletal keratin, vimentin, and β-actin in MIA PaCa-2 cells. This finding suggests that vimentin protein may potentially serve as a unique ^{13}C labeling signature to distinguish MIA PaCa-2 from HPDE cells.

C. Identification of ^{13}C Labeling in MIA PaCa-2 Xenograft Mouse Tumor Tissue

Xenograft mouse PDAC tumor was transplanted by injection of MIA PaCa-2 cell line into mouse pancreas. [U-$^{13}C_6$]-glucose (99%) was pumped to tumor site via transplanted pump for 24 hours at constant flow. Mouse tumor tissues were dissected and tissue proteins were lysed. Cellular proteins were separated by 2-dimensional gel electrophoresis based on charge and size. Protein spots were stained, exercised, trypsin digested, and analyzed with LC-MS/MS and database search. Mass spectrums of ^{13}C labeled protein peptides were compared with control ^{12}C unlabeled protein peptides. In total, we identified 20 potential ^{13}C labeled proteins (571 peptides) with 2 unique peptides match from mouse tumor tissue (**Table 3-4**). ^{13}C labeled protein accounted for ~1%-2% in comparison with total identified (unlabeled and labeled) proteins. Poor sensitivity of ^{13}C labeling presented uncertainty in determination of ^{13}C labeled peptides. This in part, may be due to short [U-$^{13}C_6$]-glucose (99%) infusion time into MIA PaCa-2 cells for protein turnover, or reduced purity of MIA PaCa-2 cells due to presence of adjacent cells in the mouse pancreas. In addition, numerous precursor peaks were excluded from database search due

to complexity in ^{13}C peptide isotopomer distribution and further limited matching labeled MS spectrum with the correct peptide sequence for comparison.

D. Analysis of ^{13}C Labeled Peptide Isotopomers in MIA PaCa-2 Xenograft Mouse Tumor Tissue

MS spectrum of ^{13}C labeled MIA PaCa-2 xenograft mouse tumor tissue is shown in **Figure 3-3**. In comparison with ^{13}C labeled PDAC cell lines, mouse tissue presented rapid decay in isotope peak abundance that resembles natural ^{12}C unlabeled peptide isotopomer distribution, which may suggests poor ^{13}C enrichment compared to cell lines (**Figure 3-3)**. However numerous potential ^{13}C labeled peptides did not match monoisotopic precursor (1^{st} isotopic peak) to database search since mass shift complicated automated MS detection to select the correct monoisotopic peak for fragmentation. Therefore, manual inclusion parameters to fragment all isotope peaks (M_0, M_1, M_2, M_3, M_4, M_5…) within a ^{13}C labeled peptide may be necessary to help overcome the limitation for determining specific position of amino acids that are labeled with ^{13}C.

E. ^{13}C Labeled Proteins and Related Pathways in in Human Pancreatic Duct Epithelial Cells and Pancreatic Adenocarcinoma Cells

^{13}C labeled proteins with single matched peptide were analyzed with Database for Annotation, Visualization and Integrated Discovery (DAVID) v6.7 according to UNIGENE protein code that was converted from UniProtKB/Swiss-Prot protein accession number (**Tables 3-5, 3-6, 3-7, 3-8**). ^{13}C labeled proteins in HPDE, BxPC-3 and MIA PaCa-2 cells were categorized based on their related cellular pathways (**Tables 3-9, 3-10, 3-11, 3-12**). Our finding indicated many ^{13}C labeled enzymes involved in glycolysis, p53 signaling, and spliceosome pathways.

DISCUSSION

Cancer cells can reprogram their metabolic pathways in favor of aerobic glycolysis for selective growth advantages. Many modulators such as p53, Myc, Ras, and HIF-1 can play a key role in this process. For example, Ras signaling can increase glycolytic flux into lactate [19] and p53 can stimulate glycolysis by transcriptional activation of hexokinase II [20]. When glucose enters glycolysis, it gets converted into pyruvate. Pyruvate and other α-keto acid substrates of TCA cycle such as oxaloacetate and α-ketoglutarate can serve critical importance in the synthesis of non-essential amino acids via transamination reaction. Non-essential amino acids are the building block for protein synthesis, which includes alanine, aspartate, cysteine, glutamate, glycine, proline, serine, and tyrosine [21]. For example, alanine is an α-amino acid analog of pyruvate, catalyzed by aminotransferase via transamination reaction [22]. The mechanism of this reaction occurs by transferring the amino group from glutamate onto pyruvate to form alanine and α-ketoglutarate. Since alanine can be synthesized from break down of glucose through glycolysis in a single step transamination reaction, synthesis of alanine can occur in a rapid process. Rapid synthesis of alanine may corroborate with ^{13}C labeling pattern observed by 3 Da mass shift in the isotopic envelops of the isotopomer distribution due to alanine's three carbon molecular compositions (**Figure 3-2A**).

Differential expression of ^{13}C labeled protein for vimentin observed in MIA PaCa-2 compared to HPDE confirms metabolic differences in glucose directed synthesis. Vimentin overexpression has been linked with accelerated tumor growth and invasion. It was also recognized to induce cell shape, motility, and adhesion during epithelial–mesenchymal transition [18, 23]. The increased ^{13}C labeling for vimentin in MIA PaCa-2 in comparison with HPDE also correlates with the adherent, loosely attached clustering phenotype observed in MIA PaCa-2 cell

culture. Cytoskeletal keratins are highly abundance intermediate filament proteins of mammalian epithelia cells. Keratin has been recognized in cancers to regulate many cellular properties and functions, including apico-basal polarization, motility, cell size, protein synthesis, membrane trafficking, and membrane signaling [16]. The high frequency of ^{13}C labeled keratin protein observed in BxPC-3 was multi-fold greater in comparison with HPDE and MIA PaCa-2 (**Tables 3-1, 3-2, 3-3**). This finding may suggest that cytoskeletal keratin synthesis may be a primary modes by which end products of [U-$^{13}C_6$]-glucose are directed to; reflecting the distinctive metabolic state and physiological phenotype of BxPC-3 cells.

Previously, Wykes et al. infused pigs with [U-^{13}C]-glucose and observed a significant labeling in those amino acids in close exchange with the keto acids of the Krebs cycle [24,25]. We followed this study by infusing mouse pancreas with [U-13C_6]-glucose. In theory, we would expect high degree of ^{13}C labeling in amino acids connected to glucose metabolism [24]. However we achieved relatively low yield in ^{13}C labeled protein from mouse study following 24 hour infusion time. This may be partly due short infusion time, since we achieved less than 10% relative yield of ^{13}C labeled proteins in cell lines cultured with [U-13C_6]-glucose for 5 days. Repression by endogenous glucose and perfusion of [U-13C_6]-glucose into circulation may have contributed to the low labeling yield in mouse tumor tissue. Infusing higher concentration of [U-13C_6]-glucose and longer infusion time of weeks may be a valid experimental design for mouse model investigation.

Consistent with previous study, we demonstrated that metabolic labeling via [U$^{13}C_6$]-glucose can generate complex labeling patterns in ^{13}C labeled peptides. This makes it difficult to link labeled peptide patterns to its constituent amino acids. High enrichment of ^{13}C was prominently represented in raw data spectra by extended decay mass isotopomer distributions.

High enrichment of ^{13}C label (99%) contributed to a relatively high abundance in the 2nd isotopic peak (^{13}C), because the natural abundance of ^{13}C in nature is about 1.1%. Protein database search to match protein peptide sequences depends on the isotopic peaks selected for fragmentation into respective 'y' and 'b' ions; usually the highest peak or the monoisotopic peak (M0, ^{12}C) is selected for sequence match. When there is high enrichment of ^{13}C labeling in the peptide, the 2nd isotopic peak may often present relatively greater intensity than the peak intensity of natural ^{13}C (1.1% abundance in nature). In many cases, the 2nd peak (^{13}C) may displays higher intensity than the 1st peak (^{12}C), and can get selected for peptide sequencing via database search instead of the monoisotopic peak. In addition, due to high ^{13}C enriched labeling (99%) used for this study, all peaks within the peptide isotopomer distribution may contain ^{13}C labeling, particularly in the presence of multiple isotopic envelops that are labeled. Since ^{13}C labeling may be present in any of the peaks within a peptide mass distribution, this complicates the process for determining specific amino acid that are ^{13}C labeled based only on monoisotopic fragmentation analysis. To overcome this limitation, fragmentation of all precursor peaks (parent ion) within the peptide mass distribution would allow direct comparison of mass difference in daughter ions ('b' and 'y' ion) of all sequenced/fragmented peaks, and in turn, may be a valid approach to determine the specific amino acid that is labeled with ^{13}C.

Our methods demonstrated ^{13}C labeling of proteins in cancers cells via 2-dimensional gel electrophoresis and LC-MS. 2-dimensional gel electrophoresis method showed useful application for analysis of single or multiple protein spots, but face limitations in low abundant proteins analysis. Development of a method for studying ^{13}C labeling of single protein may be a feasible method to overcome the current issues in ^{13}C labeling and peptide mass isotopomer analysis.

In this study, stable isotope tracers have demonstrated its feasibility to investigate cellular dynamics for protein turnover and nutrient-gene interaction. But current application is limited by high cost of stable isotope tracers and relatively low sensitivity of ^{13}C. For example, to study gluconeogenesis from lactate, an amount in excess of 10g of [U-^{13}C]-lactate would be required for a mature person [24]. There is no doubt that the current field of metabolomics and cancer biology face many inherent and long standing challenges. Advancement in technology and bioinformatics data processing in the future may serve as valuable assets to reveal the underlying ontology of cancer cells.

CONCLUSION

In this study, we have demonstrated a novel tracer-based methodology to study the utilization of glucose for de novo protein synthesis in HPDE and PDAC cells through *in-vitro* cell line and *in-vivo* xengraft mouse models. Both HPDE and PDAC cells demonstrated incorporation of ^{13}C into amino acids of protein peptides. Labeling of protein peptide by ^{13}C generated a greater mass shift difference in the mass isotopomer distribution compared to natural ^{12}C unlabeled peptides. Mass isotopomer patterns displayed multiple isotopic envelops with relatively high peak intensities tailing the highest monoisotopic peak. Extended isotopic distribution correlated with longer peptide sequences which suggested greater probability of ^{13}C enrichment into amino acid sequences. Differential expression of ^{13}C labeled peptides was observed among all cells in this study. We observed relatively high frequency of ^{13}C labeled peptides encoding vimentin protein in MIA PaCa-2 cells and in MIA PaCa-2 xenograft mouse tumor tissue. β-tubulin protein was highly labeled only in PDAC cells. Cytoskeletal keratin was the most abundantly labeled protein among all cell lines, with BxPC-3 displaying multi-fold greater frequency of ^{13}C peptide labeling in comparison with HPDE and MIA PaCa-2 cells.

These finds suggests that the directed flow of ^{13}C into proteins is a highly regulated process dependent of cancer cells metabolic state. The specificity of carbon flow and the enrichment of ^{13}C into specific non-essential amino acids sequences may reflect nutrient-gene interaction and the metabolic pathways regulating de novo synthesis in cancer cells. The current method for tracing protein synthesis in cancer cells, combined with mathematical algorithm of mass isotopomer distribution analysis, may serve as a valuable technology to quantify protein synthesis rate and dynamics of protein turnover to reflect the differences in regulation of protein expression. Thus, revealing the reprogrammed metabolic mechanisms for oncogenesis.

References

1. National Cancer Institute (2013). http://www.cancer.gov/cancertopics/types/pancreatic.

2. Yao JC, Eisner MP, Leary C, et al. Population-based study of islet cell carcinoma . Annals of Surgical Oncology. 2007; 14: 3492–3500.

3. Amado, R.G., et al., *Low-dose trimetrexate glucuronate and protracted 5-fluorouracil infusion in previously untreated patients with advanced pancreatic cancer.* Ann Oncol, 2002. 13(4): p. 582-8.

4. Eibl G, Reber HA, Hines OJ, Go VL. COX and PPAR: possible interactions in pancreatic cancer Pancreas, 2004; 29(4): 247-53.

5. Eibl Guido, Reber Howard A, Hines Oscar J, Go Vay L W COX and PPAR: possible interactions in pancreatic cancer. Pancreas, 2004; 29(4): 247-53.

6. Baysal, B.E., et al., *Mutations in SDHD, a mitochondrial complex II gene, in hereditary paraganglioma.* Science, 2000. 287(5454): p. 848-51.

7. Pollard, P.J., N.C. Wortham, and I.P. Tomlinson, *The TCA cycle and tumorigenesis: the examples of fumarate hydratase and succinate dehydrogenase.* Ann Med, 2003. 35(8): p. 632-9.

8. Bleeker, F.E., et al., *IDH1 mutations at residue p.R132 (IDH1(R132)) occur frequently in high-grade gliomas but not in other solid tumors.* Hum Mutat, 2009. 30(1): p. 7-11.

9. Yan, H., et al., *IDH1 and IDH2 mutations in gliomas.* N Engl J Med, 2009. 360(8): p. 765-73.

10. Liu, X., et al., *Membrane proteomic analysis of pancreatic cancer cells.* J Biomed Sci. 17: p. 74.

11. Arellano-Garcia, M.E., et al., *Identification of tetranectin as a potential biomarker for metastatic oral cancer.* Int J Mol Sci. 11(9): p. 3106-21.

12. Tan MH, Nowak NJ, Loor R, Ochi H, Sandberg AA, Lopez C, Pickren JW, Berjian R, Douglass HO Jr, Chu TM: Characterization of a new primary human pancreatic tumor line. Cancer Invest 1986, 4(1):15-23.

13. Tan M, Chu T: Characterization of the tumorigenic and metastatic properties of a human pancreatic tumor cell line (AsPC-1) implanted orthotopically into nude mice. Tumour Biol 1985, 6(1):89-98.

14. Deer EL, González-Hernández J, Coursen JD, Shea JE, Ngatia J, Scaife CL, Firpo MA, Mulvihill SJ: Phenotype and genotype of pancreatic cancer cell lines. Pancreas 2010, 39(4):425-35.

15. Joosse, S.A., et al., *Changes in keratin expression during metastatic progression of breast cancer: impact on the detection of circulating tumor cells.* Clin Cancer Res. 18(4): p. 993-1003.

16. Karantza, V., *Keratins in health and cancer: more than mere epithelial cell markers.* Oncogene. 30(2): p. 127-38.

17. Lee K, Cao D, Itami A, Pour P, Hruban R, Maitra A, Ouellette M (2007) Class III beta-tubulin, a marker of resistance to paclitaxel, is overexpressed in pancreatic ductal adenocarcinoma and intraepithelial neoplasia. Histopathology 51:539–546.

18. Satelli, A. and S. Li, *Vimentin in cancer and its potential as a molecular target for cancer therapy.* Cell Mol Life Sci. 68(18): p. 3033-46.

19. Chesney, J. and S. Telang, *Regulation of glycolytic and mitochondrial metabolism by ras.* Curr Pharm Biotechnol. 14(3): p. 251-60.

20. Maddocks, O.D. and K.H. Vousden, *Metabolic regulation by p53.* J Mol Med (Berl). 89(3): p. 237-45.

21. Smolke, C.D., The Metabolic Pathway Engineering Handbook: Tools and Applications. 2009, CRC Press. p. 1259.

22. Miles, B. (April 21, 2003) Biosynthesis of Amino Acids.

23. Mendez, M.G., S. Kojima, and R.D. Goldman, *Vimentin induces changes in cell shape, motility, and adhesion during the epithelial to mesenchymal transition.* FASEB J. 24(6): p. 1838-51.

24. Vogt, J.A., et al., *Determination of fractional synthesis rates of mouse hepatic proteins via metabolic 13C-labeling, MALDI-TOF MS and analysis of relative isotopologue abundances using average masses.* Anal Chem, 2005. 77(7): p. 2034-42.

25. Wykes, L. J.; Jahoor, F.; Reeds, P. J. Am. J. Physiol. 1998, 274, E365-E376.

26. Selak, M.A., et al., *Succinate links TCA cycle dysfunction to oncogenesis by inhibiting HIF-alpha prolyl hydroxylase.* Cancer Cell, 2005. 7(1): p. 77-85.

27. Eeva-Mari Jouhilahti., Sirkku Peltonen., Juha Peltonen. *Class III beta-tubulin is a component of the mitotic spindle in multiple cell types.*Journal of Histochemistry and Cytochemistry 10/2008; 56(12):1113-9.

FIGURES

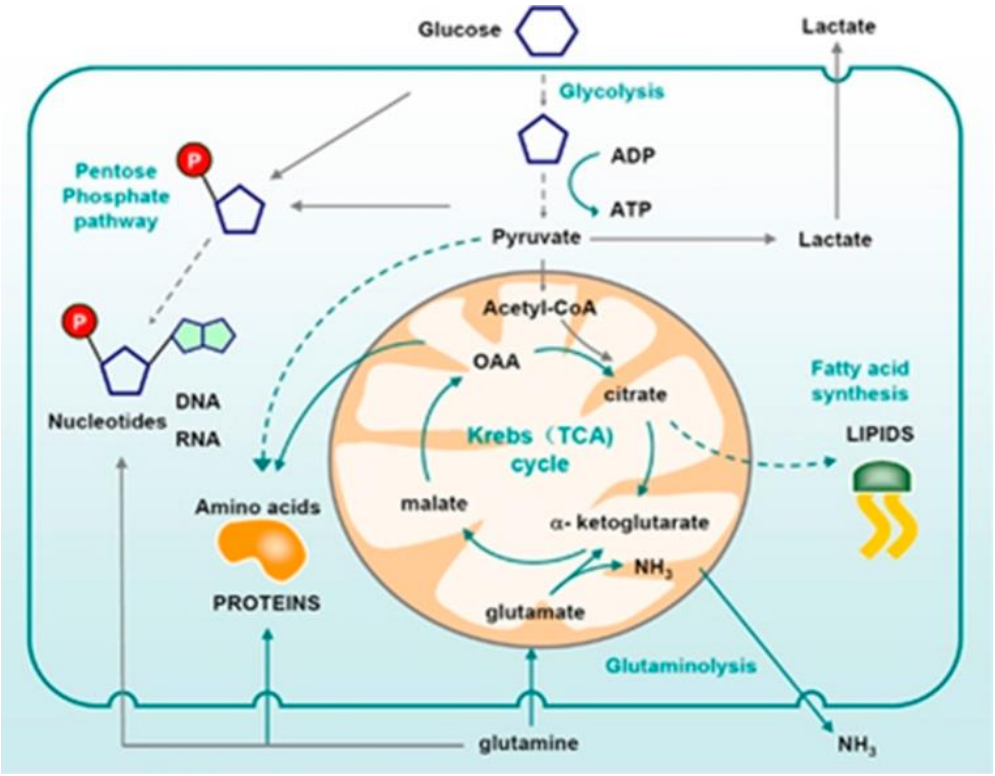

*Figures adopted from Munoz-Pinedo et al., 2012.

Figure 1. A schematic diagram of metabolism of proliferating cells. The diagram illustrates the paths by which glucose can be broken down and utilized by the cell. Glucose can take path through glycolysis to produce pyruvate. Pyruvate contributes to lactate production and non-essential amino acids synthesis. Pyruvate can enter the Krebs cycle via acetyl-CoA. Intermediates of the Krebs cycle can further contribute to fatty acid synthesis and non-essential amino acid synthesis. Glucose can take path through pentose phosphate pathway to synthesis nucleotides.

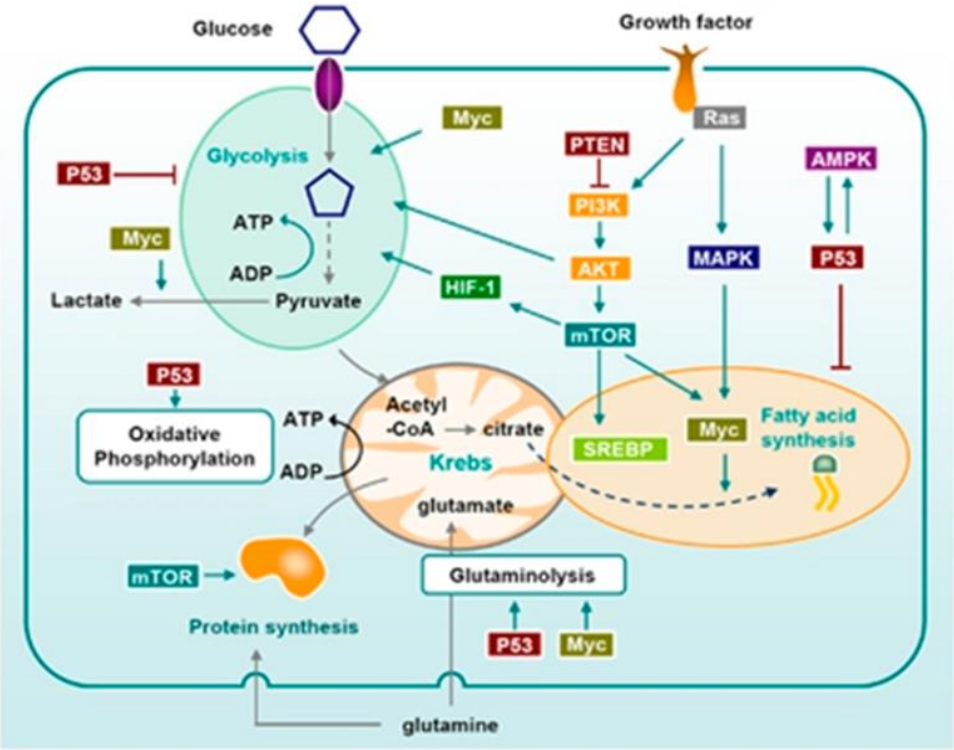

*Figures adopted from Munoz-Pinedo et al., 2012.

Figure 2. A schematic diagram of signaling pathways that regulate metabolism of cancer cells. The diagram illustrates importance of AMPK, mTOR, p53, HIF-1, and Myc regulation on glucose metabolism in the cell. AMPK can activate p53 to inhibit fatty acid synthesis. Activation of p53 can also directly inhibit intermediate steps in glycolysis. Activation of AKT, HIF-1, and Myc can directly induce glycolysis.

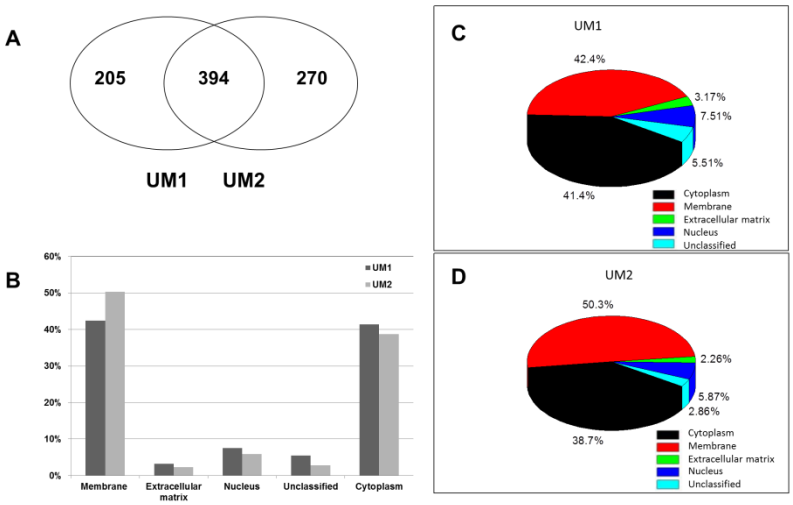

Figure 1-1. Analysis and identification of the membrane and membrane-associated proteins in UM1 and UM2 oral cancer cells using LC-MS/MS. (A) Venn diagrams for the number of proteins identified in each cell lines. (B-D) Localization of membrane and membrane-associated proteins.

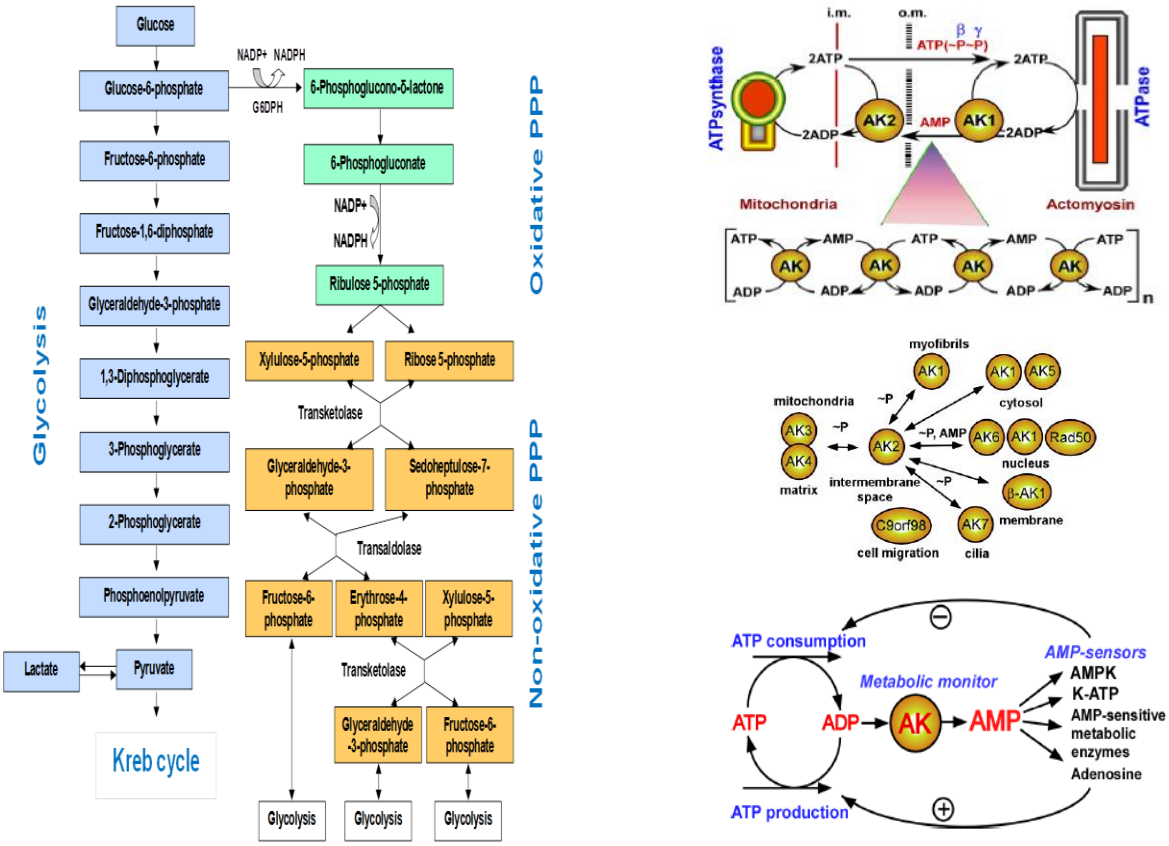

** Figures adopted from P. Dzeja and A. Terzic., 2009

Figure 1-2. A schematic diagram of glycolysis and pentose phosphate pathways and adenylate kinase metabolic monitoring systems in cells. Tranketolase is a major enzyme of the non-oxidative phase of PPP. Adenylate Kinases represent a set of enzymes that regulate phosphorylation of intracellular adenine nucleotides by catalyzing the phosphoryl exchange reaction 2ADP ↔ ATP + AMP.

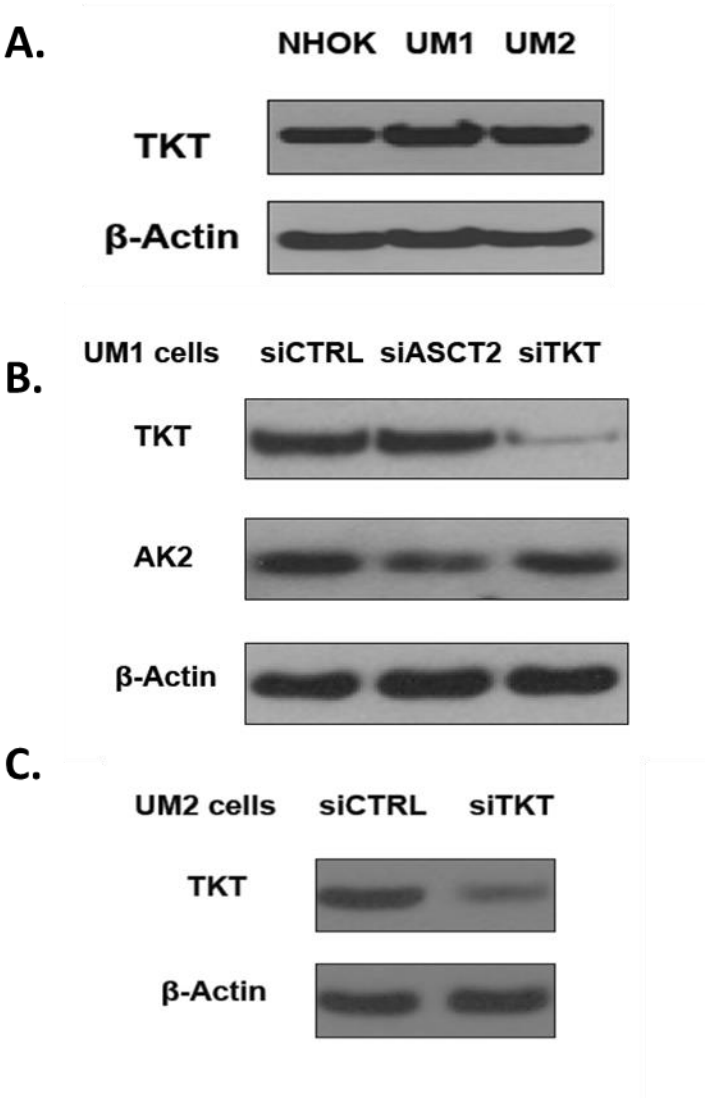

Figure 1-3. siRNA knockdown of TKT expression in UM1 and UM2 oral cancer cells. (A) Western blot analysis of TKT protein expression in NHOK, UM1 and UM2 cells. (B) Western blot analysis of TKT and AK2 expression in UM1 cells transfected with scrambled control siRNA (siCTRL), TKT siRNA (siTKT) or ASCT2 siRNA (siASCT2). (C) Western blot analysis of TKT in UM2 cells transfected with siTKT or siCTRL.

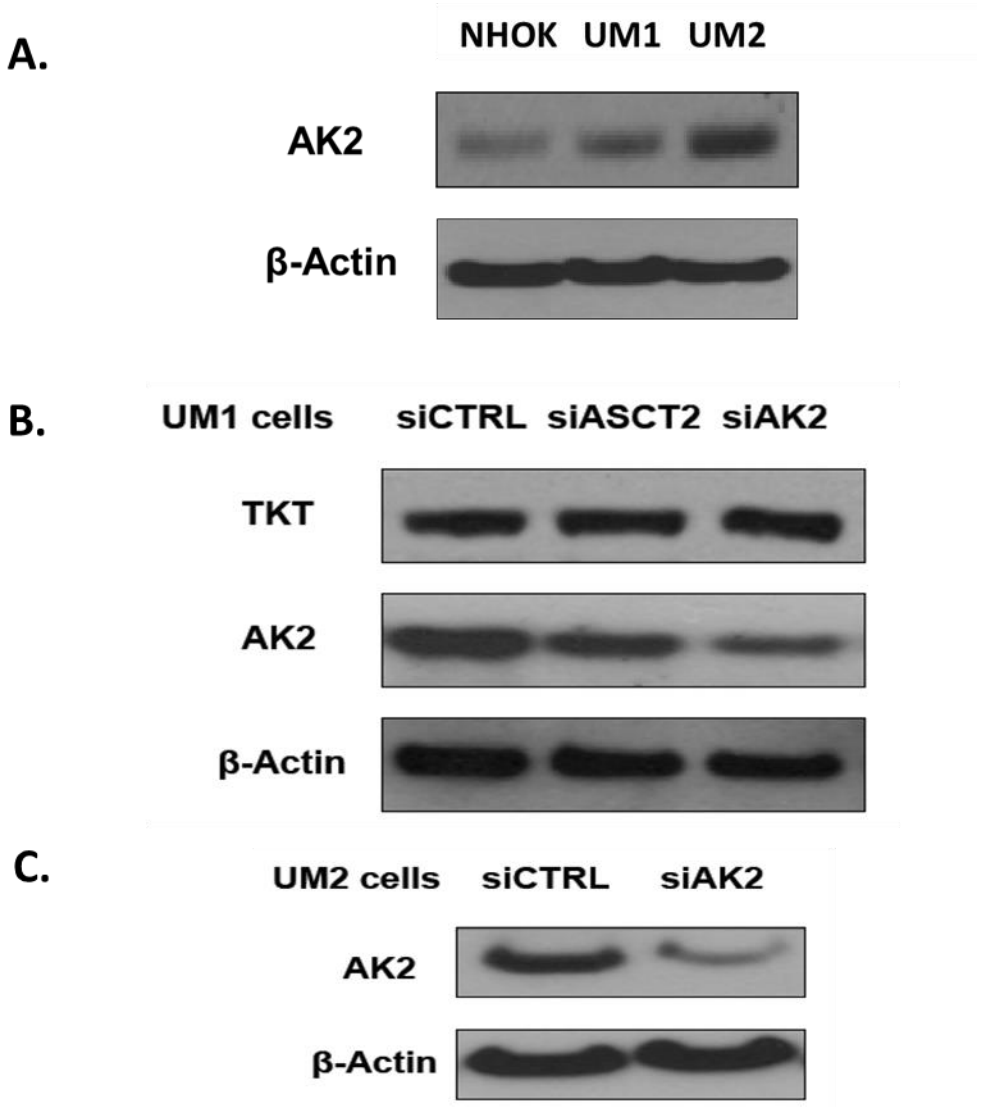

Figure 1-4. siRNA knockdown of AK2 expression in UM1 and UM2 oral cancer cells. (A) Western blot analysis of AK2 protein expression in NHOKs and oral/head and neck cancer cells. (B) Western blot analysis of AK2 expression in UM1 and UM2 cells transfected with scrambled siCTRL or siTKT. (C) Western blot analysis of AK2 and TKT in UM1 cells transfected with siCTRL, siAK2 or siCTRL.

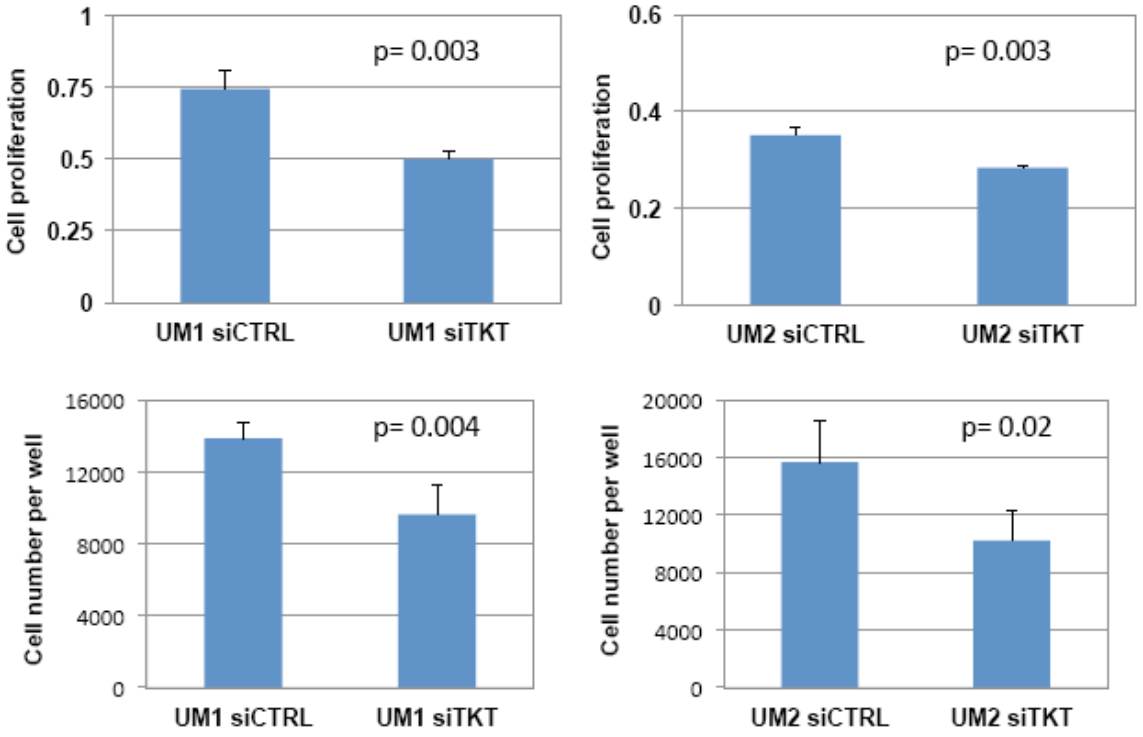

Figure 1-5. siRNA knockdown of TKT effect on cell proliferation in UM1 and UM2 cells. siRNA silencing of TKT significantly inhibited the proliferation of UM1 cells (n=4, p=0.003) and UM2 cells (n=4, p=0.003). Knockdown of TKT also had significantly inhibitory effects on the cell viability assays of UM1 (n=4, p=0.004) and UM2 (n=4, p=0.02) cells.

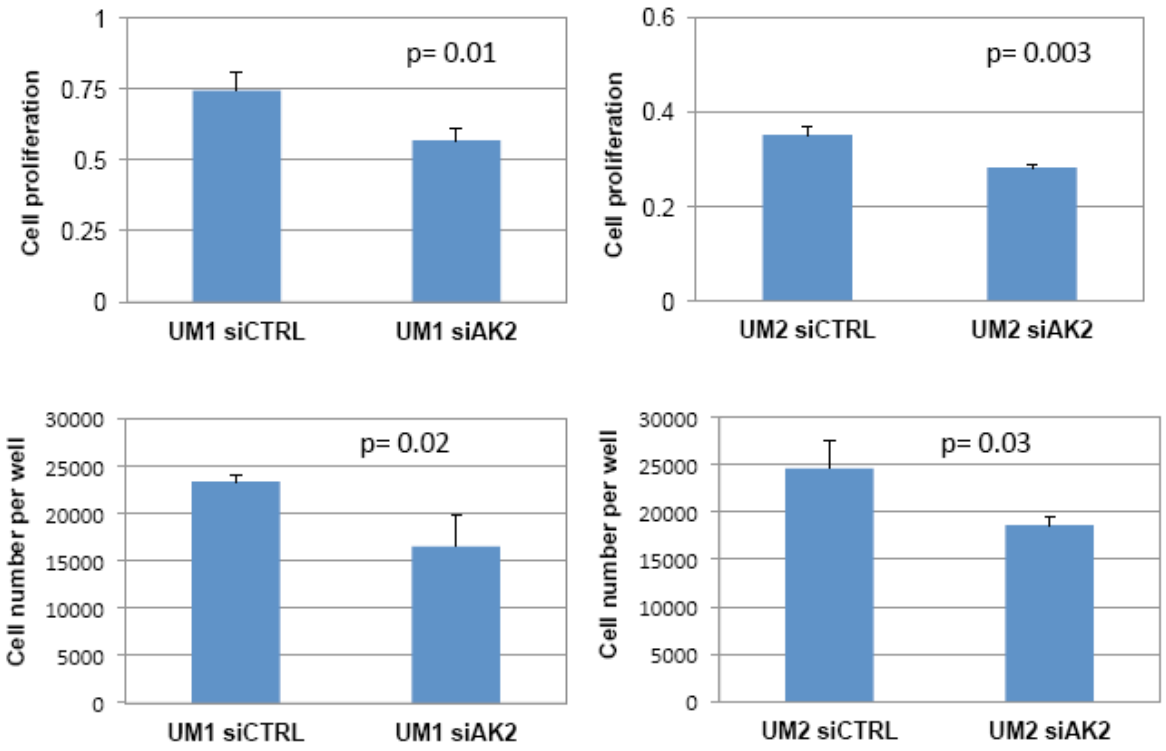

Figure 1-6. siRNA knockdown of AK2 effect on cell proliferation in UM1 and UM2 cells. MTT assays suggested that the cell proliferation was significantly inhibited in UM1 (n=4, p=0.01) and UM2 (n=4, p=0.003) cells transfected with siAK2. siRNA silencing of AK2 also had significantly inhibitory effects on the cell viability assays of UM1 (n=4, p=0.02) and UM2 (n=4, p=0.03) cells.

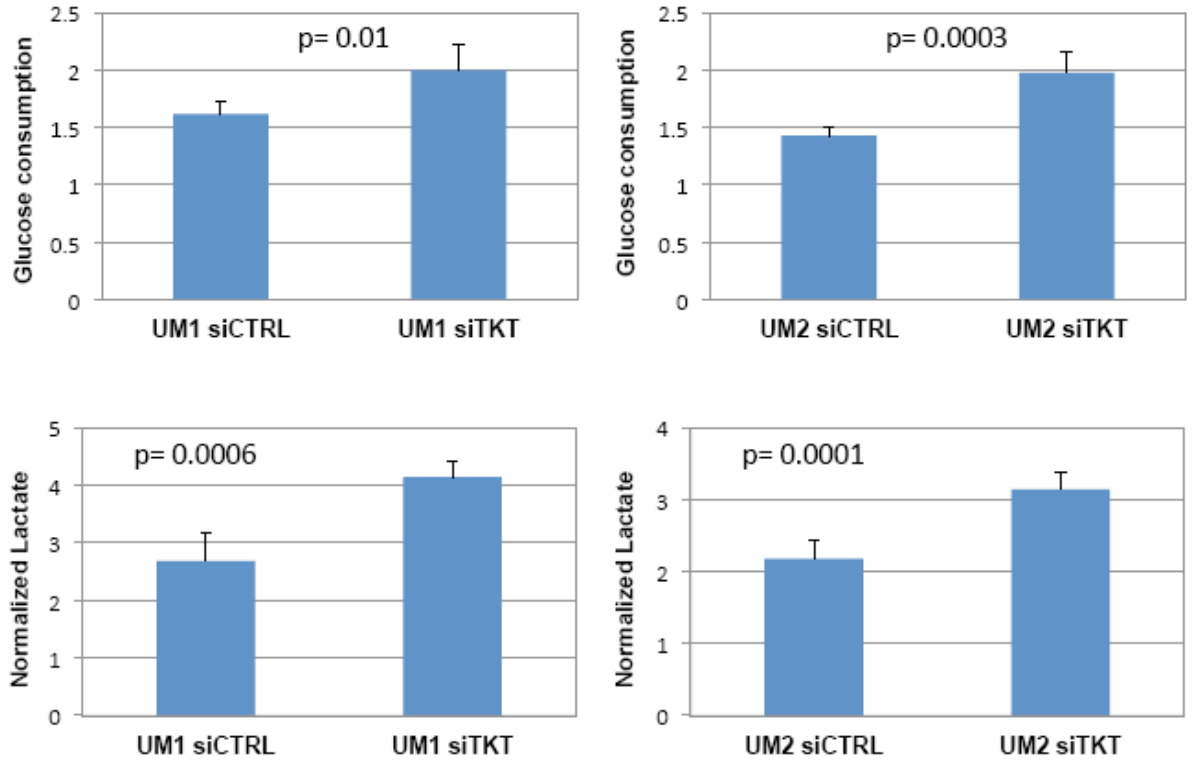

Figure 1-7. siRNA knockdown of TKT effect on glucose uptake and lactate production in UM1 and UM2 cells. When TKT expression was inhibited by siRNA silencing, a significantly higher amount of glucose was consumed by UM1 (n=5, p=0.01) and UM2 (n=5, p=0.0003) cells. siTKT-transfected UM1 (n=5, p=0.0006) and UM2 (n=5, p=0.0001) cells also produced a significantly higher amount of lactate compared to the cells transfected with siCTRL.

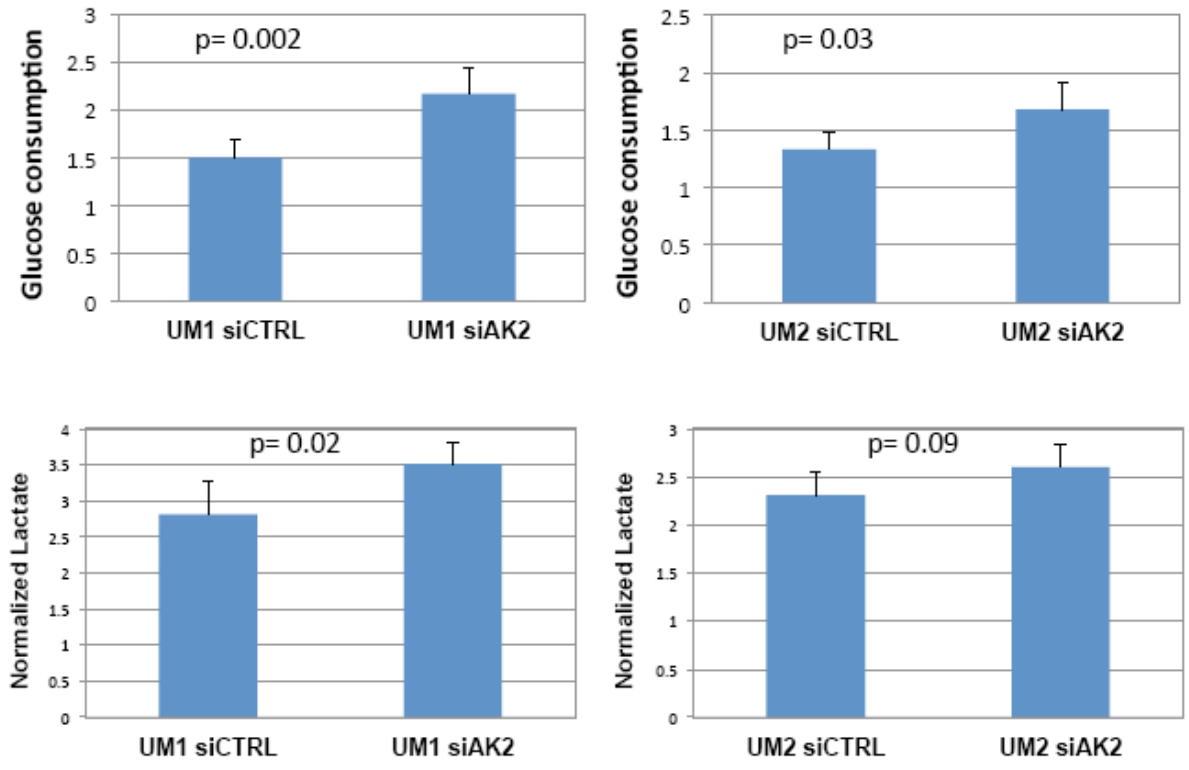

Figure 1-8. siRNA knockdown of AK2 effect on glucose uptake and lactate production in UM1 and UM2 cells. UM1 and UM2 cells consumed a significantly higher amount of glucose (n=5, p=0.002 and p=0.03, respectively) and secreted more lactate (n=5, p=0.02 and p=0.09, respectively) when AK2 expression was inhibited by siRNA silencing.

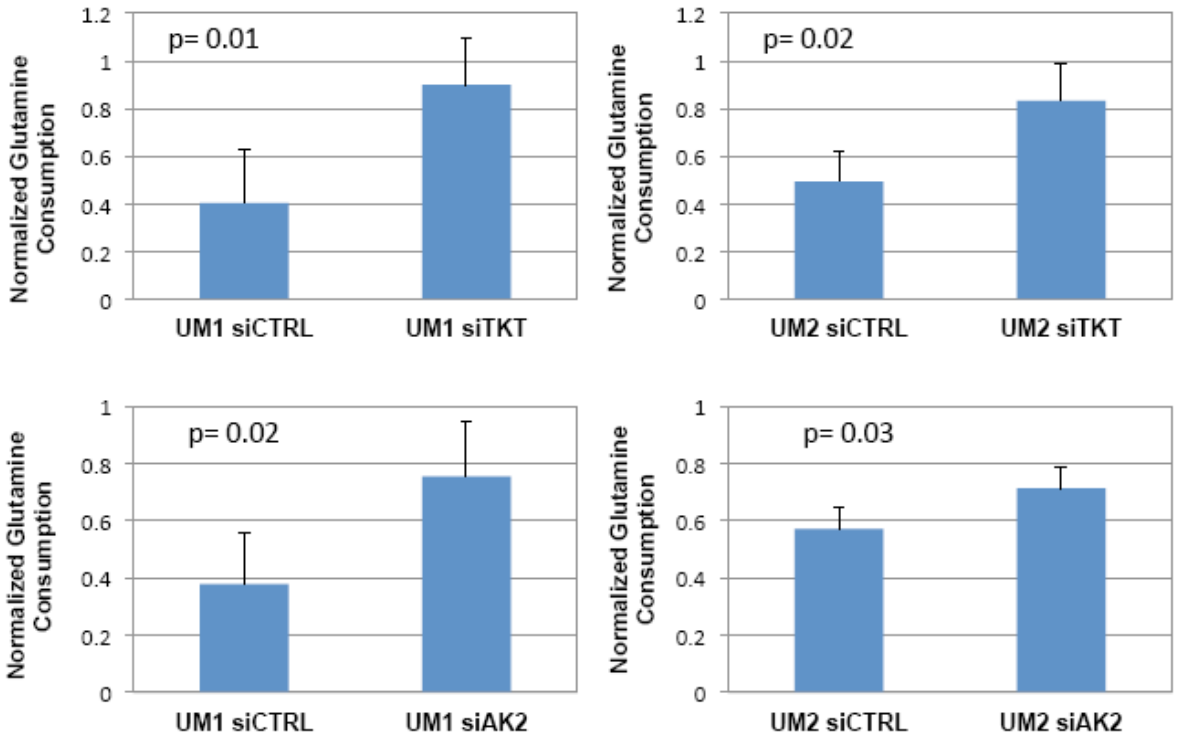

Figure 1-9. siRNA knockdown of TKT or AK2 effect on glutamine uptake in UM1 and UM2 cells. When TKT expression was inhibited by siTKT, a significantly higher amount of glutamine was consumed by UM1 (n=4, p=0.01) and UM2 (n=4, p=0.02) cells. Similarly, when AK2 expression was suppressed by siAK2, UM1 and UM2 cells exhibited a significantly more uptake of glutamine (n=4, p=0.02 and p=0.03, respectively).

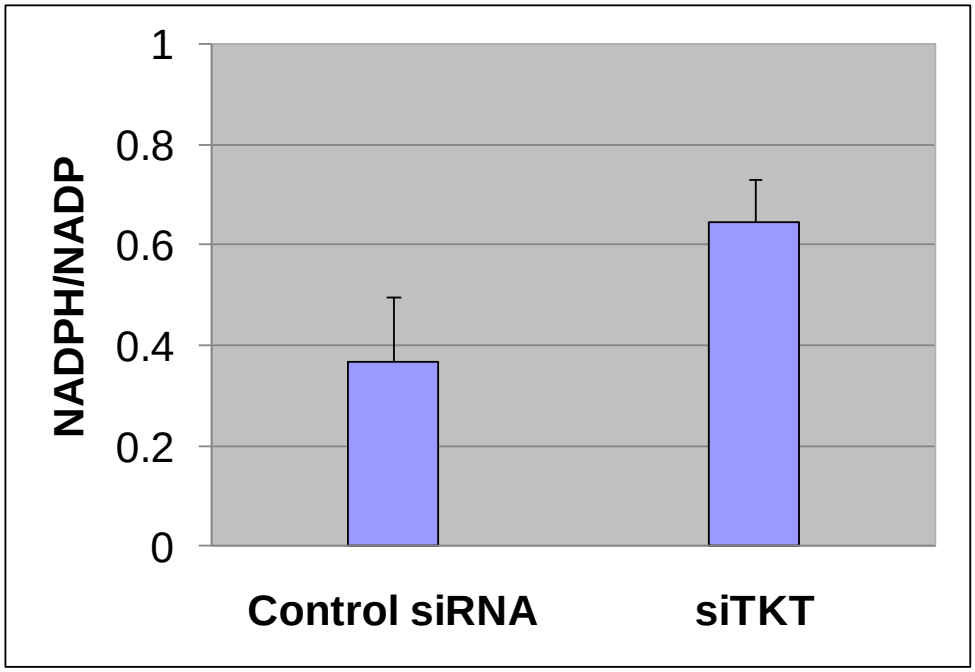

Figure 1-10: **siRNA knockdown of TKT- effect on NADPH/NADP production in UM1 cells.** When TKT expression was inhibited by siTKT in UM1 cells, siTKT-transfected UM1 cells produced 1.5-fold more NADPH than siCTRL-transfected UM1 cells.

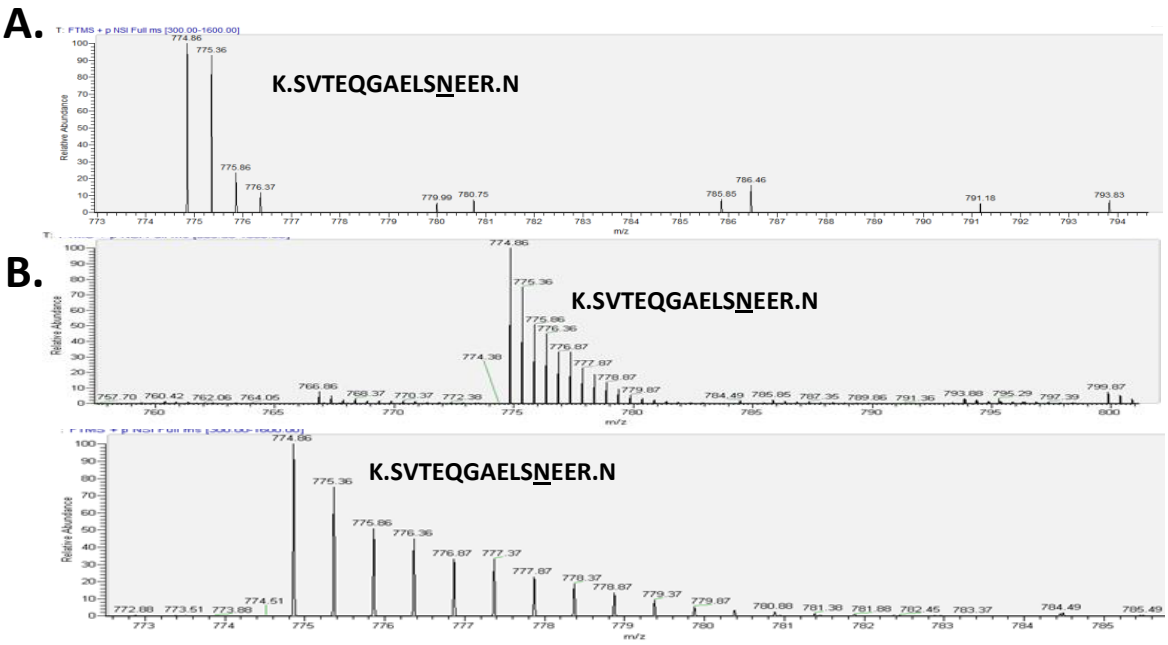

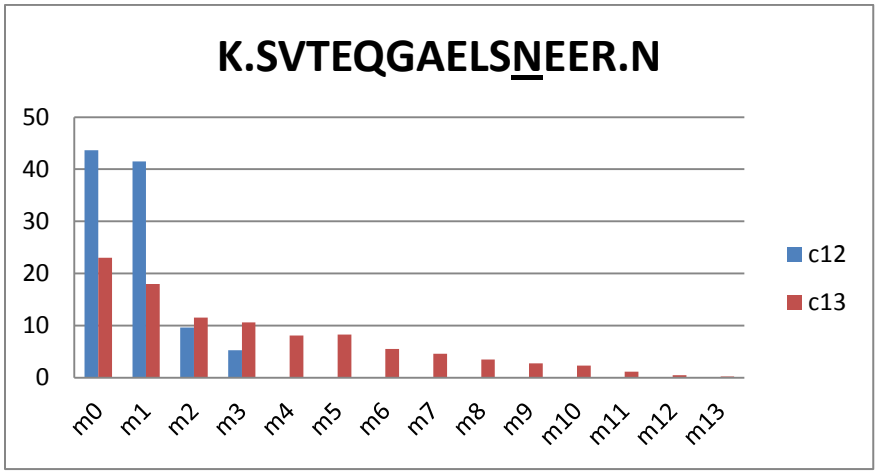

Figure 2-1. LC-MS analysis of peptide isotopomers of 14-3-3 protein zeta/delta in UM1 oral cancer cells. (A) ^{12}C unlabeled peptide mass isotopomer distribution of 14-3-3 protein zeta/delta. (B) ^{13}C labeled peptide mass isotopomer distribution of 14-3-3 protein zeta/delta. (C) Comparison of relative abundance for ^{12}C unlabeled and ^{13}C labeled peptide isotopomer distribution of 14-3-3 protein zeta/delta.

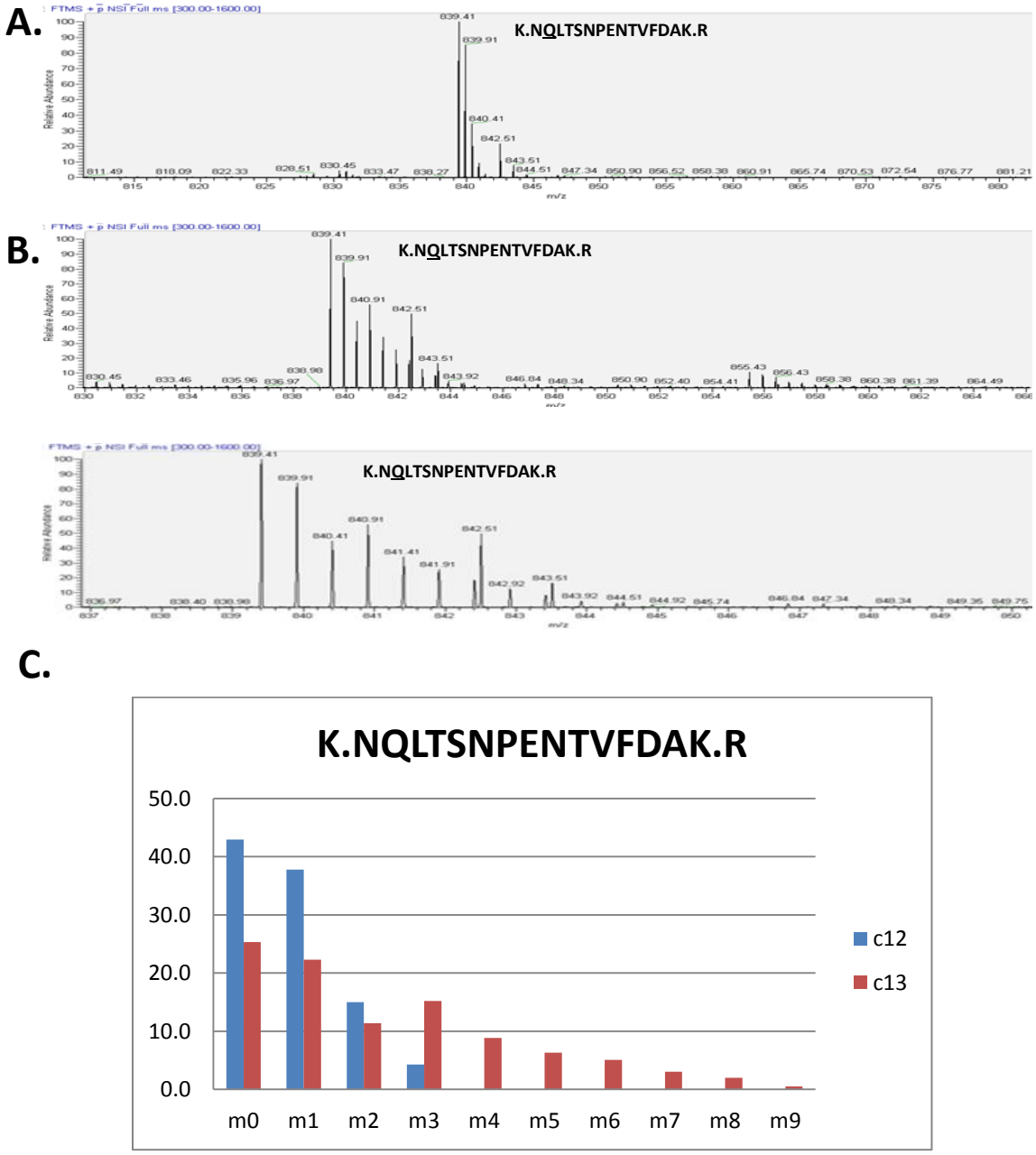

Figure 2-2. LC-MS analysis of peptide isotopomers of 78k Da glucose-related protein in UM1 oral cancer cells. (A) ^{12}C unlabeled peptide mass isotopomer distribution of 78k Da glucose-related protein. (B) ^{13}C labeled peptide mass isotopomer distribution of 78k Da glucose-related protein. (C) Comparison of relative abundance for ^{12}C unlabeled and ^{13}C labeled peptide isotopomer distribution of 78k Da glucose-related protein. Two isotopic envelops are observed.

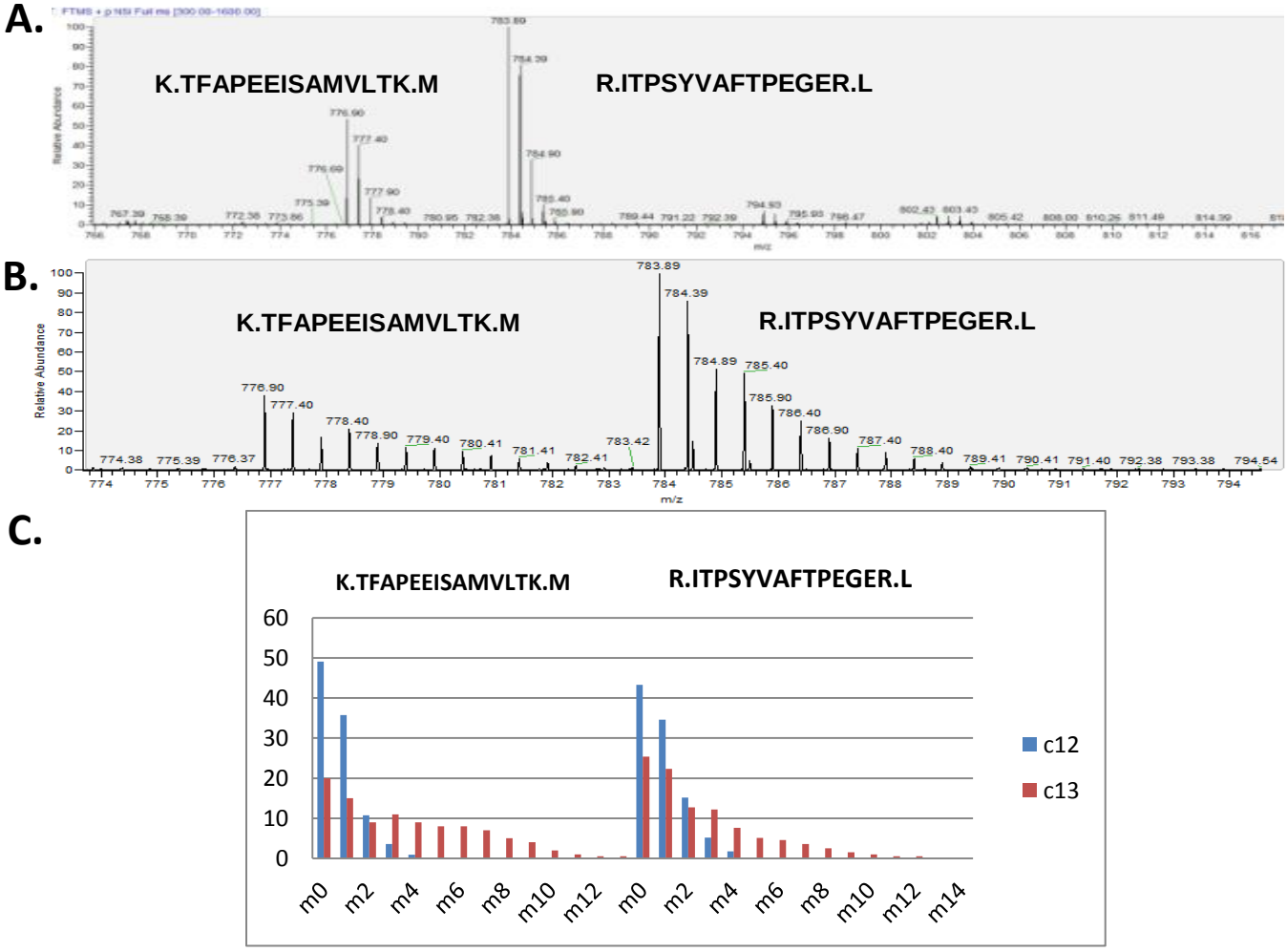

Figure 2-3. LC-MS analysis of peptide isotopomers of 78k Da glucose-related protein in UM1 oral cancer cells. (A) ^{12}C unlabeled peptide mass isotopomer distribution of 78k Da glucose-related protein. (B) ^{13}C labeled peptide mass isotopomer distribution of 78k Da glucose-related protein. (C) Comparison of relative abundance for ^{12}C unlabeled and ^{13}C labeled peptide isotopomer distribution of 78k Da glucose-related protein.

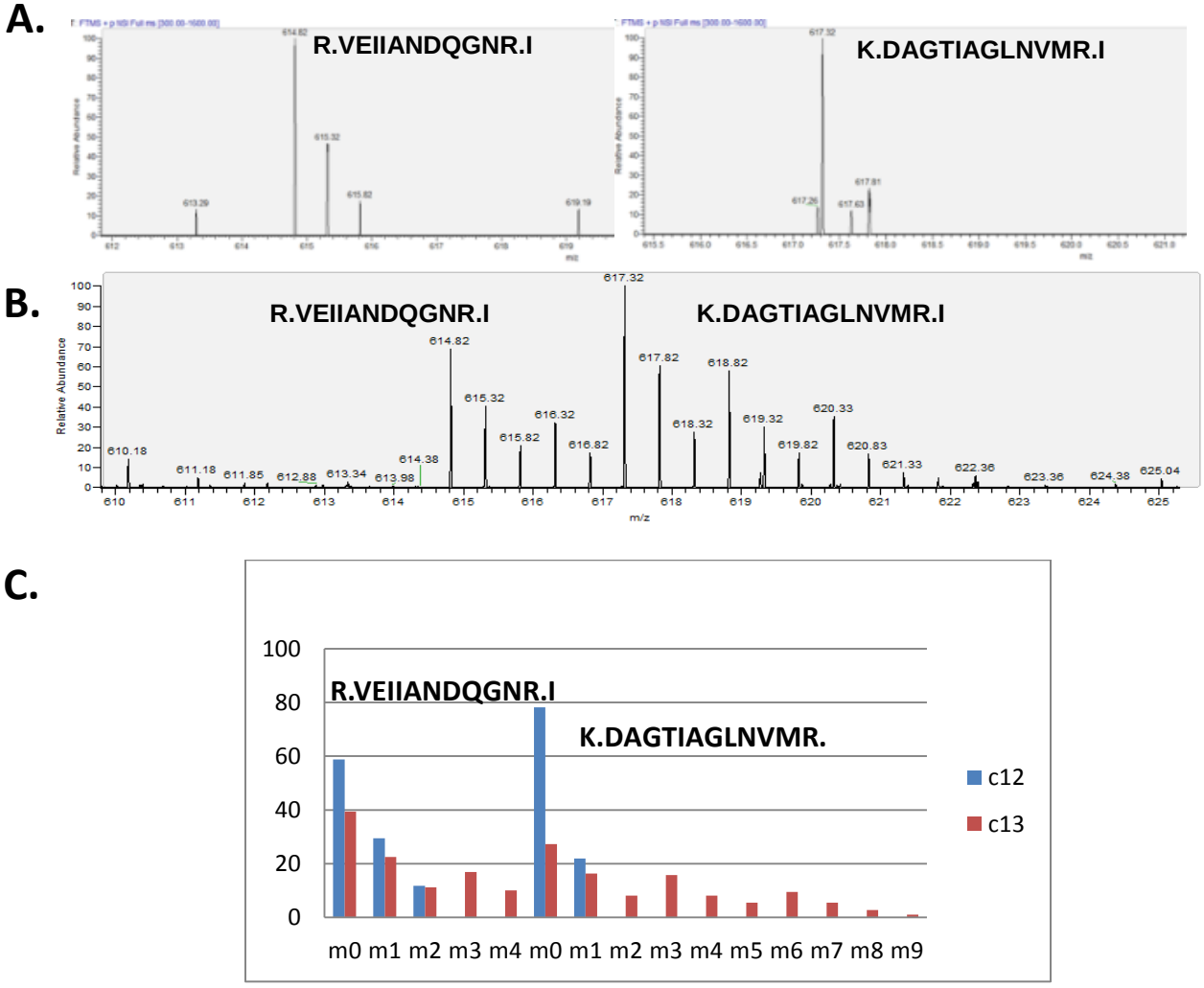

Figure 2-4. LC-MS analysis of peptide isotopomers of 78k Da glucose-related protein in UM1 oral cancer cells. (A) ^{12}C unlabeled peptide mass isotopomer distribution of 78k Da glucose-related protein. (B) ^{13}C labeled peptide mass isotopomer distribution of 78k Da glucose-related protein. (C) Comparison of relative abundance for ^{12}C unlabeled and ^{13}C labeled peptide isotopomer distribution of 78k Da glucose-related protein. Multiple isotopic envelops are observed.

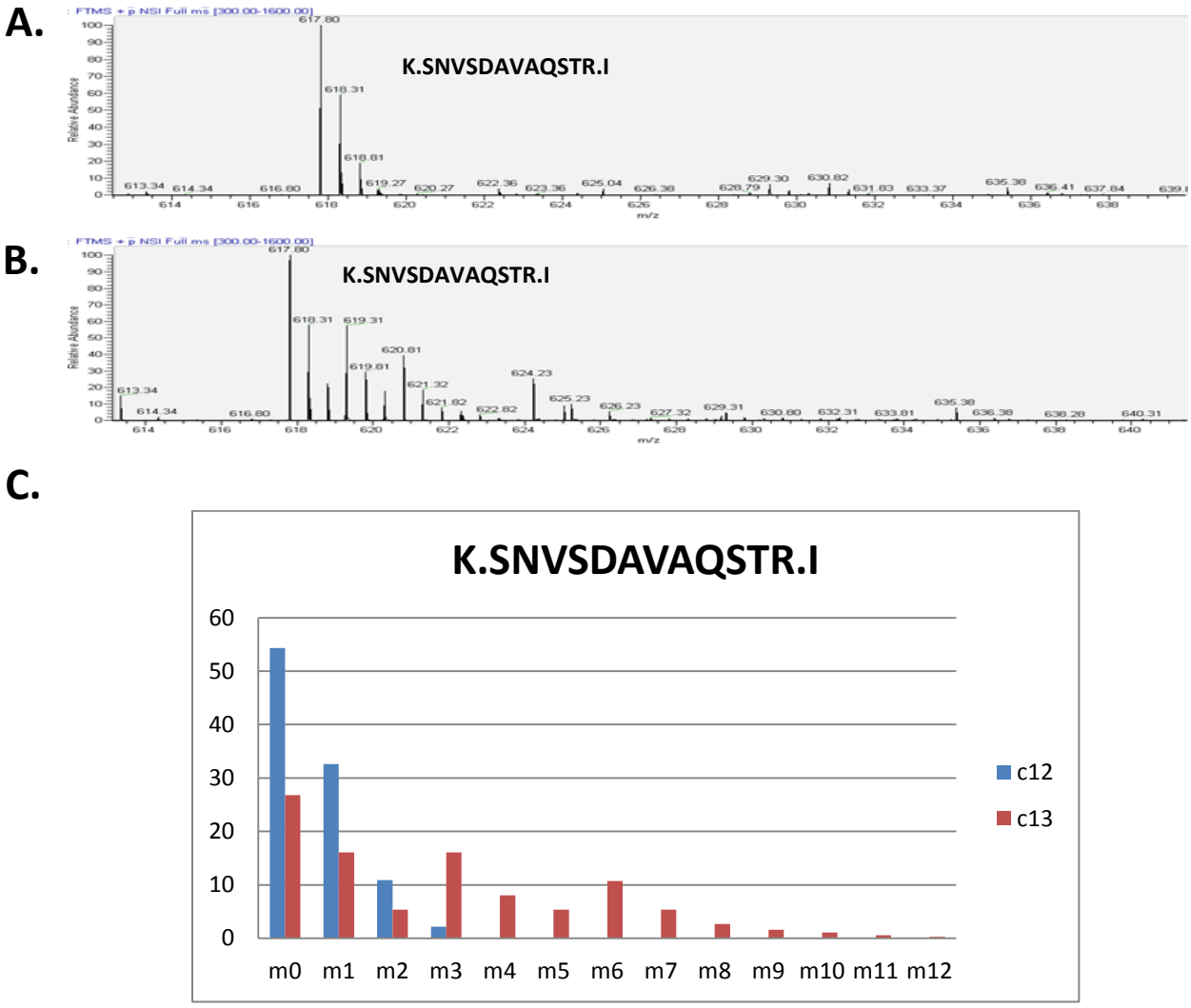

Figure 2-5. LC-MS analysis of peptide isotopomers of triosephosphate isomerase in UM1 oral cancer cells. (A) ^{12}C unlabeled peptide mass isotopomer distribution of triosephosphate isomerase. (B) ^{13}C labeled peptide mass isotopomer distribution of triosephosphate isomerase. (C) Comparison of relative abundance for ^{12}C unlabeled and ^{13}C labeled peptide isotopomer distribution of triosephosphate isomerase. Multiple isotopic envelops are observed.

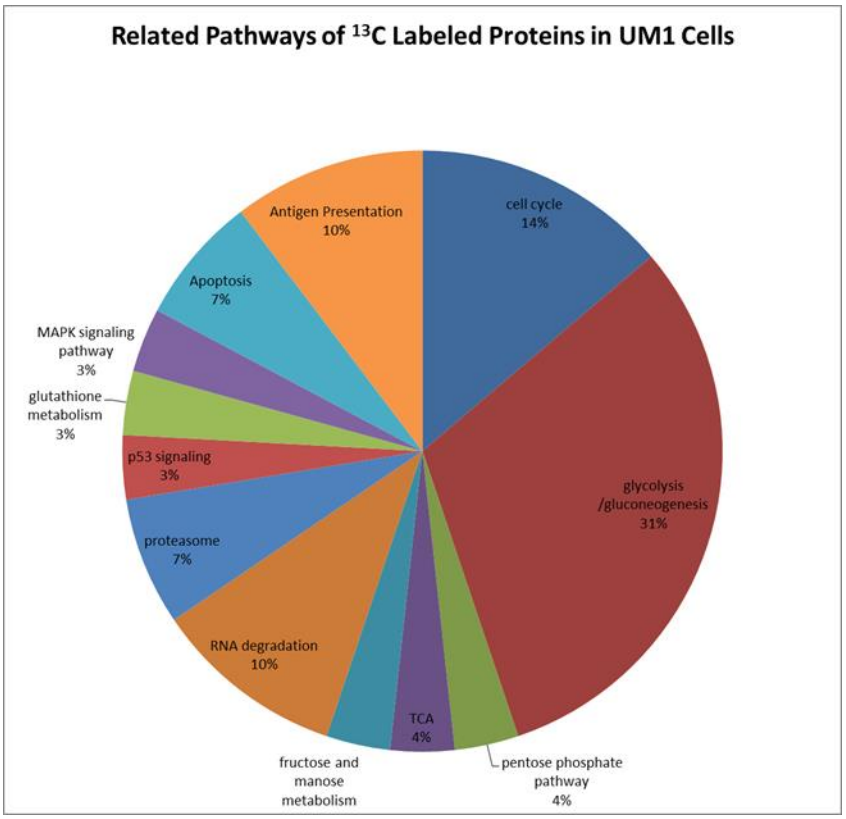

Figure 2-6. Related pathways of ^{13}C labeled proteins in UM1 oral cancer cells. Majority of ^{13}C labeled proteins in UM1 cells were involved in glycolysis/gluconeogenesis, RNA degradation, cell cycle, antigen presentation pathways.

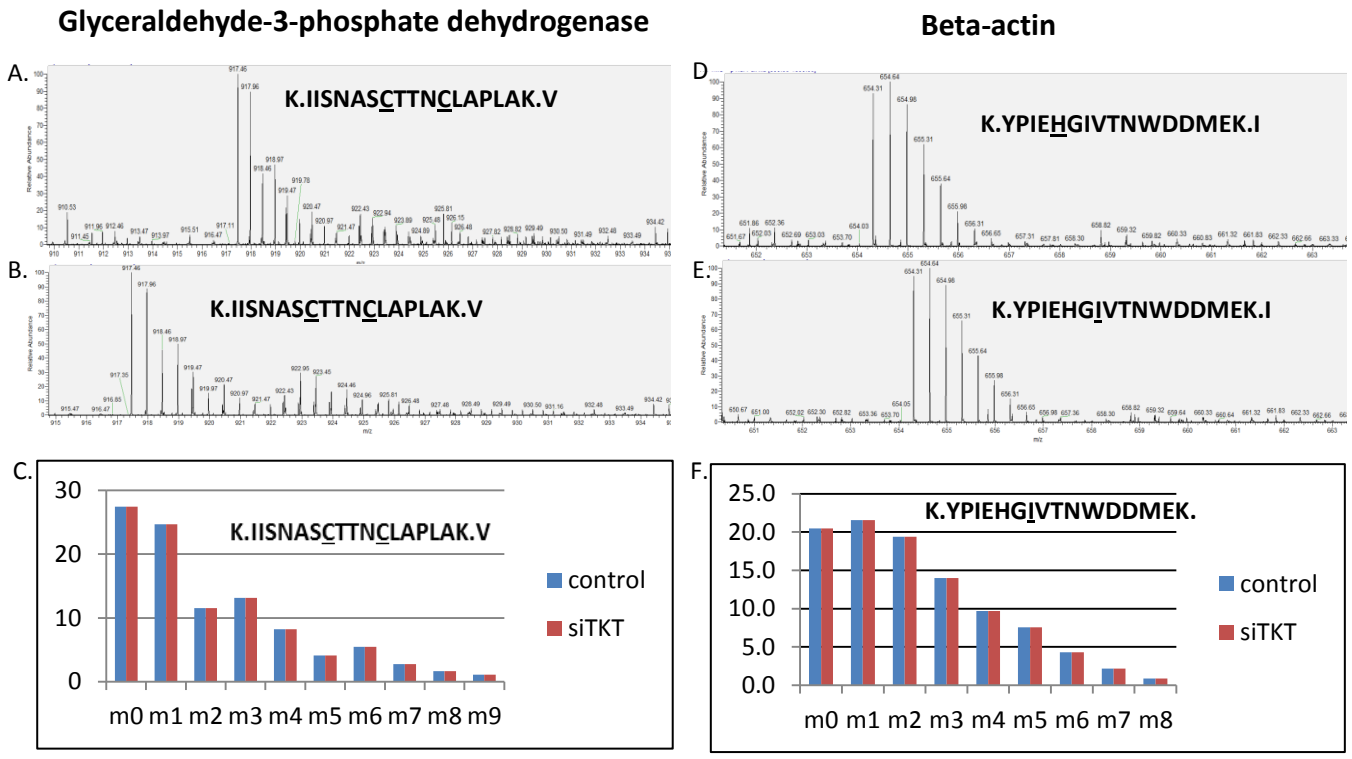

Figure 2-7. LC-MS analysis of ^{13}C labeling in siTKT transfected UM1 oral cancer cells and control scrambled siRNA transfected UM1 oral cancer cells. (A) ^{13}C labeled peptide mass isotopomer distribution of glyceraldehyde-3-phosphate dehydrogenase in siTKT UM1 cells. (B) ^{13}C labeled peptide mass isotopomer distribution of glyceraldehyde-3-phosphate dehydrogenase in siCTRL UM1 cells. (C) Comparison of relative abundance for the same ^{13}C labeled peptide isotopomer distribution in siCTRL and siTKT transfected UM1 cells. (D) ^{13}C labeled peptide mass isotopomer distribution of β-actin in siTKT UM1 cells. (E) ^{13}C labeled peptide mass isotopomer distribution of β-actin in siCTRL UM1 cells. (F) Comparison of relative abundance for the same ^{13}C labeled peptide isotopomer distribution in siCTRL and siTKT transfected UM1 cells. No significant differences were observed in the relative isotopic peak intensities and mass shifts for both glyceraldehyde-3-phosphate dehydrogenase and β-actin.

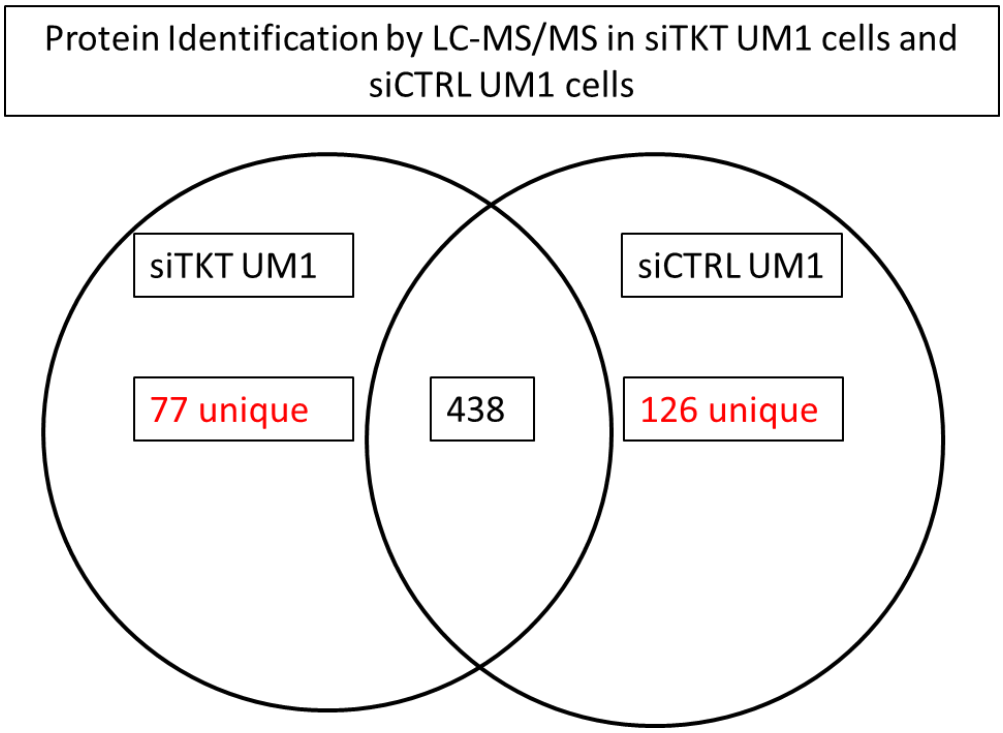

Figure 2-8. Analysis and identification of the cellular proteins in siTKT transfected UM1 oral cancer cells and control scrambled siRNA transfected UM1 oral cancer cells. We identified 564 proteins in siCTRL-transfected UM1 cells and 515 proteins in siTKT-transfected UM1 cells. Both groups had 438 proteins in common. There were 77 unique proteins identified in siTKT-transfected UM1 cells and 126 unique proteins in siCTRL-transfected UM1 cells.

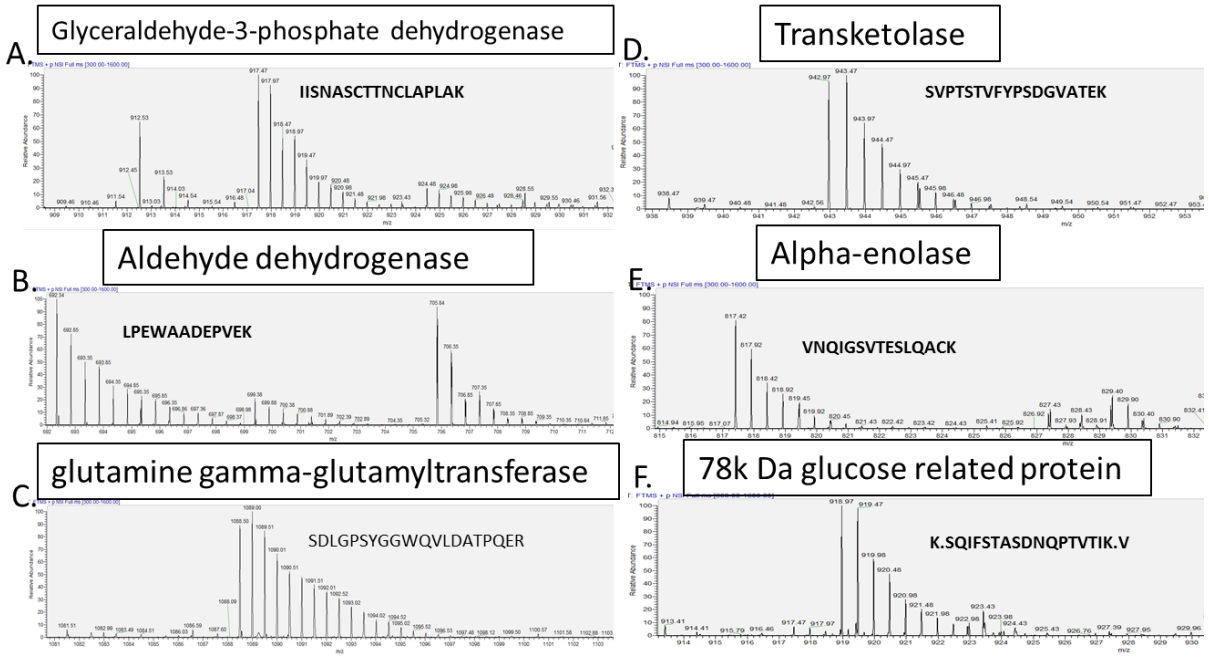

Figure 3-1. LC-MS analysis of ^{13}C labeled peptide isotopomers of proteins in primary BXPC-3 pancreas adenocarcinoma cells. (A-F) ^{13}C labeled peptide mass isotopomer distribution for glyceraldehyde-3-phosphate dehydrogenase, aldehyde dehydrogenase, glutamine gamma-glutamyltransferase, transketolase, α-enolase, and 78k Da glucose related protein in BxPC-3 cells.

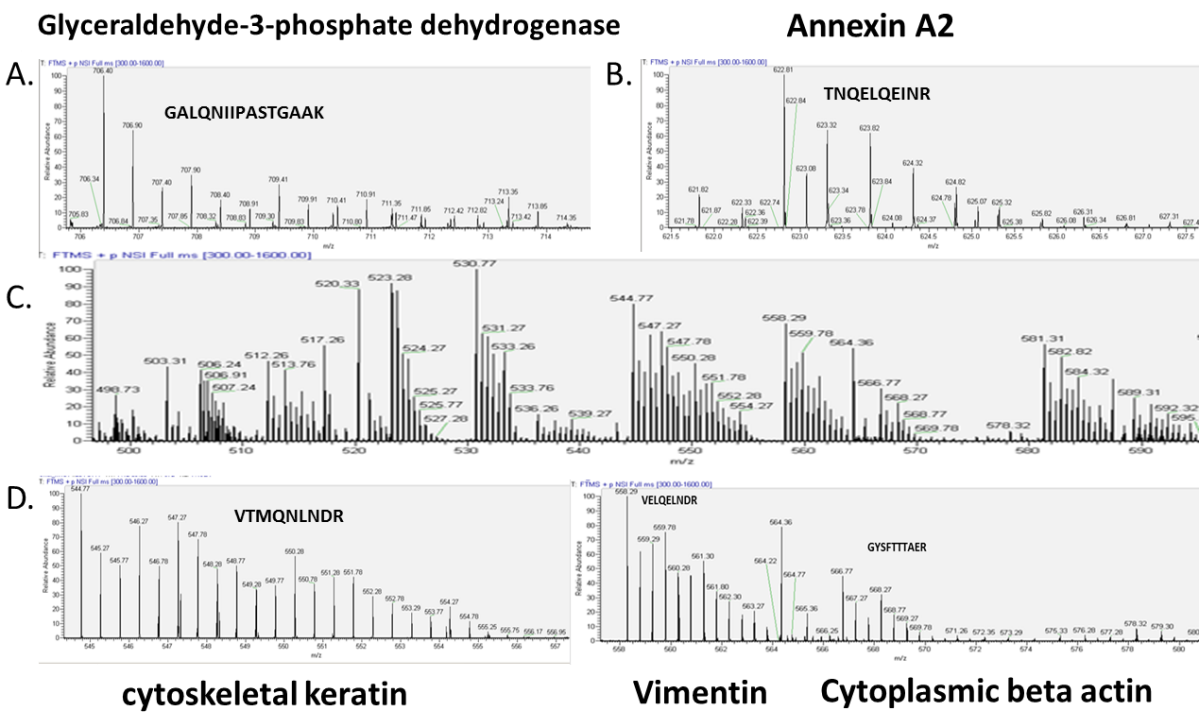

Figure 3-2. LC-MS analysis of ^{13}C labeled peptide isotopomers of proteins in human pancreatic duct epithelial cells and primary MIA PaCa-2 pancreas adenocarcinoma cells. (A) ^{13}C labeled peptide mass isotopomer distribution of glyceraldehyde-3-phosphate dehydrogenase in HPDE cells. (B) ^{13}C labeled peptide mass isotopomer distribution of Annexin A2 in HPDE cells. (C) high frequency of ^{13}C labeled peptides observed in MS1 spectra of MIA PaCa-2 cells from m/z range 500-600. (D) ^{13}C labeled peptide mass isotopomer distribution of cytoskeletal keratin, vimentin, and cytoplasmic β-actin proteins MIA PaCa-2 cells from m/z range 500-600.

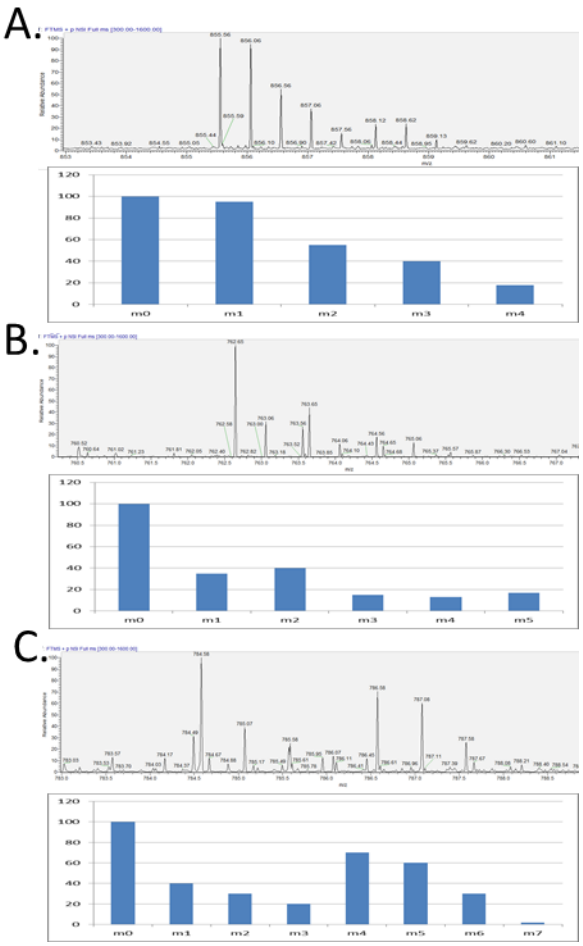

Figure 3-3. LC-MS analysis of peptide isotopomers of proteins in MIA PaCa-2 xenograft mouse pancreas tumor tissue. (A-C) Potential ^{13}C labeled peptide mass isotopomer distribution and relative isotopic peak abundance in MIA PaCa-2 mouse pancreatic tumor tissue.

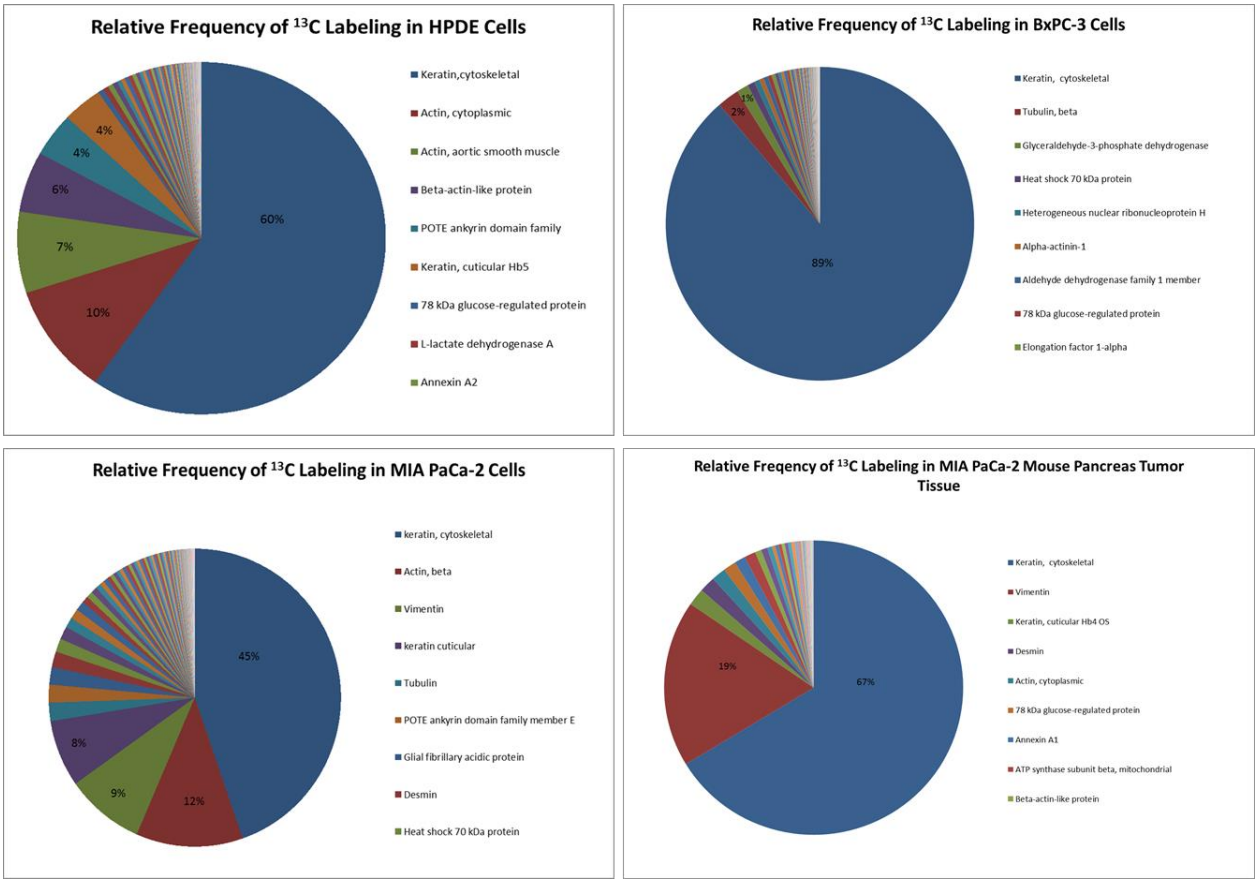

Figure 3-4. Relative frequency of ^{13}C labeling comparison in HPDE cells, BxPC-3 cells, MIA PaCa-2 cells, and mouse tumor tissue. Relative frequency of ^{13}C labeled peptides in HPDE, BxPC-3, MIA PaCa-2 and MIA PaCa-2 mouse pancreatic tumor tissue. Cytoskeletal keratin displayed greatest labeling in all cell lines. β-tubulin displayed greater labeling in PDAC cells compared to HPDE cells. Vimentin protein displayed greater labeling in MIA PaCa-2 cells compared to HPDE cells.

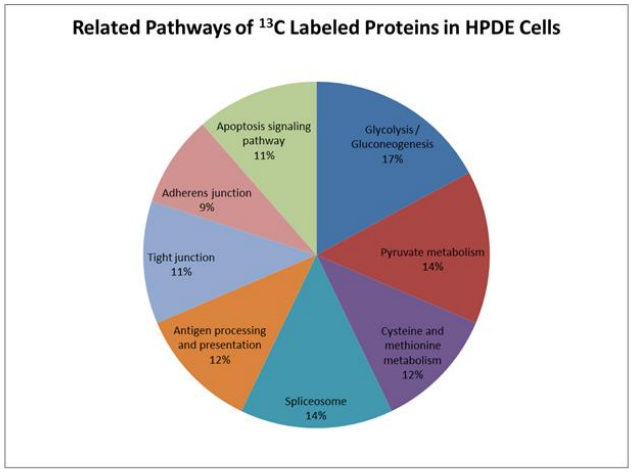

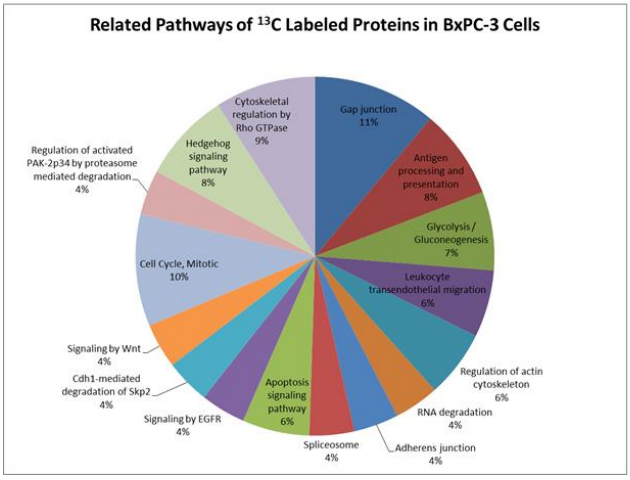

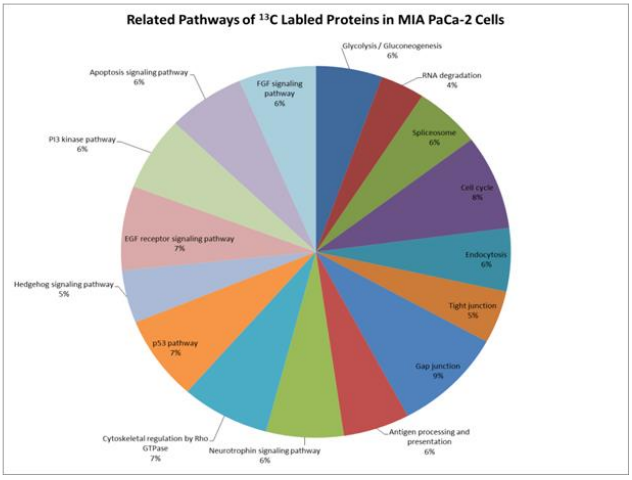

Figure 3-5. Related pathways of ^{13}C labeled proteins in HPDE cells, BxPC-3 cells, and MIA PaCa-2 cells. ^{13}C labeled proteins in HPDE, BxPC-3 and MIA PaCa-2 cells were categorized based on their related cellular pathways. Our finding indicated many ^{13}C labeled enzymes involved in glycolysis, p53 signaling, and spliceosome pathways.

Table 2-1. Identified Proteins in Human UM1 Oral Cancer Cells

Accession #	Protein Name (Peptide Scores>40)	Species
1. 1433B_HUMAN*	14-3-3 protein beta/alpha	Homo sapiens
2. 1433E_HUMAN*	14-3-3 protein epsilon	Homo sapiens
3. 1433F_HUMAN	14-3-3 protein eta	Homo sapiens
4. 1433S_HUMAN*	14-3-3 protein sigma	Homo sapiens
5. 1433T_HUMAN	14-3-3 protein theta	Homo sapiens
6. 1433Z_HUMAN*	14-3-3 protein zeta/delta	Homo sapiens
7. 6PGD_HUMAN	6-phosphogluconate dehydrogenase, decarboxylating	Homo sapiens
8. AIFM1_HUMAN	Apoptosis-inducing factor 1, mitochondrial	Homo sapiens
9. ALDOA_HUMAN	Fructose-bisphosphate aldolase A	Homo sapiens
10. ALDOC_HUMAN	Fructose-bisphosphate aldolase C	Homo sapiens
11. ANXA1_HUMAN*	Annexin A1	Homo sapiens
12. ANXA2_HUMAN*	Annexin A2	Homo sapiens
13. ANXA5_HUMAN*	Annexin A5	Homo sapiens
14. ARC1A_HUMAN	Actin-related protein 2/3 complex subunit 1A	Homo sapiens
15. ARPC2_HUMAN	Actin-related protein 2/3 complex subunit 2	Homo sapiens
16. AXA2L_HUMAN	Putative annexin A2-like protein	Homo sapiens
17. CAPG_HUMAN	Macrophage-capping protein	Homo sapiens
18. CATZ_HUMAN	Cathepsin Z	Homo sapiens
19. CAZA1_HUMAN*	F-actin-capping protein subunit alpha-1	Homo sapiens
20. CISY_HUMAN	Citrate synthase, mitochondrial	Homo sapiens
21. COPD_HUMAN	Coatomer subunit delta	Homo sapiens
22. DESP_HUMAN	Desmoplakin	Homo sapiens
23. DHE3_HUMAN	Glutamate dehydrogenase 1, mitochondrial	Homo sapiens
24. DLDH_HUMAN	Dihydrolipoyl dehydrogenase, mitochondrial	Homo sapiens
25. EF1D_HUMAN	Elongation factor 1-delta	Homo sapiens
26. ENOA_HUMAN*	Alpha-enolase	Homo sapiens
27. ENOB_HUMAN*	Beta-enolase	Homo sapiens
28. ENOG_HUMAN*	Gamma-enolase	Homo sapiens
29. ERO1A_HUMAN *	ERO1-like protein alpha	Homo sapiens
30. EZRI_HUMAN	Ezrin	Homo sapiens
31. FSCN1_HUMAN	Fascin	Homo sapiens
32. FUMH_HUMAN*	Fumarate hydratase, mitochondrial	Homo sapiens
33. G6PD_HUMAN*	Glucose-6-phosphate 1-dehydrogenase	Homo sapiens
34. GBB1_HUMAN	Guanine nucleotide-binding protein G(I)/G(S)/G(T) subunit beta-1	Homo sapiens
35. GBB4_HUMAN	Guanine nucleotide-binding protein subunit beta-4	Homo sapiens
36. GBLP_HUMAN	Guanine nucleotide-binding protein subunit beta-2-like 1	Homo sapiens
37. GFAP_HUMAN	Glial fibrillary acidic protein	Homo sapiens
38. GLU2B_HUMAN	Glucosidase 2 subunit beta	Homo sapiens

39. GRP78_HUMAN*	78 kDa glucose-regulated protein	Homo sapiens
40. GSH0_HUMAN*	Glutamate--cysteine ligase regulatory subunit	Homo sapiens
41. HNRDL_HUMAN	Heterogeneous nuclear ribonucleoprotein D-like	Homo sapiens
42. HNRH3_HUMAN*	Heterogeneous nuclear ribonucleoprotein H3	Homo sapiens
43. HNRPD_HUMAN*	Heterogeneous nuclear ribonucleoprotein D0	Homo sapiens
44. HNRPK_HUMAN*	Heterogeneous nuclear ribonucleoprotein K	Homo sapiens
45. HNRPL_HUMAN	Heterogeneous nuclear ribonucleoprotein L	Homo sapiens
46. HS71L_HUMAN	Heat shock 70 kDa protein 1-like	Homo sapiens
47. HSP71_HUMAN	Heat shock 70 kDa protein 1A/1B	Homo sapiens
48. HSP72_HUMAN	Heat shock-related 70 kDa protein 2	Homo sapiens
49. HSP76_HUMAN	Heat shock 70 kDa protein 6	Homo sapiens
50. HSP7C_HUMAN*	Heat shock cognate 71 kDa protein	Homo sapiens
51. IDHC_HUMAN	Isocitrate dehydrogenase [NADP] cytoplasmic	Homo sapiens
52. IDHP_HUMAN	Isocitrate dehydrogenase [NADP], mitochondrial	Homo sapiens
53. IMDH2_HUMAN*	Inosine-5'-monophosphate dehydrogenase 2	Homo sapiens
54. KPYM_HUMAN*	Pyruvate kinase isozymes M1/M2	Homo sapiens
55. KPYR_HUMAN	Pyruvate kinase isozymes R/L	Homo sapiens
56. LIS1_HUMAN	Platelet-activating factor acetylhydrolase IB subunit alpha	Homo sapiens
57. LMNA_HUMAN*	Lamin-A/C	Homo sapiens
58. LMNB1_HUMAN	Lamin-B1	Homo sapiens
59. LMNB2_HUMAN*	Lamin-B2	Homo sapiens
60. MOES_HUMAN	Moesin	Homo sapiens
61. OTUB1_HUMAN*	Ubiquitin thioesterase OTUB1	Homo sapiens
62. PCNA_HUMAN	Proliferating cell nuclear antigen	Homo sapiens
63. PDIA4_HUMAN	Protein disulfide-isomerase A4	Homo sapiens
64. PDLI1_HUMAN*	PDZ and LIM domain protein 1	Homo sapiens
65. PDS5B_HUMAN	Sister chromatid cohesion protein PDS5 homolog B	Homo sapiens
66. PGAM1_HUMAN*	Phosphoglycerate mutase 1	Homo sapiens
67. PGAM2_HUMAN	Phosphoglycerate mutase 2	Homo sapiens
68. PGAM4_HUMAN	Probable phosphoglycerate mutase 4	Homo sapiens
69. PGK1_HUMAN	Phosphoglycerate kinase 1	Homo sapiens
70. PGK2_HUMAN	Phosphoglycerate kinase 2	Homo sapiens
71. PRS10_HUMAN*	26S protease regulatory subunit S10B	Homo sapiens
72. PSB7_HUMAN	Proteasome subunit beta type-7	Homo sapiens
73. PSME1_HUMAN*	Proteasome activator complex subunit 1	Homo sapiens
74. RADI_HUMAN	Radixin	Homo sapiens
75. RAN_HUMAN*	GTP-binding nuclear protein Ran	Homo sapiens
76. ROAA_HUMAN	Heterogeneous nuclear ribonucleoprotein A/B	Homo sapiens
77. RSSA_HUMAN	40S ribosomal protein SA	Homo sapiens
78. SHRM3_HUMAN	Protein Shroom3	Homo sapiens
79. SODM_HUMAN*	Superoxide dismutase [Mn], mitochondrial	Homo sapiens

80. STIP1_HUMAN	Stress-induced-phosphoprotein 1	Homo sapiens
81. SYYC_HUMAN	Tyrosyl-tRNA synthetase, cytoplasmic	Homo sapiens
82. TAGL2_HUMAN	Transgelin-2	Homo sapiens
83. TCPD_HUMAN	T-complex protein 1 subunit delta	Homo sapiens
84. TCPG_HUMAN	T-complex protein 1 subunit gamma	Homo sapiens
85. TCPH_HUMAN	T-complex protein 1 subunit eta	Homo sapiens
86. TCPQ_HUMAN	T-complex protein 1 subunit theta	Homo sapiens
87. TKT_HUMAN*	Transketolase	Homo sapiens
88. TPIS_HUMAN*	Triosephosphate isomerase	Homo sapiens
89. TPISL_HUMAN	Putative triosephosphate isomerase-like protein LOC286016	Homo sapiens
90. TPM1_HUMAN*	Tropomyosin alpha-1 chain	Homo sapiens
91. TPM2_HUMAN *	Tropomyosin beta chain	Homo sapiens
92. TPM3_HUMAN *	Tropomyosin alpha-3 chain OS=Homo sapiens	Homo sapiens
93. TPM3L_HUMAN	Putative tropomyosin alpha-3 chain-like protein	Homo sapiens
94. TPM4_HUMAN*	Tropomyosin alpha-4 chain	Homo sapiens
95. U17L1_HUMAN	Putative ubiquitin carboxyl-terminal hydrolase 17-like protein 1	Homo sapiens
96. UGDH_HUMAN*	UDP-glucose 6-dehydrogenase	Homo sapiens
97. VATA_HUMAN	V-type proton ATPase catalytic subunit A	Homo sapiens
98. VDAC1_HUMAN	Voltage-dependent anion-selective channel protein 1	Homo sapiens
99. VDAC2_HUMAN*	Voltage-dependent anion-selective channel protein 2	Homo sapiens
100. VDAC3_HUMAN	Voltage-dependent anion-selective channel protein 3	Homo sapiens

Table 2-2. ^{13}C Labeled Proteins of UM1: DAVID Converted Gene List

UNIPROT ACCESSION #	UNIGENE CODE	SPECIES	DATABASE FOR ANNOTATION,VISUALIZATION AND INTEGRATED DISCOVERY (DAVID) GENE NAME
FUMH_HUMAN	Hs.592490	Homo sapiens	fumarate hydratase
HNRH3_HUMAN	Hs.643472	Homo sapiens	heterogeneous nuclear ribonucleoprotein H3 (2H9)
1433Z_HUMAN	Hs.492407	Homo sapiens	tyrosine 3-monooxygenase/tryptophan 5-monooxygenase activation protein, zeta polypeptide
GSH0_HUMAN	Hs.315562	Homo sapiens	glutamate-cysteine ligase, modifier subunit
IMDH2_HUMAN	Hs.654400	Homo sapiens	IMP (inosine monophosphate) dehydrogenase 2
GRP78_HUMAN	Hs.710890	Homo sapiens	hypothetical gene supported by AF216292; NM_005347; heat shock 70kDa protein 5 (glucose-regulated protein, 78kDa)
GRP78_HUMAN	Hs.605502	Homo sapiens	hypothetical gene supported by AF216292; NM_005347; heat shock 70kDa protein 5 (glucose-regulated protein, 78kDa)
TPM2_HUMAN	Hs.300772	Homo sapiens	tropomyosin 2 (beta)
HNRPK_HUMAN	Hs.632565	Homo sapiens	heterogeneous nuclear ribonucleoprotein K; similar to heterogeneous nuclear ribonucleoprotein K
HNRPK_HUMAN	Hs.522257	Homo sapiens	heterogeneous nuclear ribonucleoprotein K; similar to heterogeneous nuclear ribonucleoprotein K
CAZA1_HUMAN	Hs.514934	Homo sapiens	capping protein (actin filament) muscle Z-line, alpha 1
TPM4_HUMAN	Hs.631618	Homo sapiens	tropomyosin 4
HSP7C_HUMAN	Hs.180414	Homo sapiens	heat shock 70kDa protein 8
KPYM_HUMAN	Hs.534770	Homo sapiens	similar to Pyruvate kinase, isozymes M1/M2 (Pyruvate kinase muscle isozyme) (Cytosolic thyroid hormone-binding protein) (CTHBP) (THBP1); pyruvate kinase, muscle
ANXA1_HUMAN	Hs.494173	Homo sapiens	annexin A1
PSME1_HUMAN	Hs.75348	Homo sapiens	proteasome (prosome, macropain) activator subunit 1 (PA28 alpha)
TPIS_HUMAN	Hs.524219	Homo sapiens	TPI1 pseudogene; triosephosphate isomerase 1
PGAM1_HUMAN	Hs.592599	Homo sapiens	phosphoglycerate mutase 1 (brain)
PGAM1_HUMAN	Hs.632918	Homo sapiens	phosphoglycerate mutase 1 (brain)
LMNB2_HUMAN	Hs.538286	Homo sapiens	lamin B2
1433E_HUMAN	Hs.591239	Homo sapiens	similar to 14-3-3 protein epsilon (14-3-3E) (Mitochondrial import stimulation factor L subunit) (MSF L); tyrosine 3-monooxygenase/tryptophan 5-monooxygenase activation protein, epsilon polypeptide
1433E_HUMAN	Hs.513851	Homo sapiens	similar to 14-3-3 protein epsilon (14-3-3E) (Mitochondrial import stimulation factor L subunit) (MSF L); tyrosine 3-monooxygenase/tryptophan 5-monooxygenase activation protein, epsilon polypeptide
PDLI1_HUMAN	Hs.368525	Homo sapiens	PDZ and LIM domain 1
OTUB1_HUMAN	Hs.473788	Homo sapiens	OTU domain, ubiquitin aldehyde binding 1
LMNA_HUMAN	Hs.594444	Homo sapiens	lamin A/C
ENOA_HUMAN	Hs.517145	Homo sapiens	enolase 1, (alpha)
SODM_HUMAN	Hs.487046	Homo sapiens	superoxide dismutase 2, mitochondrial
UGDH_HUMAN	Hs.572518	Homo sapiens	UDP-glucose dehydrogenase
ANXA5_HUMAN	Hs.480653	Homo sapiens	annexin A5
ENOG_HUMAN	Hs.511915	Homo sapiens	enolase 2 (gamma, neuronal)
ERO1A_HUMAN	Hs.592304	Homo sapiens	ERO1-like (S. cerevisiae)
RAN_HUMAN	Hs.10842	Homo sapiens	RAN, member RAS oncogene family
TPM1_HUMAN	Hs.133892	Homo sapiens	tropomyosin 1 (alpha)
VDAC2_HUMAN	Hs.355927	Homo sapiens	voltage-dependent anion channel 2
1433B_HUMAN	Hs.643544	Homo sapiens	tyrosine 3-monooxygenase/tryptophan 5-monooxygenase

			activation protein, beta polypeptide
ENOB_HUMAN	Hs.224171	Homo sapiens	enolase 3 (beta, muscle)
1433S_HUMAN	Hs.523718	Homo sapiens	stratifin
TPM3_HUMAN	Hs.654421	Homo sapiens	tropomyosin 3
TPM3_HUMAN	Hs.535581	Homo sapiens	tropomyosin 3
TPM3_HUMAN	Hs.644306	Homo sapiens	tropomyosin 3
TKT_HUMAN	Hs.89643	Homo sapiens	transketolase
HNRPD_HUMAN	Hs.480073	Homo sapiens	heterogeneous nuclear ribonucleoprotein D (AU-rich element RNA binding protein 1, 37kDa)
PRS10_HUMAN	Hs.156171	Homo sapiens	proteasome (prosome, macropain) 26S subunit, ATPase, 6
ANXA2_HUMAN	Hs.591361	Homo sapiens	annexin A2 pseudogene 3; annexin A2; annexin A2 pseudogene 1
ANXA2_HUMAN	Hs.546235	Homo sapiens	annexin A2 pseudogene 3; annexin A2; annexin A2 pseudogene 1
ANXA2_HUMAN	Hs.511605	Homo sapiens	annexin A2 pseudogene 3; annexin A2; annexin A2 pseudogene 1

Table 2-3. Biological Function and Related Pathways of ^{13}C Labeled Proteins in Human UM1 Oral Cancer Cells

UNIGENE ID	Gene name	Related Pathway
Hs.643544	14-3-3 protein beta	Cell cycle, Oocyte meiosis, Neurotrophin signaling pathway
Hs.513851, Hs.591239	14-3-3 protein epsilon	Cell cycle, Oocyte meiosis, Neurotrophin signaling pathway
Hs.492407	14-3-3 protein zeta	Cell cycle, Oocyte meiosis, Neurotrophin signaling pathway, Pathogenic Escherichia coli infection
Hs.494173	annexin A1	Corticosteroids and cardioprotection
Hs.517145	enolase 1, (alpha)	Glycolysis Pathway
Hs.517145	enolase 1, (alpha)	Glycolysis / Gluconeogenesis, RNA degradation
Hs.511915	enolase 2 (gamma, neuronal)	Glycolysis / Gluconeogenesis, RNA degradation
Hs.224171	enolase 3 (beta, muscle)	Glycolysis / Gluconeogenesis, RNA degradation
Hs.592304	ERO1-like (S. cerevisiae)	Vibrio cholerae infection
Hs.592490	fumarate hydratase	Citrate cycle (TCA cycle), Pathways in cancer, Renal cell carcinoma
Hs.605502, Hs.710890	glucose-regulated protein, 78kDa	Prion Pathway, Stathmin and breast cancer resistance to antimicrotubule agents, Antigen processing and presentation, Prion diseases
Hs.315562	glutamate-cysteine ligase, modifier subunit	Glutathione metabolism
Hs.180414	heat shock 70kDa protein 8	Spliceosome, MAPK signaling pathway, Endocytosis, Antigen processing and presentation
Hs.522257, Hs.632565	heterogeneous nuclear ribonucleoprotein K	Spliceosome
Hs.654400	IMP (inosine monophosphate) dehydrogenase 2	Purine metabolism, Drug metabolism
Hs.594444	lamin A/C	Caspase Cascade in Apoptosis, Induction of apoptosis through DR3 and DR4/5 Death Receptors , FAS signaling pathway (CD95), HIV-I Nef, TNFR1 Signaling Pathway,Hypertrophic cardiomyopathy (HCM), Arrhythmogenic right ventricular cardiomyopathy (ARVC), Dilated cardiomyopathy
Hs.538286	lamin B2	Caspase Cascade in Apoptosis, FAS signaling pathway (CD95), TNFR1 Signaling Pathway
Hs.592599, Hs.632918	phosphoglycerate mutase 1 (brain)	Glycolysis Pathway
Hs.592599, Hs.632918	phosphoglycerate mutase 1 (brain)	Glycolysis / Gluconeogenesis
Hs.632918	phosphoglycerate mutase 1 pseudogene	Glycolysis Pathway
Hs.156171	proteasome (prosome, macropain) 26S subunit, ATPase, 6	Proteasome
Hs.75348	proteasome (prosome, macropain) activator subunit 1 (PA28 alpha)	Proteasome, Antigen processing and presentation
Hs.534770	Pyruvate kinase, isozymes M1/M2	Glycolysis / Gluconeogenesis, Purine metabolism, Pyruvate metabolism, Type II diabetes mellitus

Hs.10842	RAN, member RAS oncogene family	Mechanism of Protein Import into the Nucleus, Sumoylation by RanBP2 Regulates Transcriptional Repression, Role of Ran in mitotic spindle regulation, Cycling of Ran in nucleocytoplasmic transport
Hs.523718	stratifin	Estrogen-responsive protein Efp controls cell cycle and breast tumors growth
Hs.523718	stratifin	Cell cycle, p53 signaling pathway, Aldosterone-regulated sodium reabsorption
Hs.487046	superoxide dismutase 2, mitochondrial	Erythropoietin mediated neuroprotection through NF-kB
Hs.487046	superoxide dismutase 2, mitochondrial	Huntington's disease
Hs.524219	TPI1 pseudogene; triosephosphate isomerase 1	Glycolysis / Gluconeogenesis, Fructose and mannose metabolism, Inositol phosphate metabolism
Hs.89643	transketolase	Pentose phosphate pathway
Hs.133892	tropomyosin 1 (alpha)	Cardiac muscle contraction, Hypertrophic cardiomyopathy (HCM), Dilated cardiomyopathy
Hs.300772	tropomyosin 2 (beta)	Cardiac muscle contraction, Hypertrophic cardiomyopathy (HCM), Dilated cardiomyopathy
Hs.535581, Hs.644306, Hs.654421	tropomyosin 3	Cardiac muscle contraction, Pathways in cancer, Thyroid cancer, Hypertrophic cardiomyopathy (HCM), Dilated cardiomyopathy
Hs.631618	tropomyosin 4	Cardiac muscle contraction, Hypertrophic cardiomyopathy (HCM), Dilated cardiomyopathy
Hs.572518	UDP-glucose dehydrogenase	Pentose and glucuronate interconversions, Ascorbate and aldarate metabolism, Starch and sucrose metabolism, Amino sugar and nucleotide sugar metabolism
Hs.355927	voltage-dependent anion channel 2	Calcium signaling pathway, Parkinson's disease, Huntington's disease

Table 2-4. Differential Identification of Proteins siCtrl UM1 Cells amd siTKT UM1 Cells

siCtrl UM1		**siTKT UM1**	
CH10_HUMAN	10 kDa heat shock protein, mitochondrial OS=Homo sapiens GN=HSPE1 PE=1 SV=2	ADT2_HUMAN	ADP/ATP translocase 2 OS=Homo sapiens GN=SLC25A5 PE=1 SV=6
1A1L1_HUMAN	1-aminocyclopropane-1-carboxylate synthase-like protein 1 OS=Homo sapiens GN=ACCS PE=2 SV=1	ARF5_HUMAN	ADP-ribosylation factor 5 OS=Homo sapiens GN=ARF5 PE=1 SV=2
PRS6A_HUMAN	26S protease regulatory subunit 6A OS=Homo sapiens GN=PSMC3 PE=1 SV=3	ALPK3_HUMAN	Alpha-protein kinase 3 OS=Homo sapiens GN=ALPK3 PE=2 SV=1
PRS6B_HUMAN	26S protease regulatory subunit 6B OS=Homo sapiens GN=PSMC4 PE=1 SV=2	APIP_HUMAN	APAF1-interacting protein OS=Homo sapiens GN=APIP PE=1 SV=1
AIM1_HUMAN	Absent in melanoma 1 protein OS=Homo sapiens GN=AIM1 PE=1 SV=3	ATX2L_HUMAN	Ataxin-2-like protein OS=Homo sapiens GN=ATXN2L PE=1 SV=2
ARP2_HUMAN	Actin-related protein 2 OS=Homo sapiens GN=ACTR2 PE=1 SV=1	BZW1_HUMAN	Basic leucine zipper and W2 domain-containing protein 1 OS=Homo sapiens GN=BZW1 PE=1 SV=1
AARD_HUMAN	Alanine and arginine-rich domain-containing protein OS=Homo sapiens GN=AARD PE=2 SV=1	C1TC_HUMAN	C-1-tetrahydrofolate synthase, cytoplasmic OS=Homo sapiens GN=MTHFD1 PE=1 SV=3
AK1A1_HUMAN	Alcohol dehydrogenase [NADP+] OS=Homo sapiens GN=AKR1A1 PE=1 SV=3	C4BPB_HUMAN	C4b-binding protein beta chain OS=Homo sapiens GN=C4BPB PE=1 SV=1
ACTZ_HUMAN	Alpha-centractin OS=Homo sapiens GN=ACTR1A PE=1 SV=1	CCAR1_HUMAN	Cell division cycle and apoptosis regulator protein 1 OS=Homo sapiens GN=CCAR1 PE=1 SV=2
ALMS1_HUMAN	Alstrom syndrome protein 1 OS=Homo sapiens GN=ALMS1 PE=1 SV=2	COPB2_HUMAN	Coatomer subunit beta' OS=Homo sapiens GN=COPB2 PE=1 SV=2
AMPD1_HUMAN	AMP deaminase 1 OS=Homo sapiens GN=AMPD1 PE=1 SV=1	CYC_HUMAN	Cytochrome c OS=Homo sapiens GN=CYCS PE=1 SV=2
ANR31_HUMAN	Ankyrin repeat domain-containing protein 31 OS=Homo sapiens GN=ANKRD31 PE=5 SV=2	CX6B1_HUMAN	Cytochrome c oxidase subunit 6B1 OS=Homo sapiens GN=COX6B1 PE=1 SV=2
ACINU_HUMAN	Apoptotic chromatin condensation inducer in the nucleus OS=Homo sapiens GN=ACIN1 PE=1 SV=1	NCK1_HUMAN	Cytoplasmic protein NCK1 OS=Homo sapiens GN=NCK1 PE=1 SV=1
ATD3A_HUMAN	ATPase family AAA domain-containing protein 3A OS=Homo sapiens GN=ATAD3A PE=1 SV=2	DUT_HUMAN	Deoxyuridine 5'-triphosphate nucleotidohydrolase, mitochondrial OS=Homo sapiens GN=DUT PE=1 SV=3
KU70_HUMAN	ATP-dependent DNA helicase 2 subunit 1 OS=Homo sapiens GN=XRCC6 PE=1 SV=2	DEST_HUMAN	Destrin OS=Homo sapiens GN=DSTN PE=1 SV=3
DDX3X_HUMAN	ATP-dependent RNA helicase	RPAB1_HUMAN	DNA-directed RNA polymerases

	DDX3X OS=Homo sapiens GN=DDX3X PE=1 SV=3		I, II, and III subunit RPABC1 OS=Homo sapiens GN=POLR2E PE=1 SV=4
DDX3Y_HUMAN	ATP-dependent RNA helicase DDX3Y OS=Homo sapiens GN=DDX3Y PE=1 SV=2	DNJA2_HUMAN	DnaJ homolog subfamily A member 2 OS=Homo sapiens GN=DNAJA2 PE=1 SV=1
B2MG_HUMAN	Beta-2-microglobulin OS=Homo sapiens GN=B2M PE=1 SV=1	MRE11_HUMAN	Double-strand break repair protein MRE11A OS=Homo sapiens GN=MRE11A PE=1 SV=3
KLOTB_HUMAN	Beta-klotho OS=Homo sapiens GN=KLB PE=1 SV=1	EPAS1_HUMAN	Endothelial PAS domain-containing protein 1 OS=Homo sapiens GN=EPAS1 PE=1 SV=3
BOD1L_HUMAN	Biorientation of chromosomes in cell division protein 1-like OS=Homo sapiens GN=BOD1L PE=1 SV=2	IF4A3_HUMAN	Eukaryotic initiation factor 4A-III OS=Homo sapiens GN=EIF4A3 PE=1 SV=4
CALD1_HUMAN	Caldesmon OS=Homo sapiens GN=CALD1 PE=1 SV=2	IF4G1_HUMAN	Eukaryotic translation initiation factor 4 gamma 1 OS=Homo sapiens GN=EIF4G1 PE=1 SV=3
CAN1_HUMAN	Calpain-1 catalytic subunit OS=Homo sapiens GN=CAPN1 PE=1 SV=1	TBL1R_HUMAN	F-box-like/WD repeat-containing protein TBL1XR1 OS=Homo sapiens GN=TBL1XR1 PE=1 SV=1
CD44_HUMAN	CD44 antigen OS=Homo sapiens GN=CD44 PE=1 SV=2	LEG12_HUMAN	Galectin-12 OS=Homo sapiens GN=LGALS12 PE=1 SV=1
CNBP_HUMAN	Cellular nucleic acid-binding protein OS=Homo sapiens GN=CNBP PE=1 SV=1	TF2H4_HUMAN	General transcription factor IIH subunit 4 OS=Homo sapiens GN=GTF2H4 PE=2 SV=1
CP250_HUMAN	Centrosome-associated protein CEP250 OS=Homo sapiens GN=CEP250 PE=1 SV=2	G6PI_HUMAN	Glucose-6-phosphate isomerase OS=Homo sapiens GN=GPI PE=1 SV=4
CISY_HUMAN	Citrate synthase, mitochondrial OS=Homo sapiens GN=CS PE=1 SV=2	G3PT_HUMAN	Glyceraldehyde-3-phosphate dehydrogenase, testis-specific OS=Homo sapiens GN=GAPDHS PE=1 SV=2
CC147_HUMAN	Coiled-coil domain-containing protein 147 OS=Homo sapiens GN=CCDC147 PE=2 SV=1	H2AX_HUMAN	Histone H2A.x OS=Homo sapiens GN=H2AFX PE=1 SV=2
CNKR2_HUMAN	Connector enhancer of kinase suppressor of ras 2 OS=Homo sapiens GN=CNKSR2 PE=1 SV=1	H2B1A_HUMAN	Histone H2B type 1-A OS=Homo sapiens GN=HIST1H2BA PE=1 SV=3
CORO7_HUMAN	Coronin-7 OS=Homo sapiens GN=CORO7 PE=1 SV=2	H2B1B_HUMAN	Histone H2B type 1-B OS=Homo sapiens GN=HIST1H2BB PE=1 SV=2
CSMD2_HUMAN	CUB and sushi domain-containing protein 2 OS=Homo sapiens GN=CSMD2 PE=1 SV=2	H2BFS_HUMAN	Histone H2B type F-S OS=Homo sapiens GN=H2BFS PE=1 SV=2
CBPC3_HUMAN	Cytosolic carboxypeptidase 3 OS=Homo sapiens GN=AGBL3 PE=2 SV=2	H33_HUMAN	Histone H3.3 OS=Homo sapiens GN=H3F3A PE=1 SV=2
DCD_HUMAN	Dermcidin OS=Homo sapiens GN=DCD PE=1 SV=2	HORN_HUMAN	Hornerin OS=Homo sapiens GN=HRNR PE=1 SV=2
DIP2C_HUMAN	Disco-interacting protein 2	IGSF1_HUMAN	Immunoglobulin superfamily

	homolog C OS=Homo sapiens GN=DIP2C PE=2 SV=2		member 1 OS=Homo sapiens GN=IGSF1 PE=1 SV=3
DDB1_HUMAN	DNA damage-binding protein 1 OS=Homo sapiens GN=DDB1 PE=1 SV=1	LPPRC_HUMAN	Leucine-rich PPR motif-containing protein, mitochondrial OS=Homo sapiens GN=LRPPRC PE=1 SV=3
DJB11_HUMAN	DnaJ homolog subfamily B member 11 OS=Homo sapiens GN=DNAJB11 PE=1 SV=1	LHPL3_HUMAN	Lipoma HMGIC fusion partner-like 3 protein OS=Homo sapiens GN=LHFPL3 PE=2 SV=2
DJC11_HUMAN	DnaJ homolog subfamily C member 11 OS=Homo sapiens GN=DNAJC11 PE=1 SV=2	SYK_HUMAN	Lysyl-tRNA synthetase OS=Homo sapiens GN=KARS PE=1 SV=3
ENC1_HUMAN	Ectoderm-neural cortex protein 1 OS=Homo sapiens GN=ENC1 PE=1 SV=2	MAP4_HUMAN	Microtubule-associated protein 4 OS=Homo sapiens GN=MAP4 PE=1 SV=3
ENC2_HUMAN	Ectoderm-neural cortex protein 2 OS=Homo sapiens GN=KLHL25 PE=2 SV=1	MARE1_HUMAN	Microtubule-associated protein RP/EB family member 1 OS=Homo sapiens GN=MAPRE1 PE=1 SV=3
EFTU_HUMAN	Elongation factor Tu, mitochondrial OS=Homo sapiens GN=TUFM PE=1 SV=2	MARE3_HUMAN	Microtubule-associated protein RP/EB family member 3 OS=Homo sapiens GN=MAPRE3 PE=1 SV=1
ERP29_HUMAN	Endoplasmic reticulum resident protein 29 OS=Homo sapiens GN=ERP29 PE=1 SV=4	M3K9_HUMAN	Mitogen-activated protein kinase kinase kinase 9 OS=Homo sapiens GN=MAP3K9 PE=1 SV=3
EIF1B_HUMAN	Eukaryotic translation initiation factor 1b OS=Homo sapiens GN=EIF1B PE=1 SV=2	MRP6_HUMAN	Multidrug resistance-associated protein 6 OS=Homo sapiens GN=ABCC6 PE=1 SV=2
IF4H_HUMAN	Eukaryotic translation initiation factor 4H OS=Homo sapiens GN=EIF4H PE=1 SV=5	MTPN_HUMAN	Myotrophin OS=Homo sapiens GN=MTPN PE=1 SV=2
IF5A1_HUMAN	Eukaryotic translation initiation factor 5A-1 OS=Homo sapiens GN=EIF5A PE=1 SV=2	NAT8L_HUMAN	N-acetyltransferase 8-like protein OS=Homo sapiens GN=NAT8L PE=2 SV=3
IF5AL_HUMAN	Eukaryotic translation initiation factor 5A-1-like OS=Homo sapiens GN=EIF5AL1 PE=1 SV=2	NCS1_HUMAN	Neuronal calcium sensor 1 OS=Homo sapiens GN=FREQ PE=1 SV=2
IF5A2_HUMAN	Eukaryotic translation initiation factor 5A-2 OS=Homo sapiens GN=EIF5A2 PE=1 SV=3	GANAB_HUMAN	Neutral alpha-glucosidase AB OS=Homo sapiens GN=GANAB PE=1 SV=3
CAZA1_HUMAN	F-actin-capping protein subunit alpha-1 OS=Homo sapiens GN=CAPZA1 PE=1 SV=3	NCOA1_HUMAN	Nuclear receptor coactivator 1 OS=Homo sapiens GN=NCOA1 PE=1 SV=3
CAZA2_HUMAN	F-actin-capping protein subunit alpha-2 OS=Homo sapiens GN=CAPZA2 PE=1 SV=3	NUCKS_HUMAN	Nuclear ubiquitous casein and cyclin-dependent kinases substrate OS=Homo sapiens GN=NUCKS1 PE=1 SV=1
CAPZB_HUMAN	F-actin-capping protein subunit beta OS=Homo sapiens GN=CAPZB PE=1 SV=4	NOLC1_HUMAN	Nucleolar and coiled-body phosphoprotein 1 OS=Homo sapiens GN=NOLC1 PE=1 SV=2
FAS_HUMAN	Fatty acid synthase OS=Homo sapiens GN=FASN PE=1 SV=3	NP1L4_HUMAN	Nucleosome assembly protein 1-like 4 OS=Homo sapiens

			GN=NAP1L4 PE=1 SV=1
FLNA_HUMAN	Filamin-A OS=Homo sapiens GN=FLNA PE=1 SV=4	PCBP3_HUMAN	Poly(rC)-binding protein 3 OS=Homo sapiens GN=PCBP3 PE=1 SV=1
FLNC_HUMAN	Filamin-C OS=Homo sapiens GN=FLNC PE=1 SV=3	PSB4_HUMAN	Proteasome subunit beta type-4 OS=Homo sapiens GN=PSMB4 PE=1 SV=4
GPTC8_HUMAN	G patch domain-containing protein 8 OS=Homo sapiens GN=GPATCH8 PE=1 SV=2	F102B_HUMAN	Protein FAM102B OS=Homo sapiens GN=FAM102B PE=1 SV=2
LG3BP_HUMAN	Galectin-3-binding protein OS=Homo sapiens GN=LGALS3BP PE=1 SV=1	F75A1_HUMAN	Protein FAM75A1 OS=Homo sapiens GN=FAM75A1 PE=2 SV=1
GFAP_HUMAN	Glial fibrillary acidic protein OS=Homo sapiens GN=GFAP PE=1 SV=1	F75A2_HUMAN	Protein FAM75A2 OS=Homo sapiens GN=FAM75A2 PE=3 SV=1
GLRX3_HUMAN	Glutaredoxin-3 OS=Homo sapiens GN=GLRX3 PE=1 SV=2	F75A4_HUMAN	Protein FAM75A4 OS=Homo sapiens GN=FAM75A4 PE=3 SV=2
C1GLT_HUMAN	Glycoprotein-N-acetylgalactosamine 3-beta-galactosyltransferase 1 OS=Homo sapiens GN=C1GALT1 PE=1 SV=1	F75A6_HUMAN	Protein FAM75A6 OS=Homo sapiens GN=FAM75A6 PE=1 SV=1
LARG2_HUMAN	Glycosyltransferase-like protein LARGE2 OS=Homo sapiens GN=GYLTL1B PE=2 SV=2	FA98C_HUMAN	Protein FAM98C OS=Homo sapiens GN=FAM98C PE=2 SV=1
KAD3_HUMAN	GTP:AMP phosphotransferase mitochondrial OS=Homo sapiens GN=AK3 PE=1 SV=4	S10AD_HUMAN	Protein S100-A13 OS=Homo sapiens GN=S100A13 PE=1 SV=1
GBB2_HUMAN	Guanine nucleotide-binding protein G(I)/G(S)/G(T) subunit beta-2 OS=Homo sapiens GN=GNB2 PE=1 SV=3	S10A6_HUMAN	Protein S100-A6 OS=Homo sapiens GN=S100A6 PE=1 SV=1
GNAL_HUMAN	Guanine nucleotide-binding protein G(olf) subunit alpha OS=Homo sapiens GN=GNAL PE=1 SV=1	NDK8_HUMAN	Putative nucleoside diphosphate kinase OS=Homo sapiens GN=NME2P1 PE=5 SV=1
GNAS1_HUMAN	Guanine nucleotide-binding protein G(s) subunit alpha isoforms XLas OS=Homo sapiens GN=GNAS PE=1 SV=2	RBM3_HUMAN	Putative RNA-binding protein 3 OS=Homo sapiens GN=RBM3 PE=1 SV=1
GBB4_HUMAN	Guanine nucleotide-binding protein subunit beta-4 OS=Homo sapiens GN=GNB4 PE=1 SV=3	GDIA_HUMAN	Rab GDP dissociation inhibitor alpha OS=Homo sapiens GN=GDI1 PE=1 SV=2
HSP74_HUMAN	Heat shock 70 kDa protein 4 OS=Homo sapiens GN=HSPA4 PE=1 SV=4	RB_HUMAN	Retinoblastoma-associated protein OS=Homo sapiens GN=RB1 PE=1 SV=2
HNRCL_HUMAN	Heterogeneous nuclear ribonucleoprotein C-like 1 OS=Homo sapiens GN=HNRNPCL1 PE=1 SV=1	RGP1_HUMAN	Retrograde Golgi transport protein RGP1 homolog OS=Homo sapiens GN=RGP1 PE=2 SV=1
H2B1C_HUMAN	Histone H2B type 1-C/E/F/G/I OS=Homo sapiens GN=HIST1H2BC PE=1 SV=4	ELOA2_HUMAN	RNA polymerase II transcription factor SIII subunit A2 OS=Homo sapiens GN=TCEB3B PE=1

			SV=2
H2B1L_HUMAN	Histone H2B type 1-L OS=Homo sapiens GN=HIST1H2BL PE=1 SV=3	RBM39_HUMAN	RNA-binding protein 39 OS=Homo sapiens GN=RBM39 PE=1 SV=2
H2B3B_HUMAN	Histone H2B type 3-B OS=Homo sapiens GN=HIST3H2BB PE=1 SV=3	METK2_HUMAN	S-adenosylmethionine synthetase isoform type-2 OS=Homo sapiens GN=MAT2A PE=1 SV=1
HJURP_HUMAN	Holliday junction recognition protein OS=Homo sapiens GN=HJURP PE=1 SV=2	SCRN1_HUMAN	Secernin-1 OS=Homo sapiens GN=SCRN1 PE=1 SV=2
ITB1_HUMAN	Integrin beta-1 OS=Homo sapiens GN=ITGB1 PE=1 SV=2	STK38_HUMAN	Serine/threonine-protein kinase 38 OS=Homo sapiens GN=STK38 PE=1 SV=1
ITB4_HUMAN	Integrin beta-4 OS=Homo sapiens GN=ITGB4 PE=1 SV=4	2AAA_HUMAN	Serine/threonine-protein phosphatase 2A 65 kDa regulatory subunit A alpha isoform OS=Homo sapiens GN=PPP2R1A PE=1 SV=4
ILF3_HUMAN	Interleukin enhancer-binding factor 3 OS=Homo sapiens GN=ILF3 PE=1 SV=3	PP1B_HUMAN	Serine/threonine-protein phosphatase PP1-beta catalytic subunit OS=Homo sapiens GN=PPP1CB PE=1 SV=3
ILRL2_HUMAN	Interleukin-1 receptor-like 2 OS=Homo sapiens GN=IL1RL2 PE=2 SV=2	SUCA_HUMAN	Succinyl-CoA ligase [GDP-forming] subunit alpha, mitochondrial OS=Homo sapiens GN=SUCLG1 PE=1 SV=4
IQEC3_HUMAN	IQ motif and SEC7 domain-containing protein 3 OS=Homo sapiens GN=IQSEC3 PE=2 SV=3	TBD2A_HUMAN	TBC1 domain family member 2A OS=Homo sapiens GN=TBC1D2 PE=1 SV=2
KBTB3_HUMAN	Kelch repeat and BTB domain-containing protein 3 OS=Homo sapiens GN=KBTBD3 PE=2 SV=2	TCPE_HUMAN	T-complex protein 1 subunit epsilon OS=Homo sapiens GN=CCT5 PE=1 SV=1
KHDR1_HUMAN	KH domain-containing, RNA-binding, signal transduction-associated protein 1 OS=Homo sapiens GN=KHDRBS1 PE=1 SV=1	TCPG_HUMAN	T-complex protein 1 subunit gamma OS=Homo sapiens GN=CCT3 PE=1 SV=4
LGUL_HUMAN	Lactoylglutathione lyase OS=Homo sapiens GN=GLO1 PE=1 SV=4	TRI29_HUMAN	Tripartite motif-containing protein 29 OS=Homo sapiens GN=TRIM29 PE=1 SV=2
LAMB3_HUMAN	Laminin subunit beta-3 OS=Homo sapiens GN=LAMB3 PE=1 SV=1	UBN1_HUMAN	Ubinuclein-1 OS=Homo sapiens GN=UBN1 PE=1 SV=2
LAMP1_HUMAN	Lysosome-associated membrane glycoprotein 1 OS=Homo sapiens GN=LAMP1 PE=1 SV=3		
LAMP2_HUMAN	Lysosome-associated membrane glycoprotein 2 OS=Homo sapiens GN=LAMP2 PE=1 SV=2		
MTBP_HUMAN	Mdm2-binding protein OS=Homo sapiens GN=MTBP PE=1 SV=1		
MT1G_HUMAN	Metallothionein-1G OS=Homo sapiens GN=MT1G PE=1 SV=2		

MT1X_HUMAN	Metallothionein-1X OS=Homo sapiens GN=MT1X PE=1 SV=1		
IMMT_HUMAN	Mitochondrial inner membrane protein OS=Homo sapiens GN=IMMT PE=1 SV=1		
MK67I_HUMAN	MKI67 FHA domain-interacting nucleolar phosphoprotein OS=Homo sapiens GN=MKI67IP PE=1 SV=1		
MUC19_HUMAN	Mucin-19 OS=Homo sapiens GN=MUC19 PE=1 SV=2		
MYL9_HUMAN	Myosin regulatory light polypeptide 9 OS=Homo sapiens GN=MYL9 PE=1 SV=4		
MYO9A_HUMAN	Myosin-IXa OS=Homo sapiens GN=MYO9A PE=1 SV=1		
MYO5C_HUMAN	Myosin-Vc OS=Homo sapiens GN=MYO5C PE=1 SV=1		
MARCS_HUMAN	Myristoylated alanine-rich C-kinase substrate OS=Homo sapiens GN=MARCKS PE=1 SV=4		
NEBU_HUMAN	Nebulin OS=Homo sapiens GN=NEB PE=1 SV=3		
OAT_HUMAN	Ornithine aminotransferase, mitochondrial OS=Homo sapiens GN=OAT PE=1 SV=1		
PAL4B_HUMAN	Peptidylprolyl cis-trans isomerase A-like 4B OS=Homo sapiens GN=PPIAL4B PE=1 SV=1		
PPIE_HUMAN	Peptidyl-prolyl cis-trans isomerase E OS=Homo sapiens GN=PPIE PE=1 SV=1		
PPIF_HUMAN	Peptidyl-prolyl cis-trans isomerase F, mitochondrial OS=Homo sapiens GN=PPIF PE=1 SV=1		
PRDX2_HUMAN	Peroxiredoxin-2 OS=Homo sapiens GN=PRDX2 PE=1 SV=5		
PRDX6_HUMAN	Peroxiredoxin-6 OS=Homo sapiens GN=PRDX6 PE=1 SV=3		
PHF5A_HUMAN	PHD finger-like domain-containing protein 5A OS=Homo sapiens GN=PHF5A PE=1 SV=1		
PGK2_HUMAN	Phosphoglycerate kinase 2 OS=Homo sapiens GN=PGK2 PE=1 SV=3		
PKP3_HUMAN	Plakophilin-3 OS=Homo sapiens GN=PKP3 PE=1 SV=1		
HCN3_HUMAN	Potassium/sodium hyperpolarization-activated cyclic nucleotide-gated channel 3 OS=Homo sapiens GN=HCN3 PE=2 SV=2		

PRP8_HUMAN	Pre-mRNA-processing-splicing factor 8 OS=Homo sapiens GN=PRPF8 PE=1 SV=2		
DDX5_HUMAN	Probable ATP-dependent RNA helicase DDX5 OS=Homo sapiens GN=DDX5 PE=1 SV=1		
DDX59_HUMAN	Probable ATP-dependent RNA helicase DDX59 OS=Homo sapiens GN=DDX59 PE=1 SV=1		
PCNA_HUMAN	Proliferating cell nuclear antigen OS=Homo sapiens GN=PCNA PE=1 SV=1		
PSME1_HUMAN	Proteasome activator complex subunit 1 OS=Homo sapiens GN=PSME1 PE=1 SV=1		
PSA1_HUMAN	Proteasome subunit alpha type-1 OS=Homo sapiens GN=PSMA1 PE=1 SV=1		
AHNK2_HUMAN	Protein AHNAK2 OS=Homo sapiens GN=AHNAK2 PE=1 SV=2		
CYR61_HUMAN	Protein CYR61 OS=Homo sapiens GN=CYR61 PE=1 SV=1		
R13AX_HUMAN	Putative 60S ribosomal protein L13a-like MGC87657 OS=Homo sapiens PE=5 SV=1		
AXA2L_HUMAN	Putative annexin A2-like protein OS=Homo sapiens GN=ANXA2P2 PE=5 SV=2		
RAB10_HUMAN	Ras-related protein Rab-10 OS=Homo sapiens GN=RAB10 PE=1 SV=1		
RAB14_HUMAN	Ras-related protein Rab-14 OS=Homo sapiens GN=RAB14 PE=1 SV=4		
RAB1A_HUMAN	Ras-related protein Rab-1A OS=Homo sapiens GN=RAB1A PE=1 SV=3		
RAB30_HUMAN	Ras-related protein Rab-30 OS=Homo sapiens GN=RAB30 PE=1 SV=2		
RALYL_HUMAN	RNA-binding Raly-like protein OS=Homo sapiens GN=RALYL PE=1 SV=2		
SAFB1_HUMAN	Scaffold attachment factor B1 OS=Homo sapiens GN=SAFB PE=1 SV=4		
SAFB2_HUMAN	Scaffold attachment factor B2 OS=Homo sapiens GN=SAFB2 PE=1 SV=1		
PP2AA_HUMAN	Serine/threonine-protein phosphatase 2A catalytic subunit alpha isoform OS=Homo sapiens GN=PPP2CA PE=1 SV=1		
PTN5_HUMAN	Tyrosine-protein phosphatase		

	non-receptor type 5 OS=Homo sapiens GN=PTPN5 PE=1 SV=3		
CV030_HUMAN	Uncharacterized protein C22orf30 OS=Homo sapiens GN=C22orf30 PE=1 SV=1		
CB034_HUMAN	Uncharacterized protein C2orf34 OS=Homo sapiens GN=C2orf34 PE=1 SV=2		
K1210_HUMAN	Uncharacterized protein KIAA1210 OS=Homo sapiens GN=KIAA1210 PE=2 SV=3		
K1614_HUMAN	Uncharacterized protein KIAA1614 OS=Homo sapiens GN=KIAA1614 PE=2 SV=2		
CV028_HUMAN	UPF0027 protein C22orf28 OS=Homo sapiens GN=C22orf28 PE=1 SV=1		
CQ028_HUMAN	UPF0663 transmembrane protein C17orf28 OS=Homo sapiens GN=C17orf28 PE=1 SV=1		
CB086_HUMAN	WD repeat-containing protein C2orf86 OS=Homo sapiens GN=C2orf86 PE=1 SV=2		

Table 3-1. ^{13}C Labeled Proteins in human BxPC-3 cells

Protein Name	# of ^{13}C Labeled Peptides	Relative % of ^{13}C Labeled Peptides
Keratin, cytoskeletal OS=Homo sapiens	2334	88.71
Tubulin beta-8 chain OS=Homo sapiens GN=TUBB8 PE=1 SV=2	61	2.32
Glyceraldehyde-3-phosphate dehydrogenase OS=Homo sapiens GN=GAPDH PE=1 SV=3	32	1.22
Heat shock 70 kDa protein OS=Homo sapiens GN=HSPA6 PE=1 SV=2	20	0.76
Heterogeneous nuclear ribonucleoprotein H OS=Homo sapiens GN=HNRNPH1 PE=1 SV=4	15	0.57
Alpha-actinin-1 OS=Homo sapiens GN=ACTN1 PE=1 SV=2	12	0.46
Aldehyde dehydrogenase family 1 member A3 OS=Homo sapiens GN=ALDH1A3 PE=1 SV=2	12	0.46
78 kDa glucose-regulated protein OS=Homo sapiens GN=HSPA5 PE=1 SV=2	11	0.42
Elongation factor 1-alpha 1 OS=Homo sapiens GN=EEF1A1 PE=1 SV=1	10	0.38
Serpin B5 OS=Homo sapiens GN=SERPINB5 PE=1 SV=2	9	0.34
Ezrin OS=Homo sapiens GN=EZR PE=1 SV=4	8	0.30
Dermcidin OS=Homo sapiens GN=DCD PE=1 SV=2	8	0.30
Alpha-enolase OS=Homo sapiens GN=ENO1 PE=1 SV=2	8	0.30
Fascin OS=Homo sapiens GN=FSCN1 PE=1 SV=3	7	0.27
Rab GDP dissociation inhibitor beta OS=Homo sapiens GN=GDI2 PE=1 SV=2	5	0.19
Neutral alpha-glucosidase AB OS=Homo sapiens GN=GANAB PE=1 SV=3	5	0.19
POTE ankyrin domain family member E OS=Homo sapiens GN=POTEE PE=1 SV=3	4	0.15
Heat shock protein beta-1 OS=Homo sapiens GN=HSPB1 PE=1 SV=2	4	0.15
Caspase-14 OS=Homo sapiens GN=CASP14 PE=1 SV=2	4	0.15
Beta-enolase OS=Homo sapiens GN=ENO3 PE=1 SV=4	4	0.15
Beta-actin-like protein 2 OS=Homo sapiens GN=ACTBL2 PE=1 SV=2	4	0.15
Actin, cytoplasmic 1 OS=Homo sapiens GN=ACTB PE=1 SV=1	4	0.15
Transketolase OS=Homo sapiens GN=TKT PE=1 SV=3	3	0.11
Transitional endoplasmic reticulum ATPase OS=Homo sapiens GN=VCP PE=1 SV=4	3	0.11
T-complex protein 1 subunit alpha OS=Homo sapiens GN=TCP1 PE=1 SV=1	3	0.11
Stress-70 protein, mitochondrial OS=Homo sapiens GN=HSPA9 PE=1 SV=2	3	0.11
Putative tubulin beta chain-like protein ENSP00000290377 OS=Homo sapiens PE=5 SV=2	3	0.11
Moesin OS=Homo sapiens GN=MSN PE=1 SV=3	3	0.11
Gamma-enolase OS=Homo sapiens GN=ENO2 PE=1 SV=3	3	0.11
Ubiquitin OS=Homo sapiens GN=RPS27A PE=1 SV=1	2	0.08

Serum albumin OS=Homo sapiens GN=ALB PE=1 SV=2	2	0.08
Rho GTPase-activating protein 1 OS=Homo sapiens GN=ARHGAP1 PE=1 SV=1	2	0.08
Protein-glutamine gamma-glutamyltransferase E OS=Homo sapiens GN=TGM3 PE=1 SV=4	2	0.08
Neutrophil gelatinase-associated lipocalin OS=Homo sapiens GN=LCN2 PE=1 SV=2	2	0.08
Junction plakoglobin OS=Homo sapiens GN=JUP PE=1 SV=3	2	0.08
Ig kappa chain C region OS=Homo sapiens GN=IGKC PE=1 SV=1	2	0.08
Fructose-bisphosphate aldolase A OS=Homo sapiens GN=ALDOA PE=1 SV=2	2	0.08
Desmoglein-1 OS=Homo sapiens GN=DSG1 PE=1 SV=1	2	0.08
Bifunctional purine biosynthesis protein PURH OS=Homo sapiens GN=ATIC PE=1 SV=3	2	0.08
Rootletin OS=Homo sapiens GN=CROCC PE=1 SV=1	1	0.04
Putative heat shock protein HSP 90-alpha A2 OS=Homo sapiens GN=HSP90AA2 PE=1 SV=2	1	0.04
Putative annexin A2-like protein OS=Homo sapiens GN=ANXA2P2 PE=5 SV=2	1	0.04
Protein-glutamine gamma-glutamyltransferase E OS=Homo sapiens GN=TGM3 PE=1 SV=4	1	0.04
Filaggrin-2 OS=Homo sapiens GN=FLG2 PE=1 SV=1	1	0.04
Corneodesmosin OS=Homo sapiens GN=CDSN PE=1 SV=2	1	0.04
Calreticulin OS=Homo sapiens GN=CALR PE=1 SV=1	1	0.04
Annexin A2 OS=Homo sapiens GN=ANXA2 PE=1 SV=2	1	0.04
Ankyrin repeat and SOCS box protein 2 OS=Homo sapiens GN=ASB2 PE=1 SV=1	1	0.04
TOTAL	**2631**	

Table 3-2. ^{13}C Labeled Proteins in human MIA PaCa-2 Cells

Protein Name	# of ^{13}C Labeled Peptides	Relative % of ^{13}C Labeled Peptides
keratin cytoskeletal	1316	44.69
Actin	348	11.82
Vimentin	256	8.69
keratin cuticular	214	7.27
Tubulin	59	2.00
POTE ankyrin domain family member E	57	1.94
Glial fibrillary acidic protein	56	1.90
Desmin	50	1.70
Heat shock 70 kDa protein	43	1.46
Putative ubiquitin carboxyl-terminal hydrolase 17-like protein 1	41	1.39
Interferon-induced guanylate-binding protein 2	33	1.12
Peripherin	32	1.09
14-3-3 protein family	31	1.05
Dynein heavy chain	21	0.71
Alpha-enolase	21	0.71
Anaphase-promoting complex subunit 5	20	0.68
Desmoplakin	17	0.58
Myosin	14	0.48
Nesprin-2	14	0.48
Alpha-internexin	12	0.41
Protocadherin Fat 1	12	0.41
Kinesin heavy chain isoform 5C	12	0.41
ATP-binding cassette transporter sub-family C	11	0.37
Neurofilament heavy polypeptide	11	0.37
Otoancorin	11	0.37
Glyceraldehyde-3-phosphate dehydrogenase	10	0.34
Neurofilament light polypeptide	10	0.34
Neurofilament medium polypeptide	10	0.34
Ezrin	9	0.31
Pyruvate kinase isozymes M1/M2	9	0.31
Putative tubulin beta chain-like protein ENSP00000290377	9	0.31
Arf-GAP with SH3 domain	8	0.27
60 kDa heat shock protein, mitochondrial	8	0.27
Girdin	8	0.27
78 kDa glucose-regulated protein	8	0.27
Annexin A1	7	0.24
Coiled-coil domain-containing protein 88B	7	0.24
Matrix-remodeling-associated protein 5	7	0.24

Thyroid hormone receptor-associated protein 3	7	0.24
Twinfilin-2	7	0.24
Nucleophosmin	6	0.20
Obscurin	6	0.20
T-complex protein	6	0.20
Moesin	5	0.17
Biotinidase	4	0.14
Rootletin	4	0.14
Probable ATP-dependent RNA helicase DDX10	4	0.14
Elongation factor 1-alpha	4	0.14
F-box only protein 18	4	0.14
Potassium voltage-gated channel subfamily H member 5	4	0.14
DNA-dependent protein kinase catalytic subunit	4	0.14
Gamma-enolase	3	0.10
Stress-70 protein, mitochondrial	3	0.10
Ig lambda chain C regions	3	0.10
Sortilin	3	0.10
A-kinase anchor protein 9	2	0.07
Retinal dehydrogenase 1	2	0.07
Uncharacterized protein C2orf67	2	0.07
Centrosome-associated protein 350	2	0.07
Forkhead-associated domain-containing protein 1	2	0.07
Keratinocyte proline-rich protein	2	0.07
Putative methyltransferase NSUN4	2	0.07
Phosphoglycerate kinase 1	2	0.07
Protein PTHB1	2	0.07
Protein PTHB1	2	0.07
Probable helicase senataxin	2	0.07
Protein Shroom3	2	0.07
Nesprin-1	2	0.07
Serine/threonine-protein kinase	2	0.07
Xin actin-binding repeat-containing protein 2	2	0.07
Afadin	1	0.03
Bullous pemphigoid antigen 1	1	0.03
Trifunctional enzyme subunit beta, mitochondrial	1	0.03
ERI1 exoribonuclease 2	1	0.03
Protein FAM98A OS	1	0.03
Leucine-rich repeat and calponin homology domain-containing protein 2	1	0.03
Neurobeachin	1	0.03
Neurofibromin	1	0.03
Putative ribosomal RNA methyltransferase NOP2	1	0.03

High affinity cAMP-specific and IBMX-insensitive 3~,5~-cyclic phosphodiesterase 8B	1	0.03
Plectin-1	1	0.03
Splicing factor 3A subunit 1	1	0.03
Schlafen family member 14	1	0.03
Structural maintenance of chromosomes protein 2	1	0.03
Succinyl-CoA ligase [GDP-forming] subunit beta, mitochondrial	1	0.03
Zinc finger protein 44	1	0.03
TOTAL	**2945**	

Table 3-3. ^{13}C Labeled Protein in Human Pancreatic Ductal Epithelial Cells

Protein Name	# of 13C Labeled Peptides	Relative % of 13C Labeled Peptides
Keratin,cytoskeletal 8 OS=Homo sapiens GN=KRT8 PE=1 SV=7	1340	59.795
Actin, cytoplasmic 1 OS=Homo sapiens GN=ACTB PE=1 SV=1	228	10.174
Actin, aortic smooth muscle OS=Homo sapiens GN=ACTA2 PE=1 SV=1	167	7.452
Beta-actin-like protein 3 OS=Homo sapiens GN=ACTBL3 PE=1 SV=1	125	5.578
POTE ankyrin domain family member E OS=Homo sapiens GN=POTEE PE=1 SV=3	90	4.016
Keratin, type II cuticular Hb5 OS=Homo sapiens GN=KRT85 PE=1 SV=1	79	3.525
78 kDa glucose-regulated protein OS=Homo sapiens GN=HSPA5 PE=1 SV=2	11	0.491
L-lactate dehydrogenase A-like 6A OS=Homo sapiens GN=LDHAL6A PE=2 SV=1	11	0.491
Annexin A2 OS=Homo sapiens GN=ANXA2 PE=1 SV=2	10	0.446
Desmoplakin OS=Homo sapiens GN=DSP PE=1 SV=3	10	0.446
60 kDa heat shock protein, mitochondrial OS=Homo sapiens GN=HSPD1 PE=1 SV=2	8	0.357
Glyceraldehyde-3-phosphate dehydrogenase OS=Homo sapiens GN=GAPDH PE=1 SV=3	8	0.357
Neurofilament heavy polypeptide OS=Homo sapiens GN=NEFH PE=1 SV=4	8	0.357
Lymphokine-activated killer T-cell-originated protein kinase OS=Homo sapiens GN=PBK PE=1 SV=3	8	0.357
WASH complex subunit 7 OS=Homo sapiens GN=KIAA1033 PE=1 SV=1	8	0.357
Pyruvate kinase isozymes M1/M2 OS=Homo sapiens GN=PKM2 PE=1 SV=4	7	0.312
Dynein heavy chain 1, axonemal OS=Homo sapiens GN=DNAH1 PE=1 SV=3	6	0.268
Heat shock 70 kDa protein 1A/1B OS=Homo sapiens GN=HSPA1A PE=1 SV=5	6	0.268
2-5A-dependent ribonuclease OS=Homo sapiens GN=RNASEL PE=1 SV=2	6	0.268
Nuclear mitotic apparatus protein 1 OS=Homo sapiens GN=NUMA1 PE=1 SV=2	5	0.223
T-complex protein 1 subunit delta OS=Homo sapiens GN=CCT4 PE=1 SV=4	5	0.223
Urotensin-2 OS=Homo sapiens GN=UTS2 PE=1 SV=1	5	0.223
Putative vomeronasal receptor-like protein 4 OS=Homo sapiens GN=VNRL4 PE=5 SV=1	5	0.223
Glial fibrillary acidic protein OS=Homo sapiens GN=GFAP PE=1 SV=1	4	0.178
Msx2-interacting protein OS=Homo sapiens GN=SPEN PE=1 SV=1	4	0.178
Myosin-1 OS=Homo sapiens GN=MYH1 PE=1 SV=3	4	0.178
High affinity cAMP-specific and IBMX-insensitive 3~,5~-cyclic phosphodiesterase 8B OS=Homo sapiens GN=PDE8B PE=1 SV=2	4	0.178
60S ribosomal protein L37a OS=Homo sapiens GN=RPL37A PE=1 SV=2	4	0.178
Nesprin-1 OS=Homo sapiens GN=SYNE1 PE=1 SV=3	4	0.178
Zinc finger protein 509 OS=Homo sapiens GN=ZNF509 PE=1 SV=2	4	0.178

Desmin OS=Homo sapiens GN=DES PE=1 SV=3	3	0.134
Hornerin OS=Homo sapiens GN=HRNR PE=1 SV=2	3	0.134
Keratinocyte proline-rich protein OS=Homo sapiens GN=KPRP PE=1 SV=1	3	0.134
Protein piccolo OS=Homo sapiens GN=PCLO PE=1 SV=3	3	0.134
Peripherin OS=Homo sapiens GN=PRPH PE=1 SV=2	3	0.134
Vimentin OS=Homo sapiens GN=VIM PE=1 SV=4	3	0.134
Forkhead-associated domain-containing protein 1 OS=Homo sapiens GN=FHAD1 PE=2 SV=2	2	0.089
Extracellular matrix protein FRAS1 OS=Homo sapiens GN=FRAS1 PE=2 SV=1	2	0.089
Golgin subfamily B member 1 OS=Homo sapiens GN=GOLGB1 PE=1 SV=2	2	0.089
RAB6-interacting golgin OS=Homo sapiens GN=GORAB PE=1 SV=1	2	0.089
Potassium voltage-gated channel subfamily KQT member 3 OS=Homo sapiens GN=KCNQ3 PE=1 SV=2	2	0.089
Keratin-like protein KRT222 OS=Homo sapiens GN=KRT222 PE=2 SV=1	2	0.089
Tyrosine-protein phosphatase non-receptor type 13 OS=Homo sapiens GN=PTPN13 PE=1 SV=2	2	0.089
Ras-related protein Rab-9A OS=Homo sapiens GN=RAB9A PE=1 SV=1	2	0.089
DNA repair protein RAD50 OS=Homo sapiens GN=RAD50 PE=1 SV=1	2	0.089
Heterogeneous nuclear ribonucleoprotein A1 OS=Homo sapiens GN=HNRNPA1 PE=1 SV=5	2	0.089
Spectrin beta chain, brain 4 OS=Homo sapiens GN=SPTBN5 PE=2 SV=1	2	0.089
Phenylalanyl-tRNA synthetase alpha chain OS=Homo sapiens GN=FARSA PE=1 SV=3	2	0.089
Tropomyosin alpha-1 chain OS=Homo sapiens GN=TPM1 PE=1 SV=2	2	0.089
Thyroid receptor-interacting protein 11 OS=Homo sapiens GN=TRIP11 PE=1 SV=2	2	0.089
Alpha-actinin-3 OS=Homo sapiens GN=ACTN3 PE=1 SV=2	1	0.045
Elongation factor Tu GTP-binding domain-containing protein 1 OS=Homo sapiens GN=EFTUD1 PE=1 SV=2	1	0.045
Serine/threonine-protein kinase mTOR OS=Homo sapiens GN=FRAP1 PE=1 SV=1	1	0.045
Interferon-induced guanylate-binding protein 2 OS=Homo sapiens GN=GBP2 PE=2 SV=3	1	0.045
Inositol 1,4,5-trisphosphate receptor type 2 OS=Homo sapiens GN=ITPR2 PE=1 SV=2	1	0.045
Antigen KI-67 OS=Homo sapiens GN=MKI67 PE=1 SV=2	1	0.045
Lysozyme C OS=Homo sapiens GN=LYZ PE=1 SV=1	1	0.045
PDZ domain-containing protein 2 OS=Homo sapiens GN=PDZD2 PE=1 SV=4	1	0.045
Heterogeneous nuclear ribonucleoprotein A1-like 2 OS=Homo sapiens GN=HNRNPA1L2 PE=2 SV=2	1	0.045
Tudor domain-containing protein 1 OS=Homo sapiens GN=TDRD1 PE=1 SV=2	1	0.045
Xin actin-binding repeat-containing protein 2 OS=Homo sapiens GN=XIRP2 PE=1 SV=2	1	0.045
Total	**2241**	

Table 3-4. ^{13}C Labeled Proteins from MIA PaCa-2 Mouse Tumor Tissue

Protein Name	# of 13C Labeled Peptides	Relative % of 13C Labeled Peptides
Keratin, cytoskeletal 80 OS=Mus musculus	384	66.32
Vimentin OS=Mus musculus GN=Vim PE=1 SV=3	106	18.31
Keratin, cuticular Hb4 OS=Mus musculus	11	1.90
Desmin OS=Mus musculus GN=Des PE=1 SV=3	10	1.73
Actin, cytoplasmic 1 OS=Mus musculus GN=Actb PE=1 SV=1	9	1.55
78 kDa glucose-regulated protein OS=Mus musculus GN=Hspa5 PE=1 SV=3	8	1.38
Annexin A1 OS=Mus musculus GN=Anxa1 PE=1 SV=2	7	1.21
ATP synthase subunit beta, mitochondrial OS=Mus musculus GN=Atp5b PE=1 SV=2	7	1.21
Beta-actin-like protein 2 OS=Mus musculus GN=Actbl2 PE=2 SV=1	4	0.69
60 kDa heat shock protein, mitochondrial OS=Mus musculus GN=Hspd1 PE=1 SV=1	4	0.69
Histone H2A type 1-F OS=Mus musculus GN=Hist1h2af PE=1 SV=3	3	0.52
Actin, alpha cardiac muscle 1 OS=Mus musculus GN=Actc1 PE=1 SV=1	2	0.35
Pancreatic alpha-amylase OS=Mus musculus GN=Amy2 PE=1 SV=1	2	0.35
Chymotrypsinogen B OS=Mus musculus GN=Ctrb1 PE=2 SV=1	2	0.35
Glycine amidinotransferase, mitochondrial OS=Mus musculus GN=Gatm PE=1 SV=1	2	0.35
Neurofilament heavy polypeptide OS=Mus musculus GN=Nefh PE=1 SV=3	2	0.35
Probable histone-lysine N-methyltransferase NSD2 OS=Mus musculus GN=Whsc1 PE=2 SV=2	2	0.35
Peripherin OS=Mus musculus GN=Prph PE=1 SV=2	2	0.35
40S ribosomal protein S24 OS=Mus musculus GN=Rps24 PE=1 SV=1	2	0.35
Tubulin alpha-1B chain OS=Mus musculus GN=Tuba1b PE=1 SV=2	2	0.35
14-3-3 protein eta OS=Mus musculus GN=Ywhah PE=1 SV=2	1	0.17
Alpha-internexin OS=Mus musculus GN=Ina PE=1 SV=2	1	0.17
Coiled-coil domain-containing protein 38 OS=Mus musculus GN=Ccdc38 PE=2 SV=1	1	0.17
Glial fibrillary acidic protein OS=Mus musculus GN=Gfap PE=1 SV=4	1	0.17
Heat shock cognate 71 kDa protein OS=Mus musculus GN=Hspa8 PE=1 SV=1	1	0.17
Myosin regulatory light chain 12B OS=Mus musculus GN=Myl12b PE=1 SV=2	1	0.17
Junction plakoglobin OS=Mus musculus GN=Jup PE=1 SV=3	1	0.17
RNA polymerase II-associated protein 1 OS=Mus musculus GN=Rpap1 PE=1 SV=2	1	0.17
Total	**579**	

Table 3-5. ^{13}C Labeled Proteins of BxPC-3 Cells: DAVID Converted Gene List

UNIPROT ACCESSION #	UNIGENE CODE	SPECIES	DATABASE FOR ANNOTATION,VISUALIZATION AND INTEGRATED DISCOVERY (DAVID) GENE NAME
ALDOA_HUMAN	Hs.513490	Homo sapiens	aldolase A, fructose-bisphosphate
UBIQ_HUMAN	Hs.546292	Homo sapiens	ribosomal protein S27a pseudogene 12
UBIQ_HUMAN	Hs.5308	Homo sapiens	ubiquitin A-52 residue ribosomal protein fusion product 1
UBIQ_HUMAN	Hs.520348	Homo sapiens	ubiquitin C
UBIQ_HUMAN	Hs.719097	Homo sapiens	ubiquitin B
UBIQ_HUMAN	Hs.356190	Homo sapiens	ubiquitin B
HNRH2_HUMAN	Hs.632828	Homo sapiens	ribosomal protein L36a pseudogene 51
K2C7_HUMAN	Hs.411501	Homo sapiens	keratin 7
CALR_HUMAN	Hs.515162	Homo sapiens	calreticulin
HSP7C_HUMAN	Hs.180414	Homo sapiens	heat shock 70kDa protein 8
K22E_HUMAN	Hs.707	Homo sapiens	keratin 2
TBB1_HUMAN	Hs.303023	Homo sapiens	tubulin, beta 1
G3P_HUMAN	Hs.592355	Homo sapiens	glyceraldehyde-3-phosphate dehydrogenase
K2C78_HUMAN	Hs.665267	Homo sapiens	keratin 78
TBB5_HUMAN	Hs.636480	Homo sapiens	tubulin, beta
K2C72_HUMAN	Hs.662013	Homo sapiens	keratin 72
K1C23_HUMAN	Hs.9029	Homo sapiens	keratin 23 (histone deacetylase inducible)
SPB5_HUMAN	Hs.55279	Homo sapiens	serpin peptidase inhibitor, clade B (ovalbumin), member 5
DSG1_HUMAN	Hs.2633	Homo sapiens	desmoglein 1
ACTN1_HUMAN	Hs.509765	Homo sapiens	actinin, alpha 1
K2C73_HUMAN	Hs.55410	Homo sapiens	keratin 73
MOES_HUMAN	Hs.87752	Homo sapiens	moesin
K22O_HUMAN	Hs.654392	Homo sapiens	keratin 76
K1C17_HUMAN	Hs.2785	Homo sapiens	keratin 17; keratin 17 pseudogene 3
HS71L_HUMAN	Hs.690634	Homo sapiens	heat shock 70kDa protein 1-like
K1C13_HUMAN	Hs.654550	Homo sapiens	keratin 13
K1C24_HUMAN	Hs.87383	Homo sapiens	keratin 24
TBB2C_HUMAN	Hs.433615	Homo sapiens	tubulin, beta 2C
NGAL_HUMAN	Hs.204238	Homo sapiens	lipocalin 2
ACTN2_HUMAN	Hs.498178	Homo sapiens	actinin, alpha 2
K2C1B_HUMAN	Hs.334989	Homo sapiens	keratin 77
K1C10_HUMAN	Hs.99936	Homo sapiens	keratin 10
HNRH1_HUMAN	Hs.604001	Homo sapiens	heterogeneous nuclear ribonucleoprotein H1 (H)
AL3A1_HUMAN	Hs.531682	Homo sapiens	aldehyde dehydrogenase 3 family, memberA1
TBB8_HUMAN	Hs.532659	Homo sapiens	tubulin, beta 8

ALBU_HUMAN	Hs.418167	Homo sapiens	albumin
GRP78_HUMAN	Hs.710890	Homo sapiens	hypothetical gene supported by AF216292; NM_005347; heat shock 70kDa protein 5 (glucose-regulated protein, 78kDa)
GRP78_HUMAN	Hs.605502	Homo sapiens	hypothetical gene supported by AF216292; NM_005347; heat shock 70kDa protein 5 (glucose-regulated protein, 78kDa)
K2C6C_HUMAN	Hs.709234	Homo sapiens	keratin 6C
FILA2_HUMAN	Hs.156124	Homo sapiens	filaggrin family member 2
H90B3_HUMAN	Hs.720330	Homo sapiens	heat shock protein 90kDa alpha (cytosolic), class B member 3 (pseudogene)
EF1A1_HUMAN	Hs.512059	Homo sapiens	eukaryotic translation elongation factor 1 alpha
K1C16_HUMAN	Hs.723586	Homo sapiens	keratin 16; keratin type 16-like
TGM3_HUMAN	Hs.2022	Homo sapiens	transglutaminase 3 (E polypeptide, protein-glutamine-gamma-glutamyltransferase)
ACTBL_HUMAN	Hs.482167	Homo sapiens	actin, beta-like 2
POTEE_HUMAN	Hs.686146	Homo sapiens	POTE ankyrin domain family, member E
AL1A3_HUMAN	Hs.459538	Homo sapiens	aldehyde dehydrogenase 1 family, member A3
GRP75_HUMAN	Hs.184233	Homo sapiens	heat shock 70kDa protein 9 (mortalin)
ENOA_HUMAN	Hs.517145	Homo sapiens	enolase 1, (alpha)
HS902_HUMAN	Hs.525600	Homo sapiens	heat shock protein 90kDa alpha (cytosolic), class A member 2; heat shock protein 90kDa alpha (cytosolic), class A member 1
ACTN4_HUMAN	Hs.270291	Homo sapiens	actinin, alpha 4
TBA4A_HUMAN	Hs.75318	Homo sapiens	tubulin, alpha 4a
K2C8_HUMAN	Hs.708445	Homo sapiens	keratin 8 pseudogene 9; similar to keratin 8; keratin 8
K2C3_HUMAN	Hs.680652	Homo sapiens	keratin 3
DCD_HUMAN	Hs.350570	Homo sapiens	dermcidin
GDIB_HUMAN	Hs.299055	Homo sapiens	GDP dissociation inhibitor 2
TBB3_HUMAN	Hs.513829	Homo sapiens	tubulin, beta 3
K1C14_HUMAN	Hs.654380	Homo sapiens	keratin 14
CDSN_HUMAN	Hs.556031	Homo sapiens	corneodesmosin
TBA3C_HUMAN	Hs.503749	Homo sapiens	tubulin, alpha 3d; tubulin, alpha 3c
TBA3C_HUMAN	Hs.349695	Homo sapiens	tubulin, alpha 3d; tubulin, alpha 3c
ANXA2_HUMAN	Hs.591361	Homo sapiens	annexin A2
K2C75_HUMAN	Hs.697046	Homo sapiens	keratin 75
K1C28_HUMAN	Hs.59736	Homo sapiens	keratin 28
TCPA_HUMAN	Hs.577662	Homo sapiens	hypothetical gene supported by BC000665; t-complex 1
TCPA_HUMAN	Hs.363137	Homo sapiens	hypothetical gene supported by BC000665; t-complex 1
GANAB_HUMAN	Hs.595071	Homo sapiens	glucosidase, alpha; neutral AB
KRT81_HUMAN	Hs.658118	Homo sapiens	keratin 81
EZRI_HUMAN	Hs.487027	Homo sapiens	hypothetical protein LOC100129652; ezrin
ASB2_HUMAN	Hs.510327	Homo sapiens	ankyrin repeat and SOCS box-containing 2

FSCN1_HUMAN	Hs.118400	Homo sapiens	fascin homolog 1, actin-bundling protein (Strongylocentrotus purpuratus)
FSCN1_HUMAN	Hs.705741	Homo sapiens	fascin homolog 1, actin-bundling protein (Strongylocentrotus purpuratus)
PUR9_HUMAN	Hs.90280	Homo sapiens	5-aminoimidazole-4-carboxamide ribonucleotide formyltransferase/IMP cyclohydrolase
PLAK_HUMAN	Hs.514174	Homo sapiens	junction plakoglobin
ACTB_HUMAN	Hs.520640	Homo sapiens	actin, beta
K2C6A_HUMAN	Hs.700779	Homo sapiens	keratin 6A
K2C4_HUMAN	Hs.654610	Homo sapiens	keratin 4
TBB2A_HUMAN	Hs.654543	Homo sapiens	tubulin, beta 2A
TBB4_HUMAN	Hs.110837	Homo sapiens	tubulin, beta 4
TBB6_HUMAN	Hs.706875	Homo sapiens	tubulin, beta 6
TBB6_HUMAN	Hs.720070	Homo sapiens	tubulin, beta 6
K1C25_HUMAN	Hs.55412	Homo sapiens	keratin 25
K2C71_HUMAN	Hs.660007	Homo sapiens	keratin 71
K2C6B_HUMAN	Hs.708950	Homo sapiens	keratin 6B
RHG01_HUMAN	Hs.138860	Homo sapiens	Rho GTPase activating protein 1
ENOG_HUMAN	Hs.511915	Homo sapiens	enolase 2 (gamma, neuronal)
IGKC_HUMAN	Hs.449621	Homo sapiens	similar to hCG26659; immunoglobulin kappa constant; similar to Ig kappa chain V-I region HK102 precursor
HS90A_HUMAN	Hs.525600	Homo sapiens	heat shock protein 90kDa alpha (cytosolic)
EF2_HUMAN	Hs.515070	Homo sapiens	eukaryotic translation elongation factor 2
ENOB_HUMAN	Hs.224171	Homo sapiens	enolase 3 (beta, muscle)
CASPE_HUMAN	Hs.466057	Homo sapiens	caspase 14, apoptosis-related cysteine peptidase
EF1A2_HUMAN	Hs.433839	Homo sapiens	eukaryotic translation elongation factor 1 alpha 2
HSPB1_HUMAN	Hs.520973	Homo sapiens	heat shock 27kDa protein-like 2 pseudogene; heat shock 27kDa protein 1
HSP76_HUMAN	Hs.654614	Homo sapiens	heat shock 70kDa protein 7 (HSP70B); heat shock 70kDa protein 6 (HSP70B')
K1C9_HUMAN	Hs.654569	Homo sapiens	keratin 9
TERA_HUMAN	Hs.529782	Homo sapiens	valosin-containing protein
DESP_HUMAN	Hs.519873	Homo sapiens	desmoplakin
K1C15_HUMAN	Hs.654570	Homo sapiens	keratin 15
K2C1_HUMAN	Hs.80828	Homo sapiens	keratin 1
K2C5_HUMAN	Hs.433845	Homo sapiens	keratin 5
CROCC_HUMAN	Hs.309403	Homo sapiens	ciliary rootlet coiled-coil, rootletin
K2C79_HUMAN	Hs.711471	Homo sapiens	keratin 79
HSP71_HUMAN	Hs.719966	Homo sapiens	heat shock 70kDa protein 1A; heat shock 70kDa protein 1B
K1C19_HUMAN	Hs.654568	Homo sapiens	keratin 19
K2C74_HUMAN	Hs.660125	Homo sapiens	keratin 74
TBA1A_HUMAN	Hs.654422	Homo sapiens	tubulin, alpha 1a
TBA1A_HUMAN	Hs.713158	Homo sapiens	tubulin, alpha 1a

K1C27_HUMAN	Hs.59363	Homo sapiens	keratin 27
K1C26_HUMAN	Hs.592133	Homo sapiens	keratin 26
HS90B_HUMAN	Hs.701787	Homo sapiens	heat shock protein 90kDa alpha (cytosolic), class B member 1
TKT_HUMAN	Hs.89643	Homo sapiens	transketolase
K1C12_HUMAN	Hs.66739	Homo sapiens	keratin 12

Table 3-6. ^{13}C Labeled Proteins of MIA PaCa-2 Cells: DAVID Converted Gene List

UNIPROT ACCESSION #	UNIGENE CODE	SPECIES	DATABASE FOR ANNOTATION,VISUALIZATION AND INTEGRATED DISCOVERY (DAVID) GENE NAME
HSP72_HUMAN	Hs.432648	Homo sapiens	heat shock 70kDa protein 2
HSP72_HUMAN	Hs.722086	Homo sapiens	heat shock 70kDa protein 2
ERI2_HUMAN	Hs.248437	Homo sapiens	exoribonuclease 2
K2C7_HUMAN	Hs.411501	Homo sapiens	keratin 7
K2C7_HUMAN	Hs.670221	Homo sapiens	keratin 7
FBX18_HUMAN	Hs.498543	Homo sapiens	F-box protein, helicase, 18
BTD_HUMAN	Hs.517830	Homo sapiens	biotinidase
CH60_HUMAN	Hs.595053	Homo sapiens	heat shock 60kDa protein 1 (chaperonin) pseudogene 5; heat shock 60kDa protein 1 (chaperonin) pseudogene 6; heat shock 60kDa protein 1 (chaperonin) pseudogene 1; heat shock 60kDa protein 1 (chaperonin) pseudogene 4; heat shock 60kDa protein 1 (chaperonin)
CH60_HUMAN	Hs.723164	Homo sapiens	heat shock 60kDa protein 1 (chaperonin) pseudogene 5; heat shock 60kDa protein 1 (chaperonin) pseudogene 6; heat shock 60kDa protein 1 (chaperonin) pseudogene 1; heat shock 60kDa protein 1 (chaperonin) pseudogene 4; heat shock 60kDa protein 1 (chaperonin)
K1C18_HUMAN	Hs.406013	Homo sapiens	keratin 18; keratin 18 pseudogene 26; keratin 18 pseudogene 19
HSP7C_HUMAN	Hs.180414	Homo sapiens	heat shock 70kDa protein 8
K22E_HUMAN	Hs.707	Homo sapiens	keratin 2
TBB1_HUMAN	Hs.303023	Homo sapiens	tubulin, beta 1
G3P_HUMAN	Hs.592355	Homo sapiens	glyceraldehyde-3-phosphate dehydrogenase-like 6; hypothetical protein LOC100133042; glyceraldehyde-3-phosphate dehydrogenase
G3P_HUMAN	Hs.598320	Homo sapiens	glyceraldehyde-3-phosphate dehydrogenase-like 6; hypothetical protein LOC100133042; glyceraldehyde-3-phosphate dehydrogenase
G3P_HUMAN	Hs.544577	Homo sapiens	glyceraldehyde-3-phosphate dehydrogenase-like 6; hypothetical protein LOC100133042; glyceraldehyde-3-phosphate dehydrogenase
CQ085_HUMAN	Hs.120963	Homo sapiens	chromosome 17 open reading frame 85
K2C78_HUMAN	Hs.665267	Homo sapiens	keratin 78
PRKDC_HUMAN	Hs.491682	Homo sapiens	similar to protein kinase, DNA-activated, catalytic polypeptide; protein kinase, DNA-activated, catalytic polypeptide
TBB5_HUMAN	Hs.636480	Homo sapiens	tubulin, beta; similar to tubulin, beta 5; tubulin, beta pseudogene 2; tubulin, beta pseudogene 1
TBB5_HUMAN	Hs.706246	Homo sapiens	tubulin, beta; similar to tubulin, beta 5; tubulin, beta pseudogene 2; tubulin, beta pseudogene 1
TBB5_HUMAN	Hs.720412	Homo sapiens	tubulin, beta; similar to tubulin, beta 5; tubulin, beta pseudogene 2; tubulin, beta pseudogene 1

MYH7_HUMAN	Hs.678918	Homo sapiens	myosin, heavy chain 7, cardiac muscle, beta
NFL_HUMAN	Hs.521461	Homo sapiens	neurofilament, light polypeptide
K2C72_HUMAN	Hs.662013	Homo sapiens	keratin 72
K1C23_HUMAN	Hs.9029	Homo sapiens	keratin 23 (histone deacetylase inducible)
PTHB1_HUMAN	Hs.372360	Homo sapiens	Bardet-Biedl syndrome 9
GFAP_HUMAN	Hs.514227	Homo sapiens	glial fibrillary acidic protein
TCPH_HUMAN	Hs.368149	Homo sapiens	chaperonin containing TCP1, subunit 7 (eta)
DSG1_HUMAN	Hs.2633	Homo sapiens	desmoglein 1
KRT84_HUMAN	Hs.272336	Homo sapiens	keratin 84
TBA8_HUMAN	Hs.137400	Homo sapiens	tubulin, alpha 8
DYH17_HUMAN	Hs.375975	Homo sapiens	dynein, axonemal, heavy chain 17
K2C73_HUMAN	Hs.55410	Homo sapiens	keratin 73
MOES_HUMAN	Hs.87752	Homo sapiens	moesin
K22O_HUMAN	Hs.654392	Homo sapiens	keratin 76
K1C17_HUMAN	Hs.2785	Homo sapiens	keratin 17; keratin 17 pseudogene 3
APC5_HUMAN	Hs.7101	Homo sapiens	anaphase promoting complex subunit 5
HS71L_HUMAN	Hs.690634	Homo sapiens	heat shock 70kDa protein 1-like
K1C20_HUMAN	Hs.84905	Homo sapiens	keratin 20
K2C80_HUMAN	Hs.140978	Homo sapiens	keratin 80
K1C13_HUMAN	Hs.654550	Homo sapiens	keratin 13
K1C24_HUMAN	Hs.87383	Homo sapiens	keratin 24
KCNH5_HUMAN	Hs.27043	Homo sapiens	potassium voltage-gated channel, subfamily H (eag-related), member 5
BPA1_HUMAN	Hs.669931	Homo sapiens	dystonin
BPA1_HUMAN	Hs.604915	Homo sapiens	dystonin
KRT85_HUMAN	Hs.182507	Homo sapiens	keratin 85
LAC_HUMAN	Hs.655198	Homo sapiens	immunoglobulin lambda variable 2-11; immunoglobulin lambda constant 2 (Kern-Oz-marker); immunoglobulin lambda variable 1-44; immunoglobulin lambda constant 1 (Mcg marker); immunoglobulin lambda variable 1-40; immunoglobulin lambda variable 3-21; immunoglobulin lambda locus; immunoglobulin lambda constant 3 (Kern-Oz+ marker)
LAC_HUMAN	Hs.449585	Homo sapiens	immunoglobulin lambda variable 2-11; immunoglobulin lambda constant 2 (Kern-Oz-marker); immunoglobulin lambda variable 1-44; immunoglobulin lambda constant 1 (Mcg marker); immunoglobulin lambda variable 1-40; immunoglobulin lambda variable 3-21; immunoglobulin lambda locus; immunoglobulin lambda constant 3 (Kern-Oz+ marker)
LAC_HUMAN	Hs.561078	Homo sapiens	immunoglobulin lambda variable 2-11; immunoglobulin lambda constant 2 (Kern-Oz-marker); immunoglobulin lambda variable 1-44; immunoglobulin lambda constant 1 (Mcg marker); immunoglobulin lambda variable 1-40;

			immunoglobulin lambda variable 3-21; immunoglobulin lambda locus; immunoglobulin lambda constant 3 (Kern-Oz+ marker)
1433T_HUMAN	Hs.74405	Homo sapiens	tyrosine 3-monooxygenase/tryptophan 5-monooxygenase activation protein, theta polypeptide
1433S_HUMAN	Hs.523718	Homo sapiens	stratifin
KRT36_HUMAN	Hs.248189	Homo sapiens	keratin 36
XIRP2_HUMAN	Hs.73680	Homo sapiens	xin actin-binding repeat containing 2
AFAD_HUMAN	Hs.614974	Homo sapiens	similar to Afadin (Protein AF-6); myeloid/lymphoid or mixed-lineage leukemia (trithorax homolog, Drosophila); translocated to, 4
AFAD_HUMAN	Hs.708726	Homo sapiens	similar to Afadin (Protein AF-6); myeloid/lymphoid or mixed-lineage leukemia (trithorax homolog, Drosophila); translocated to, 4
NFM_HUMAN	Hs.458657	Homo sapiens	neurofilament, medium polypeptide
NFM_HUMAN	Hs.723633	Homo sapiens	neurofilament, medium polypeptide
PERI_HUMAN	Hs.37044	Homo sapiens	peripherin
K2C1B_HUMAN	Hs.334989	Homo sapiens	keratin 77
SUCB2_HUMAN	Hs.644919	Homo sapiens	similar to sucb; succinate-CoA ligase, GDP-forming, beta subunit
SUCB2_HUMAN	Hs.567794	Homo sapiens	similar to sucb; succinate-CoA ligase, GDP-forming, beta subunit
TWF2_HUMAN	Hs.436439	Homo sapiens	twinfilin, actin-binding protein, homolog 2 (Drosophila)
K1C10_HUMAN	Hs.99936	Homo sapiens	keratin 10
VIME_HUMAN	Hs.628678	Homo sapiens	vimentin
VIME_HUMAN	Hs.455493	Homo sapiens	vimentin
1433Z_HUMAN	Hs.492407	Homo sapiens	tyrosine 3-monooxygenase/tryptophan 5-monooxygenase activation protein, zeta polypeptide
ACTBM_HUMAN	Hs.631267	Homo sapiens	POTE ankyrin domain family, member K
GRP78_HUMAN	Hs.710890	Homo sapiens	hypothetical gene supported by AF216292; NM_005347; heat shock 70kDa protein 5 (glucose-regulated protein, 78kDa)
GRP78_HUMAN	Hs.605502	Homo sapiens	hypothetical gene supported by AF216292; NM_005347; heat shock 70kDa protein 5 (glucose-regulated protein, 78kDa)
KDM5A_HUMAN	Hs.76272	Homo sapiens	lysine (K)-specific demethylase 5A
K2C6C_HUMAN	Hs.709234	Homo sapiens	keratin 6C
DYH1_HUMAN	Hs.655469	Homo sapiens	dynein, axonemal, heavy chain 1
TCPD_HUMAN	Hs.421509	Homo sapiens	chaperonin containing TCP1, subunit 4 (delta)
HTR5A_HUMAN	Hs.370299	Homo sapiens	HEAT repeat containing 5A
K1H1_HUMAN	Hs.41696	Homo sapiens	keratin 31
OTOAN_HUMAN	Hs.408336	Homo sapiens	otoancorin
EF1A1_HUMAN	Hs.512059	Homo sapiens	eukaryotic translation elongation factor 1 alpha-like 7; eukaryotic translation elongation factor 1 alpha-like 3; similar to eukaryotic translation elongation factor 1 alpha 1; eukaryotic translation

			elongation factor 1 alpha 1
EF1A1_HUMAN	Hs.723125	Homo sapiens	eukaryotic translation elongation factor 1 alpha-like 7; eukaryotic translation elongation factor 1 alpha-like 3; similar to eukaryotic translation elongation factor 1 alpha 1; eukaryotic translation elongation factor 1 alpha 1
EF1A1_HUMAN	Hs.713109	Homo sapiens	eukaryotic translation elongation factor 1 alpha-like 7; eukaryotic translation elongation factor 1 alpha-like 3; similar to eukaryotic translation elongation factor 1 alpha 1; eukaryotic translation elongation factor 1 alpha 1
EF1A1_HUMAN	Hs.600365	Homo sapiens	eukaryotic translation elongation factor 1 alpha-like 7; eukaryotic translation elongation factor 1 alpha-like 3; similar to eukaryotic translation elongation factor 1 alpha 1; eukaryotic translation elongation factor 1 alpha 1
EF1A1_HUMAN	Hs.586423	Homo sapiens	eukaryotic translation elongation factor 1 alpha-like 7; eukaryotic translation elongation factor 1 alpha-like 3; similar to eukaryotic translation elongation factor 1 alpha 1; eukaryotic translation elongation factor 1 alpha 1
EF1A1_HUMAN	Hs.535192	Homo sapiens	eukaryotic translation elongation factor 1 alpha-like 7; eukaryotic translation elongation factor 1 alpha-like 3; similar to eukaryotic translation elongation factor 1 alpha 1; eukaryotic translation elongation factor 1 alpha 1
EF1A1_HUMAN	Hs.520703	Homo sapiens	eukaryotic translation elongation factor 1 alpha-like 7; eukaryotic translation elongation factor 1 alpha-like 3; similar to eukaryotic translation elongation factor 1 alpha 1; eukaryotic translation elongation factor 1 alpha 1
K1C16_HUMAN	Hs.655160	Homo sapiens	keratin 16; keratin type 16-like
K1C16_HUMAN	Hs.723586	Homo sapiens	keratin 16; keratin type 16-like
ACTBL_HUMAN	Hs.482167	Homo sapiens	actin, beta-like 2
POTEE_HUMAN	Hs.686146	Homo sapiens	POTE ankyrin domain family, member E
GRP75_HUMAN	Hs.184233	Homo sapiens	heat shock 70kDa protein 9 (mortalin)
MXRA5_HUMAN	Hs.369422	Homo sapiens	matrix-remodelling associated 5
DDX10_HUMAN	Hs.591931	Homo sapiens	DEAD (Asp-Glu-Ala-Asp) box polypeptide 10
DYH14_HUMAN	Hs.133977	Homo sapiens	dynein, axonemal, heavy chain 14
DDX41_HUMAN	Hs.484288	Homo sapiens	DEAD (Asp-Glu-Ala-Asp) box polypeptide 41
ENOA_HUMAN	Hs.517145	Homo sapiens	enolase 1, (alpha)
AL1A1_HUMAN	Hs.76392	Homo sapiens	aldehyde dehydrogenase 1 family, member A1
TBA4A_HUMAN	Hs.75318	Homo sapiens	tubulin, alpha 4a
KRT35_HUMAN	Hs.73082	Homo sapiens	keratin 35
K2C8_HUMAN	Hs.708445	Homo sapiens	keratin 8 pseudogene 9; similar to keratin 8; keratin 8
K2C8_HUMAN	Hs.533782	Homo sapiens	keratin 8 pseudogene 9; similar to keratin 8; keratin 8
K2C8_HUMAN	Hs.647727	Homo sapiens	keratin 8 pseudogene 9; similar to keratin 8; keratin 8

ECHB_HUMAN	Hs.515848	Homo sapiens	hydroxyacyl-Coenzyme A dehydrogenase/3-ketoacyl-Coenzyme A thiolase/enoyl-Coenzyme A hydratase (trifunctional protein), beta subunit
K2C3_HUMAN	Hs.680652	Homo sapiens	keratin 3
1433G_HUMAN	Hs.520974	Homo sapiens	tyrosine 3-monooxygenase/tryptophan 5-monooxygenase activation protein, gamma polypeptide
FHAD1_HUMAN	Hs.659997	Homo sapiens	forkhead-associated (FHA) phosphopeptide binding domain 1
OBSCN_HUMAN	Hs.650039	Homo sapiens	obscurin, cytoskeletal calmodulin and titin-interacting RhoGEF
OBSCN_HUMAN	Hs.656999	Homo sapiens	obscurin, cytoskeletal calmodulin and titin-interacting RhoGEF
LRCH2_HUMAN	Hs.65366	Homo sapiens	leucine-rich repeats and calponin homology (CH) domain containing 2
TBB3_HUMAN	Hs.513829	Homo sapiens	tubulin, beta 3; melanocortin 1 receptor (alpha melanocyte stimulating hormone receptor)
TBB3_HUMAN	Hs.511743	Homo sapiens	tubulin, beta 3; melanocortin 1 receptor (alpha melanocyte stimulating hormone receptor)
SF3A1_HUMAN	Hs.406277	Homo sapiens	splicing factor 3a, subunit 1, 120kDa
K1C14_HUMAN	Hs.654380	Homo sapiens	keratin 14
FA98A_HUMAN	Hs.468140	Homo sapiens	family with sequence similarity 98, member A
1433B_HUMAN	Hs.643544	Homo sapiens	tyrosine 3-monooxygenase/tryptophan 5-monooxygenase activation protein, beta polypeptide
SORT_HUMAN	Hs.703487	Homo sapiens	sortilin 1
SORT_HUMAN	Hs.485195	Homo sapiens	sortilin 1
TBA3C_HUMAN	Hs.503749	Homo sapiens	tubulin, alpha 3d; tubulin, alpha 3c
TBA3C_HUMAN	Hs.349695	Homo sapiens	tubulin, alpha 3d; tubulin, alpha 3c
1433F_HUMAN	Hs.226755	Homo sapiens	tyrosine 3-monooxygenase/tryptophan 5-monooxygenase activation protein, eta polypeptide
K2C75_HUMAN	Hs.697046	Homo sapiens	keratin 75
SMC2_HUMAN	Hs.119023	Homo sapiens	structural maintenance of chromosomes 2
NFH_HUMAN	Hs.198760	Homo sapiens	neurofilament, heavy polypeptide
FAT1_HUMAN	Hs.481371	Homo sapiens	FAT tumor suppressor homolog 1 (Drosophila)
KPRP_HUMAN	Hs.149386	Homo sapiens	keratinocyte proline-rich protein
CC88B_HUMAN	Hs.98564	Homo sapiens	coiled-coil domain containing 88B
ASAP2_HUMAN	Hs.555902	Homo sapiens	ArfGAP with SH3 domain, ankyrin repeat and PH domain 2
K1C28_HUMAN	Hs.59736	Homo sapiens	keratin 28
TCPB_HUMAN	Hs.189772	Homo sapiens	chaperonin containing TCP1, subunit 2 (beta)
NF1_HUMAN	Hs.113577	Homo sapiens	neurofibromin 1
KRT81_HUMAN	Hs.658118	Homo sapiens	keratin 81
EZRI_HUMAN	Hs.487027	Homo sapiens	hypothetical protein LOC100129652; ezrin
ANXA1_HUMAN	Hs.494173	Homo sapiens	annexin A1
CB067_HUMAN	Hs.591638	Homo sapiens	chromosome 2 open reading frame 67
CB067_HUMAN	Hs.282260	Homo sapiens	chromosome 2 open reading frame 67

KPYM_HUMAN	Hs.534770	Homo sapiens	similar to Pyruvate kinase, isozymes M1/M2 (Pyruvate kinase muscle isozyme) (Cytosolic thyroid hormone-binding protein) (CTHBP) (THBP1); pyruvate kinase, muscle
SLN14_HUMAN	Hs.591193	Homo sapiens	schlafen family member 14
ACTB_HUMAN	Hs.520640	Homo sapiens	actin, beta
K2C4_HUMAN	Hs.654610	Homo sapiens	keratin 4
K2C6A_HUMAN	Hs.700779	Homo sapiens	keratin 6A
KRT38_HUMAN	Hs.248188	Homo sapiens	keratin 38
TBB4_HUMAN	Hs.110837	Homo sapiens	tubulin, beta 4
1433E_HUMAN	Hs.591239	Homo sapiens	similar to 14-3-3 protein epsilon (14-3-3E) (Mitochondrial import stimulation factor L subunit) (MSF L); tyrosine 3-monooxygenase/tryptophan 5-monooxygenase activation protein, epsilon polypeptide
1433E_HUMAN	Hs.513851	Homo sapiens	similar to 14-3-3 protein epsilon (14-3-3E) (Mitochondrial import stimulation factor L subunit) (MSF L); tyrosine 3-monooxygenase/tryptophan 5-monooxygenase activation protein, epsilon polypeptide
SHRM3_HUMAN	Hs.702168	Homo sapiens	shroom family member 3
KPYR_HUMAN	Hs.95990	Homo sapiens	pyruvate kinase, liver and RBC
TBB6_HUMAN	Hs.706875	Homo sapiens	tubulin, beta 6
TBB6_HUMAN	Hs.720070	Homo sapiens	tubulin, beta 6
ABCCB_HUMAN	Hs.652267	Homo sapiens	ATP-binding cassette, sub-family C (CFTR/MRP), member 11
K1614_HUMAN	Hs.647760	Homo sapiens	KIAA1614
K1C25_HUMAN	Hs.55412	Homo sapiens	keratin 25
K2C71_HUMAN	Hs.660007	Homo sapiens	keratin 71
K2C6B_HUMAN	Hs.708950	Homo sapiens	keratin 6B
NOP2_HUMAN	Hs.534334	Homo sapiens	NOP2 nucleolar protein homolog (yeast)
GBP2_HUMAN	Hs.386567	Homo sapiens	guanylate binding protein 2, interferon-inducible
PLEC1_HUMAN	Hs.434248	Homo sapiens	similar to Plectin 1 (PLTN) (PCN) (Hemidesmosomal protein 1) (HD1); plectin 1, intermediate filament binding protein 500kDa
DYH8_HUMAN	Hs.520106	Homo sapiens	dynein, axonemal, heavy chain 8
PDE8B_HUMAN	Hs.584830	Homo sapiens	phosphodiesterase 8B
ENOG_HUMAN	Hs.511915	Homo sapiens	enolase 2 (gamma, neuronal)
CE350_HUMAN	Hs.413045	Homo sapiens	centrosomal protein 350kDa
HS905_HUMAN	Hs.581644	Homo sapiens	heat shock protein 90kDa alpha (cytosolic), class A member 5 (pseudogene)
MYH9_HUMAN	Hs.474751	Homo sapiens	myosin, heavy chain 9, non-muscle
ZNF44_HUMAN	Hs.296731	Homo sapiens	zinc finger protein 44
ZNF44_HUMAN	Hs.720085	Homo sapiens	zinc finger protein 44
ZNF44_HUMAN	Hs.693933	Homo sapiens	zinc finger protein 44
MYH15_HUMAN	Hs.225968	Homo sapiens	myosin, heavy chain 15
KIF5C_HUMAN	Hs.435557	Homo sapiens	kinesin family member 5C

KIF5C_HUMAN	Hs.660699	Homo sapiens	kinesin family member 5C
EF1A2_HUMAN	Hs.433839	Homo sapiens	eukaryotic translation elongation factor 1 alpha 2
SYNE1_HUMAN	Hs.12967	Homo sapiens	spectrin repeat containing, nuclear envelope 1
K1H2_HUMAN	Hs.41752	Homo sapiens	keratin 32
NPM_HUMAN	Hs.634598	Homo sapiens	nucleophosmin 1 (nucleolar phosphoprotein B23, numatrin) pseudogene 21; hypothetical LOC100131044; similar to nucleophosmin 1; nucleophosmin (nucleolar phosphoprotein B23, numatrin)
NPM_HUMAN	Hs.646505	Homo sapiens	nucleophosmin 1 (nucleolar phosphoprotein B23, numatrin) pseudogene 21; hypothetical LOC100131044; similar to nucleophosmin 1; nucleophosmin (nucleolar phosphoprotein B23, numatrin)
NPM_HUMAN	Hs.621182	Homo sapiens	nucleophosmin 1 (nucleolar phosphoprotein B23, numatrin) pseudogene 21; hypothetical LOC100131044; similar to nucleophosmin 1; nucleophosmin (nucleolar phosphoprotein B23, numatrin)
NPM_HUMAN	Hs.557550	Homo sapiens	nucleophosmin 1 (nucleolar phosphoprotein B23, numatrin) pseudogene 21; hypothetical LOC100131044; similar to nucleophosmin 1; nucleophosmin (nucleolar phosphoprotein B23, numatrin)
HSP76_HUMAN	Hs.654614	Homo sapiens	heat shock 70kDa protein 7 (HSP70B); heat shock 70kDa protein 6 (HSP70B')
AKAP9_HUMAN	Hs.651221	Homo sapiens	A kinase (PRKA) anchor protein (yotiao) 9
K1C9_HUMAN	Hs.654569	Homo sapiens	keratin 9
DESP_HUMAN	Hs.519873	Homo sapiens	desmoplakin
K1C15_HUMAN	Hs.654570	Homo sapiens	keratin 15
TR150_HUMAN	Hs.160211	Homo sapiens	thyroid hormone receptor associated protein 3
AINX_HUMAN	Hs.500916	Homo sapiens	internexin neuronal intermediate filament protein, alpha
TNI3K_HUMAN	Hs.480085	Homo sapiens	TNNI3 interacting kinase; fucose-1-phosphate guanylyltransferase
TBA3E_HUMAN	Hs.433336	Homo sapiens	tubulin, alpha 3e
INT1_HUMAN	Hs.532188	Homo sapiens	integrator complex subunit 1
K2C1_HUMAN	Hs.80828	Homo sapiens	keratin 1
K2C5_HUMAN	Hs.433845	Homo sapiens	keratin 5
ACTA_HUMAN	Hs.500483	Homo sapiens	actin, alpha 2, smooth muscle, aorta
PGK1_HUMAN	Hs.78771	Homo sapiens	phosphoglycerate kinase 1
SYNE2_HUMAN	Hs.525392	Homo sapiens	spectrin repeat containing, nuclear envelope 2
NSUN4_HUMAN	Hs.163424	Homo sapiens	NOL1/NOP2/Sun domain family, member 4
GRDN_HUMAN	Hs.292925	Homo sapiens	coiled-coil domain containing 88A
SETX_HUMAN	Hs.460317	Homo sapiens	senataxin
CROCC_HUMAN	Hs.309403	Homo sapiens	ciliary rootlet coiled-coil, rootletin
NBEA_HUMAN	Hs.491172	Homo sapiens	neurobeachin
K2C79_HUMAN	Hs.711471	Homo sapiens	keratin 79

HSP71_HUMAN	Hs.719966	Homo sapiens	heat shock 70kDa protein 1A; heat shock 70kDa protein 1B
HSP71_HUMAN	Hs.274402	Homo sapiens	heat shock 70kDa protein 1A; heat shock 70kDa protein 1B
HSP71_HUMAN	Hs.702139	Homo sapiens	heat shock 70kDa protein 1A; heat shock 70kDa protein 1B
MCAF2_HUMAN	Hs.513343	Homo sapiens	activating transcription factor 7 interacting protein 2
KRT37_HUMAN	Hs.673852	Homo sapiens	keratin 37
KRT37_HUMAN	Hs.463024	Homo sapiens	keratin 37
K1C19_HUMAN	Hs.654568	Homo sapiens	keratin 19
K2C74_HUMAN	Hs.660125	Homo sapiens	keratin 74
TBA1A_HUMAN	Hs.654422	Homo sapiens	tubulin, alpha 1a
TBA1A_HUMAN	Hs.713158	Homo sapiens	tubulin, alpha 1a
CJ068_HUMAN	Hs.585464	Homo sapiens	chromosome 10 open reading frame 68
K1C26_HUMAN	Hs.592133	Homo sapiens	keratin 26
DESM_HUMAN	Hs.594952	Homo sapiens	desmin
K1C12_HUMAN	Hs.66739	Homo sapiens	keratin 12
CRY2_HUMAN	Hs.532491	Homo sapiens	cryptochrome 2 (photolyase-like)

Table 3-7. ^{13}C Labeled Proteins of HPDE Cells: DAVID Converted Gene List

UNIPROT ACCESSION #	UNIGENE CODE	SPECIES	DATABASE FOR ANNOTATION,VISUALIZATION AND INTEGRATED DISCOVERY (DAVID) GENE NAME
ACTA_HUMAN	Hs.500483	Homo sapiens	actin, alpha 2, smooth muscle, aorta
ACTB_HUMAN	Hs.520640	Homo sapiens	actin, beta
ACTBL_HUMAN	Hs.482167	Homo sapiens	actin, beta-like 2
ACTBM_HUMAN	Hs.631267	Homo sapiens	POTE ankyrin domain family, member K
ACTN3_HUMAN	Hs.654432	Homo sapiens	actinin, alpha 3
AFAD_HUMAN	Hs.614974	Homo sapiens	similar to Afadin (Protein AF-6); myeloid/lymphoid or mixed-lineage leukemia (trithorax homolog, Drosophila); translocated to, 4
AFAD_HUMAN	Hs.708726	Homo sapiens	similar to Afadin (Protein AF-6); myeloid/lymphoid or mixed-lineage leukemia (trithorax homolog, Drosophila); translocated to, 4
ANXA2_HUMAN	Hs.591361	Homo sapiens	annexin A2 pseudogene 3; annexin A2; annexin A2 pseudogene 1
ANXA2_HUMAN	Hs.546235	Homo sapiens	annexin A2 pseudogene 3; annexin A2; annexin A2 pseudogene 1
ANXA2_HUMAN	Hs.511605	Homo sapiens	annexin A2 pseudogene 3; annexin A2; annexin A2 pseudogene 1
ASAP2_HUMAN	Hs.555902	Homo sapiens	ArfGAP with SH3 domain, ankyrin repeat and PH domain 2
CH60_HUMAN	Hs.595053	Homo sapiens	heat shock 60kDa protein 1 (chaperonin) pseudogene 5; heat shock 60kDa protein 1 (chaperonin) pseudogene 6; heat shock 60kDa protein 1 (chaperonin) pseudogene 1; heat shock 60kDa protein 1 (chaperonin) pseudogene 4; heat shock 60kDa protein 1 (chaperonin)
CH60_HUMAN	Hs.723164	Homo sapiens	heat shock 60kDa protein 1 (chaperonin) pseudogene 5; heat shock 60kDa protein 1 (chaperonin) pseudogene 6; heat shock 60kDa protein 1 (chaperonin) pseudogene 1; heat shock 60kDa protein 1 (chaperonin) pseudogene 4; heat shock 60kDa protein 1 (chaperonin)
CJ068_HUMAN	Hs.585464	Homo sapiens	chromosome 10 open reading frame 68
DCD_HUMAN	Hs.350570	Homo sapiens	dermcidin
DESM_HUMAN	Hs.594952	Homo sapiens	desmin
DESP_HUMAN	Hs.519873	Homo sapiens	desmoplakin
DNLI3_HUMAN	Hs.100299	Homo sapiens	ligase III, DNA, ATP-dependent
DYH1_HUMAN	Hs.655469	Homo sapiens	dynein, axonemal, heavy chain 1
DYH11_HUMAN	Hs.520245	Homo sapiens	dynein, axonemal, heavy chain 11
DYH11_HUMAN	Hs.723198	Homo sapiens	dynein, axonemal, heavy chain 11
DYH12_HUMAN	Hs.201378	Homo sapiens	dynein, axonemal, heavy chain 12
DYH5_HUMAN	Hs.212360	Homo sapiens	dynein, axonemal, heavy chain 5

ETUD1_HUMAN	Hs.459114	Homo sapiens	elongation factor Tu GTP binding domain containing 1
FHAD1_HUMAN	Hs.659997	Homo sapiens	forkhead-associated (FHA) phosphopeptide binding domain 1
FRAP_HUMAN	Hs.338207	Homo sapiens	mechanistic target of rapamycin (serine/threonine kinase)
FRAS1_HUMAN	Hs.721814	Homo sapiens	Fraser syndrome 1
FRAS1_HUMAN	Hs.369448	Homo sapiens	Fraser syndrome 1
G3P_HUMAN	Hs.592355	Homo sapiens	glyceraldehyde-3-phosphate dehydrogenase-like 6; hypothetical protein LOC100133042; glyceraldehyde-3-phosphate dehydrogenase
G3P_HUMAN	Hs.598320	Homo sapiens	glyceraldehyde-3-phosphate dehydrogenase-like 6; hypothetical protein LOC100133042; glyceraldehyde-3-phosphate dehydrogenase
G3P_HUMAN	Hs.544577	Homo sapiens	glyceraldehyde-3-phosphate dehydrogenase-like 6; hypothetical protein LOC100133042; glyceraldehyde-3-phosphate dehydrogenase
G3PT_HUMAN	Hs.248017	Homo sapiens	glyceraldehyde-3-phosphate dehydrogenase, spermatogenic
GBP2_HUMAN	Hs.386567	Homo sapiens	guanylate binding protein 2, interferon-inducible
GFAP_HUMAN	Hs.514227	Homo sapiens	glial fibrillary acidic protein
GOGB1_HUMAN	Hs.213389	Homo sapiens	golgin B1, golgi integral membrane protein
GORAB_HUMAN	Hs.183702	Homo sapiens	golgin, RAB6-interacting
GRP78_HUMAN	Hs.710890	Homo sapiens	hypothetical gene supported by AF216292; NM_005347; heat shock 70kDa protein 5 (glucose-regulated protein, 78kDa)
GRP78_HUMAN	Hs.605502	Homo sapiens	hypothetical gene supported by AF216292; NM_005347; heat shock 70kDa protein 5 (glucose-regulated protein, 78kDa)
HORN_HUMAN	Hs.490162	Homo sapiens	hornerin
HSP71_HUMAN	Hs.719966	Homo sapiens	heat shock 70kDa protein 1A; heat shock 70kDa protein 1B
HSP71_HUMAN	Hs.274402	Homo sapiens	heat shock 70kDa protein 1A; heat shock 70kDa protein 1B
HSP71_HUMAN	Hs.702139	Homo sapiens	heat shock 70kDa protein 1A; heat shock 70kDa protein 1B
HSP72_HUMAN	Hs.432648	Homo sapiens	heat shock 70kDa protein 2
HSP72_HUMAN	Hs.722086	Homo sapiens	heat shock 70kDa protein 2
HSP7C_HUMAN	Hs.180414	Homo sapiens	heat shock 70kDa protein 8
ITPR2_HUMAN	Hs.512235	Homo sapiens	inositol 1,4,5-triphosphate receptor, type 2
K1C10_HUMAN	Hs.99936	Homo sapiens	keratin 10
K1C12_HUMAN	Hs.66739	Homo sapiens	keratin 12
K1C13_HUMAN	Hs.654550	Homo sapiens	keratin 13
K1C14_HUMAN	Hs.654380	Homo sapiens	keratin 14
K1C15_HUMAN	Hs.654570	Homo sapiens	keratin 15
K1C16_HUMAN	Hs.655160	Homo sapiens	keratin 16; keratin type 16-like
K1C16_HUMAN	Hs.723586	Homo sapiens	keratin 16; keratin type 16-like
K1C17_HUMAN	Hs.2785	Homo sapiens	keratin 17; keratin 17 pseudogene 3

K1C18_HUMAN	Hs.406013	Homo sapiens	keratin 18; keratin 18 pseudogene 26; keratin 18 pseudogene 19
K1C19_HUMAN	Hs.654568	Homo sapiens	keratin 19
K1C20_HUMAN	Hs.84905	Homo sapiens	keratin 20
K1C23_HUMAN	Hs.9029	Homo sapiens	keratin 23 (histone deacetylase inducible)
K1C24_HUMAN	Hs.87383	Homo sapiens	keratin 24
K1C25_HUMAN	Hs.55412	Homo sapiens	keratin 25
K1C26_HUMAN	Hs.592133	Homo sapiens	keratin 26
K1C27_HUMAN	Hs.59363	Homo sapiens	keratin 27
K1C28_HUMAN	Hs.59736	Homo sapiens	keratin 28
K1C9_HUMAN	Hs.654569	Homo sapiens	keratin 9
K1H2_HUMAN	Hs.41752	Homo sapiens	keratin 32
K22E_HUMAN	Hs.707	Homo sapiens	keratin 2
K22O_HUMAN	Hs.654392	Homo sapiens	keratin 76
K2C1_HUMAN	Hs.80828	Homo sapiens	keratin 1
K2C1B_HUMAN	Hs.334989	Homo sapiens	keratin 77
K2C3_HUMAN	Hs.680652	Homo sapiens	keratin 3
K2C4_HUMAN	Hs.654610	Homo sapiens	keratin 4
K2C5_HUMAN	Hs.433845	Homo sapiens	keratin 5
K2C6A_HUMAN	Hs.700779	Homo sapiens	keratin 6A
K2C6B_HUMAN	Hs.708950	Homo sapiens	keratin 6B
K2C6C_HUMAN	Hs.709234	Homo sapiens	keratin 6C
K2C7_HUMAN	Hs.411501	Homo sapiens	keratin 7
K2C7_HUMAN	Hs.670221	Homo sapiens	keratin 7
K2C71_HUMAN	Hs.660007	Homo sapiens	keratin 71
K2C72_HUMAN	Hs.662013	Homo sapiens	keratin 72
K2C73_HUMAN	Hs.55410	Homo sapiens	keratin 73
K2C74_HUMAN	Hs.660125	Homo sapiens	keratin 74
K2C75_HUMAN	Hs.697046	Homo sapiens	keratin 75
K2C78_HUMAN	Hs.665267	Homo sapiens	keratin 78
K2C79_HUMAN	Hs.711471	Homo sapiens	keratin 79
K2C8_HUMAN	Hs.708445	Homo sapiens	keratin 8 pseudogene 9; similar to keratin 8; keratin 8
K2C8_HUMAN	Hs.533782	Homo sapiens	keratin 8 pseudogene 9; similar to keratin 8; keratin 8
K2C8_HUMAN	Hs.647727	Homo sapiens	keratin 8 pseudogene 9; similar to keratin 8; keratin 8
KCNQ3_HUMAN	Hs.374023	Homo sapiens	potassium voltage-gated channel, KQT-like subfamily, member 3
KI67_HUMAN	Hs.80976	Homo sapiens	antigen identified by monoclonal antibody Ki-67
KI67_HUMAN	Hs.689823	Homo sapiens	antigen identified by monoclonal antibody Ki-67
KPRP_HUMAN	Hs.149386	Homo sapiens	keratinocyte proline-rich protein
KPYM_HUMAN	Hs.534770	Homo sapiens	similar to Pyruvate kinase, isozymes M1/M2 (Pyruvate kinase muscle isozyme) (Cytosolic

			thyroid hormone-binding protein) (CTHBP) (THBP1); pyruvate kinase, muscle
KRT35_HUMAN	Hs.73082	Homo sapiens	keratin 35
KRT36_HUMAN	Hs.248189	Homo sapiens	keratin 36
KRT37_HUMAN	Hs.673852	Homo sapiens	keratin 37
KRT37_HUMAN	Hs.463024	Homo sapiens	keratin 37
KRT38_HUMAN	Hs.248188	Homo sapiens	keratin 38
KRT81_HUMAN	Hs.658118	Homo sapiens	keratin 81
KRT84_HUMAN	Hs.272336	Homo sapiens	keratin 84
KRT85_HUMAN	Hs.182507	Homo sapiens	keratin 85
KT222_HUMAN	Hs.6920	Homo sapiens	keratin 222 pseudogene
LDH6A_HUMAN	Hs.668877	Homo sapiens	lactate dehydrogenase A-like 6A
LDHA_HUMAN	Hs.2795	Homo sapiens	lactate dehydrogenase A
LDHB_HUMAN	Hs.446149	Homo sapiens	lactate dehydrogenase B
LDHC_HUMAN	Hs.654377	Homo sapiens	lactate dehydrogenase C
LYSC_HUMAN	Hs.524579	Homo sapiens	lysozyme (renal amyloidosis)
MINT_HUMAN	Hs.558463	Homo sapiens	spen homolog, transcriptional regulator (Drosophila)
MYH1_HUMAN	Hs.689619	Homo sapiens	myosin, heavy chain 1, skeletal muscle, adult
NFH_HUMAN	Hs.198760	Homo sapiens	neurofilament, heavy polypeptide
NUMA1_HUMAN	Hs.325978	Homo sapiens	nuclear mitotic apparatus protein 1
PCLO_HUMAN	Hs.12376	Homo sapiens	piccolo (presynaptic cytomatrix protein)
PDE8B_HUMAN	Hs.584830	Homo sapiens	phosphodiesterase 8B
PDZD2_HUMAN	Hs.481819	Homo sapiens	PDZ domain containing 2
PERI_HUMAN	Hs.37044	Homo sapiens	peripherin
POTEE_HUMAN	Hs.686146	Homo sapiens	POTE ankyrin domain family, member E
PTN13_HUMAN	Hs.436142	Homo sapiens	protein tyrosine phosphatase, non-receptor type 13 (APO-1/CD95 (Fas)-associated phosphatase)
PTPRU_HUMAN	Hs.19718	Homo sapiens	protein tyrosine phosphatase, receptor type, U
RA1L2_HUMAN	Hs.447506	Homo sapiens	heterogeneous nuclear ribonucleoprotein A1-like 2
RAB9A_HUMAN	Hs.495704	Homo sapiens	RAB9A, member RAS oncogene family
RAD50_HUMAN	Hs.655835	Homo sapiens	RAD50 homolog (S. cerevisiae)
RL37A_HUMAN	Hs.433701	Homo sapiens	ribosomal protein L37a
RN5A_HUMAN	Hs.518545	Homo sapiens	ribonuclease L (2',5'-oligoisoadenylate synthetase-dependent)
ROA1_HUMAN	Hs.711067	Homo sapiens	heterogeneous nuclear ribonucleoprotein A1-like 3; similar to heterogeneous nuclear ribonucleoprotein A1; heterogeneous nuclear ribonucleoprotein A1 pseudogene 2; heterogeneous nuclear ribonucleoprotein A1; heterogeneous nuclear ribonucleoprotein A1 pseudogene
ROA1_HUMAN	Hs.655424	Homo sapiens	heterogeneous nuclear ribonucleoprotein A1-like 3; similar to heterogeneous nuclear ribonucleoprotein A1; heterogeneous nuclear

			ribonucleoprotein A1 pseudogene 2; heterogeneous nuclear ribonucleoprotein A1; heterogeneous nuclear ribonucleoprotein A1 pseudogene
ROA1_HUMAN	Hs.631978	Homo sapiens	heterogeneous nuclear ribonucleoprotein A1-like 3; similar to heterogeneous nuclear ribonucleoprotein A1; heterogeneous nuclear ribonucleoprotein A1 pseudogene 2; heterogeneous nuclear ribonucleoprotein A1; heterogeneous nuclear ribonucleoprotein A1 pseudogene
ROA1_HUMAN	Hs.534822	Homo sapiens	heterogeneous nuclear ribonucleoprotein A1-like 3; similar to heterogeneous nuclear ribonucleoprotein A1; heterogeneous nuclear ribonucleoprotein A1 pseudogene 2; heterogeneous nuclear ribonucleoprotein A1; heterogeneous nuclear ribonucleoprotein A1 pseudogene
ROA1_HUMAN	Hs.632537	Homo sapiens	heterogeneous nuclear ribonucleoprotein A1-like 3; similar to heterogeneous nuclear ribonucleoprotein A1; heterogeneous nuclear ribonucleoprotein A1 pseudogene 2; heterogeneous nuclear ribonucleoprotein A1; heterogeneous nuclear ribonucleoprotein A1 pseudogene
ROA1_HUMAN	Hs.546261	Homo sapiens	heterogeneous nuclear ribonucleoprotein A1-like 3; similar to heterogeneous nuclear ribonucleoprotein A1; heterogeneous nuclear ribonucleoprotein A1 pseudogene 2; heterogeneous nuclear ribonucleoprotein A1; heterogeneous nuclear ribonucleoprotein A1 pseudogene
SPTN5_HUMAN	Hs.709819	Homo sapiens	spectrin, beta, non-erythrocytic 5
SYFA_HUMAN	Hs.23111	Homo sapiens	phenylalanyl-tRNA synthetase, alpha subunit
SYNE1_HUMAN	Hs.12967	Homo sapiens	spectrin repeat containing, nuclear envelope 1
SYNE2_HUMAN	Hs.525392	Homo sapiens	spectrin repeat containing, nuclear envelope 2
TCPD_HUMAN	Hs.421509	Homo sapiens	chaperonin containing TCP1, subunit 4 (delta)
TCPH_HUMAN	Hs.368149	Homo sapiens	chaperonin containing TCP1, subunit 7 (eta)
TDRD1_HUMAN	Hs.333132	Homo sapiens	tudor domain containing 1
TOPK_HUMAN	Hs.104741	Homo sapiens	PDZ binding kinase
TPM1_HUMAN	Hs.133892	Homo sapiens	tropomyosin 1 (alpha)
TPM3_HUMAN	Hs.654421	Homo sapiens	tropomyosin 3
TPM3_HUMAN	Hs.535581	Homo sapiens	tropomyosin 3
TPM3_HUMAN	Hs.644306	Homo sapiens	tropomyosin 3
TRIPB_HUMAN	Hs.632339	Homo sapiens	hypothetical LOC341378; thyroid hormone receptor interactor 11
UTS2_HUMAN	Hs.715862	Homo sapiens	urotensin 2
VIME_HUMAN	Hs.628678	Homo sapiens	vimentin
VIME_HUMAN	Hs.455493	Homo sapiens	vimentin
WAHS7_HUMAN	Hs.12144	Homo sapiens	KIAA1033

WDR85_HUMAN	Hs.292570	Homo sapiens	WD repeat domain 85
XIRP2_HUMAN	Hs.73680	Homo sapiens	xin actin-binding repeat containing 2
ZN509_HUMAN	Hs.419997	Homo sapiens	zinc finger protein 509

Table 3-8. ^{13}C Labeled Proteins in MIA PaCa-2 Mouse Tumor Tissue: DAVID Converted Gene List

UNIPROT ACCESSION #	UNIGENE CODE	SPECIES	DATABASE FOR ANNOTATION,VISUALIZATION AND INTEGRATED DISCOVERY (DAVID) GENE NAME
K2C74_MOUSE	Mm.359153	Mus musculus	keratin 74
K1C25_MOUSE	Mm.268173	Mus musculus	keratin 25
HSP7C_MOUSE	Mm.412745	Mus musculus	similar to heat shock protein 8; heat shock protein 8
HSP7C_MOUSE	Mm.336743	Mus musculus	similar to heat shock protein 8; heat shock protein 8
HSP7C_MOUSE	Mm.351377	Mus musculus	similar to heat shock protein 8; heat shock protein 8
HSP7C_MOUSE	Mm.290774	Mus musculus	similar to heat shock protein 8; heat shock protein 8
NFM_MOUSE	Mm.242832	Mus musculus	neurofilament, medium polypeptide
NFM_MOUSE	Mm.390700	Mus musculus	neurofilament, medium polypeptide
K1C28_MOUSE	Mm.180256	Mus musculus	similar to keratin 25D (predicted); keratin 28
K2C5_MOUSE	Mm.451847	Mus musculus	keratin 5
K1C18_MOUSE	Mm.22479	Mus musculus	keratin 18
ANXA1_MOUSE	Mm.248360	Mus musculus	annexin A1
AINX_MOUSE	Mm.276251	Mus musculus	internexin neuronal intermediate filament protein, alpha
ACTB_MOUSE	Mm.328431	Mus musculus	actin, beta
ACTB_MOUSE	Mm.391967	Mus musculus	actin, beta
ACTB_MOUSE	Mm.469717	Mus musculus	actin, beta
H2A1F_MOUSE	Mm.377878	Mus musculus	histone cluster 1, H2af
CH60_MOUSE	Mm.1777	Mus musculus	predicted gene 12141; heat shock protein 1 (chaperonin)
CH60_MOUSE	Mm.476770	Mus musculus	predicted gene 12141; heat shock protein 1 (chaperonin)
K2C75_MOUSE	Mm.106868	Mus musculus	keratin 75
GFAP_MOUSE	Mm.1239	Mus musculus	glial fibrillary acidic protein
K2C1_MOUSE	Mm.183137	Mus musculus	keratin 1
K2C6A_MOUSE	Mm.302399	Mus musculus	keratin 6A
NFH_MOUSE	Mm.298283	Mus musculus	similar to neurofilament protein; neurofilament, heavy polypeptide
K2C73_MOUSE	Mm.291498	Mus musculus	keratin 73
RPAP1_MOUSE	Mm.259223	Mus musculus	RNA polymerase II associated protein 1
K22O_MOUSE	Mm.195788	Mus musculus	keratin 76
ML12B_MOUSE	Mm.261329	Mus musculus	predicted gene 2805; similar to myosin regulatory light chain-like; predicted gene 6242; myosin, light chain 12B, regulatory

PLAK_MOUSE	Mm.299774	Mus musculus	junction plakoglobin
H4_MOUSE	Mm.478233	Mus musculus	histone cluster 1, H4k; histone cluster 1, H4m; histone cluster 4, H4; similar to germinal histone H4 gene; histone cluster 1, H4h; histone cluster 1, H4j; histone cluster 1, H4i; histone cluster 1, H4d; histone cluster 1, H4c; histone cluster 1, H4f; histone cluster 1, H4b; histone cluster 1, H4a; histone cluster 2, H4; similar to histone H4
H4_MOUSE	Mm.261664	Mus musculus	histone cluster 1, H4k; histone cluster 1, H4m; histone cluster 4, H4; similar to germinal histone H4 gene; histone cluster 1, H4h; histone cluster 1, H4j; histone cluster 1, H4i; histone cluster 1, H4d; histone cluster 1, H4c; histone cluster 1, H4f; histone cluster 1, H4b; histone cluster 1, H4a; histone cluster 2, H4; similar to histone H4
H4_MOUSE	Mm.227295	Mus musculus	histone cluster 1, H4k; histone cluster 1, H4m; histone cluster 4, H4; similar to germinal histone H4 gene; histone cluster 1, H4h; histone cluster 1, H4j; histone cluster 1, H4i; histone cluster 1, H4d; histone cluster 1, H4c; histone cluster 1, H4f; histone cluster 1, H4b; histone cluster 1, H4a; histone cluster 2, H4; similar to histone H4
H4_MOUSE	Mm.261662	Mus musculus	histone cluster 1, H4k; histone cluster 1, H4m; histone cluster 4, H4; similar to germinal histone H4 gene; histone cluster 1, H4h; histone cluster 1, H4j; histone cluster 1, H4i; histone cluster 1, H4d; histone cluster 1, H4c; histone cluster 1, H4f; histone cluster 1, H4b; histone cluster 1, H4a; histone cluster 2, H4; similar to histone H4
H4_MOUSE	Mm.261642	Mus musculus	histone cluster 1, H4k; histone cluster 1, H4m; histone cluster 4, H4; similar to germinal histone H4 gene; histone cluster 1, H4h; histone cluster 1, H4j; histone cluster 1, H4i; histone cluster 1, H4d; histone cluster 1, H4c; histone cluster 1, H4f; histone cluster 1, H4b; histone cluster 1, H4a; histone cluster 2, H4; similar to histone H4
H4_MOUSE	Mm.14775	Mus musculus	histone cluster 1, H4k; histone cluster 1, H4m; histone cluster 4, H4; similar to germinal histone H4 gene; histone cluster 1, H4h; histone cluster 1, H4j; histone cluster 1, H4i; histone cluster 1, H4d; histone cluster 1, H4c; histone cluster 1, H4f; histone cluster 1, H4b; histone cluster 1, H4a; histone cluster 2, H4; similar to histone H4

H4_MOUSE	Mm.158272	Mus musculus	histone cluster 1, H4k; histone cluster 1, H4m; histone cluster 4, H4; similar to germinal histone H4 gene; histone cluster 1, H4h; histone cluster 1, H4j; histone cluster 1, H4i; histone cluster 1, H4d; histone cluster 1, H4c; histone cluster 1, H4f; histone cluster 1, H4b; histone cluster 1, H4a; histone cluster 2, H4; similar to histone H4
H4_MOUSE	Mm.260530	Mus musculus	histone cluster 1, H4k; histone cluster 1, H4m; histone cluster 4, H4; similar to germinal histone H4 gene; histone cluster 1, H4h; histone cluster 1, H4j; histone cluster 1, H4i; histone cluster 1, H4d; histone cluster 1, H4c; histone cluster 1, H4f; histone cluster 1, H4b; histone cluster 1, H4a; histone cluster 2, H4; similar to histone H4
H4_MOUSE	Mm.255646	Mus musculus	histone cluster 1, H4k; histone cluster 1, H4m; histone cluster 4, H4; similar to germinal histone H4 gene; histone cluster 1, H4h; histone cluster 1, H4j; histone cluster 1, H4i; histone cluster 1, H4d; histone cluster 1, H4c; histone cluster 1, H4f; histone cluster 1, H4b; histone cluster 1, H4a; histone cluster 2, H4; similar to histone H4
H4_MOUSE	Mm.442307	Mus musculus	histone cluster 1, H4k; histone cluster 1, H4m; histone cluster 4, H4; similar to germinal histone H4 gene; histone cluster 1, H4h; histone cluster 1, H4j; histone cluster 1, H4i; histone cluster 1, H4d; histone cluster 1, H4c; histone cluster 1, H4f; histone cluster 1, H4b; histone cluster 1, H4a; histone cluster 2, H4; similar to histone H4
H4_MOUSE	Mm.228709	Mus musculus	histone cluster 1, H4k; histone cluster 1, H4m; histone cluster 4, H4; similar to germinal histone H4 gene; histone cluster 1, H4h; histone cluster 1, H4j; histone cluster 1, H4i; histone cluster 1, H4d; histone cluster 1, H4c; histone cluster 1, H4f; histone cluster 1, H4b; histone cluster 1, H4a; histone cluster 2, H4; similar to histone H4
H4_MOUSE	Mm.377875	Mus musculus	histone cluster 1, H4k; histone cluster 1, H4m; histone cluster 4, H4; similar to germinal histone H4 gene; histone cluster 1, H4h; histone cluster 1, H4j; histone cluster 1, H4i; histone cluster 1, H4d; histone cluster 1, H4c; histone cluster 1, H4f; histone cluster 1, H4b; histone cluster 1, H4a; histone cluster 2, H4; similar to histone H4
H4_MOUSE	Mm.246720	Mus musculus	histone cluster 1, H4k; histone cluster 1, H4m; histone cluster 4, H4; similar

			to germinal histone H4 gene; histone cluster 1, H4h; histone cluster 1, H4j; histone cluster 1, H4i; histone cluster 1, H4d; histone cluster 1, H4c; histone cluster 1, H4f; histone cluster 1, H4b; histone cluster 1, H4a; histone cluster 2, H4; similar to histone H4
1433Z_MOUSE	Mm.465895	Mus musculus	tyrosine 3-monooxygenase/tryptophan 5-monooxygenase activation protein, zeta polypeptide; predicted gene 4202
1433Z_MOUSE	Mm.3360	Mus musculus	tyrosine 3-monooxygenase/tryptophan 5-monooxygenase activation protein, zeta polypeptide; predicted gene 4202
K2C4_MOUSE	Mm.46425	Mus musculus	keratin 4
KRT84_MOUSE	Mm.25292	Mus musculus	keratin 84
K2C7_MOUSE	Mm.289377	Mus musculus	keratin 7
CCD38_MOUSE	Mm.477086	Mus musculus	coiled-coil domain containing 38
K22E_MOUSE	Mm.358616	Mus musculus	keratin 2
K2C6B_MOUSE	Mm.441891	Mus musculus	keratin 6B
VIME_MOUSE	Mm.268000	Mus musculus	vimentin
K2C72_MOUSE	Mm.298210	Mus musculus	keratin 72
NSD2_MOUSE	Mm.456405	Mus musculus	Wolf-Hirschhorn syndrome candidate 1 (human)
NSD2_MOUSE	Mm.332320	Mus musculus	Wolf-Hirschhorn syndrome candidate 1 (human)
NSD2_MOUSE	Mm.19892	Mus musculus	Wolf-Hirschhorn syndrome candidate 1 (human)
NSD2_MOUSE	Mm.460382	Mus musculus	Wolf-Hirschhorn syndrome candidate 1 (human)
K2C8_MOUSE	Mm.358618	Mus musculus	predicted gene 5604; keratin 8
K2C8_MOUSE	Mm.289759	Mus musculus	predicted gene 5604; keratin 8
GATM_MOUSE	Mm.29975	Mus musculus	glycine amidinotransferase (L-arginine:glycine amidinotransferase)
K1C13_MOUSE	Mm.4646	Mus musculus	keratin 13
1433F_MOUSE	Mm.332314	Mus musculus	tyrosine 3-monooxygenase/tryptophan 5-monooxygenase activation protein, eta polypeptide
DESM_MOUSE	Mm.6712	Mus musculus	desmin
RS24_MOUSE	Mm.429854	Mus musculus	predicted gene 11878; predicted gene 4832; predicted gene 8942; predicted gene 6030; predicted gene 9320; predicted gene 5271; predicted gene 7363; ribosomal protein S24; similar to ribosomal protein S24; predicted gene 8292; predicted gene 6948
RS24_MOUSE	Mm.312053	Mus musculus	predicted gene 11878; predicted gene 4832; predicted gene 8942; predicted gene 6030; predicted gene 9320; predicted gene 5271; predicted gene 7363; ribosomal protein S24; similar to ribosomal protein S24; predicted

			gene 8292; predicted gene 6948
RS24_MOUSE	Mm.16775	Mus musculus	predicted gene 11878; predicted gene 4832; predicted gene 8942; predicted gene 6030; predicted gene 9320; predicted gene 5271; predicted gene 7363; ribosomal protein S24; similar to ribosomal protein S24; predicted gene 8292; predicted gene 6948
ACTBL_MOUSE	Mm.107293	Mus musculus	actin, beta-like 2
PERI_MOUSE	Mm.2477	Mus musculus	peripherin
1433S_MOUSE	Mm.44482	Mus musculus	predicted gene 5279; stratifin; similar to 14-3-3 protein sigma (Stratifin); predicted gene 7850
K2C80_MOUSE	Mm.440055	Mus musculus	keratin 80
GRP78_MOUSE	Mm.330160	Mus musculus	heat shock protein 5
GRP78_MOUSE	Mm.470180	Mus musculus	heat shock protein 5
ANXA2_MOUSE	Mm.238343	Mus musculus	similar to Annexin A2 (Annexin II) (Lipocortin II) (Calpactin I heavy chain) (Chromobindin-8) (p36) (Protein I) (Placental anticoagulant protein IV) (PAP-IV); annexin A2
K1C15_MOUSE	Mm.440010	Mus musculus	keratin 15
TBA1B_MOUSE	Mm.392113	Mus musculus	predicted gene 3756; tubulin, alpha 1B; predicted gene 5620; similar to alpha-tubulin isotype M-alpha-2; predicted gene 14150; predicted gene 3226
TBA1B_MOUSE	Mm.479337	Mus musculus	predicted gene 3756; tubulin, alpha 1B; predicted gene 5620; similar to alpha-tubulin isotype M-alpha-2; predicted gene 14150; predicted gene 3226
TBA1B_MOUSE	Mm.326103	Mus musculus	predicted gene 3756; tubulin, alpha 1B; predicted gene 5620; similar to alpha-tubulin isotype M-alpha-2; predicted gene 14150; predicted gene 3226
K2C71_MOUSE	Mm.358677	Mus musculus	keratin 71
ATPB_MOUSE	Mm.238973	Mus musculus	ATP synthase, H+ transporting mitochondrial F1 complex, beta subunit
CTRB1_MOUSE	Mm.34374	Mus musculus	chymotrypsinogen B1
K1C10_MOUSE	Mm.22662	Mus musculus	keratin 10
AMYP_MOUSE	Mm.439729	Mus musculus	amylase 2a2, pancreatic; amylase 2a3, pancreatic; amylase 2b, pancreatic; amylase 2a1, pancreatic; amylase 2a4, pancreatic; amylase 2a5, pancreatic
AMYP_MOUSE	Mm.331313	Mus musculus	amylase 2a2, pancreatic; amylase 2a3, pancreatic; amylase 2b, pancreatic; amylase 2a1, pancreatic; amylase 2a4, pancreatic; amylase 2a5, pancreatic
ACTC_MOUSE	Mm.686	Mus musculus	actin, alpha, cardiac muscle 1; similar

			to alpha-actin (AA 27-375)
K1C14_MOUSE	Mm.439898	Mus musculus	keratin 14
K2C1B_MOUSE	Mm.292992	Mus musculus	keratin 77
K2C79_MOUSE	Mm.162744	Mus musculus	keratin 79
K1C27_MOUSE	Mm.440476	Mus musculus	keratin 27

Table. 3-9. Related Pathways of ^{13}C Labeled Proteins in Human BxPC-3 Cells

Hs.90280	**5-aminoimidazole-4-carboxamide ribonucleotide formyltransferase/IMP cyclohydrolase**
Related Pathways	Purine metabolism, One carbon pool by folate,
Hs.520640	**actin, beta**
Related Pathways	Focal adhesion, Adherens junction, Tight junction, Leukocyte transendothelial migration, Regulation of actin cytoskeleton, Vibrio cholerae infection, Pathogenic Escherichia coli infection, Hypertrophic cardiomyopathy (HCM),Arrhythmogenic right ventricular cardiomyopathy (ARVC), Dilated cardiomyopathy, Viral myocarditis
Hs.509765	**actinin, alpha 1**
Related Pathways	Focal adhesion, Adherens junction, Tight junction, Leukocyte transendothelial migration, Regulation of actin cytoskeleton, Systemic lupus erythematosus, Arrhythmogenic right ventricular cardiomyopathy (ARVC)
Hs.498178	**actinin, alpha 2**
Related Pathways	Focal adhesion, Adherens junction, Tight junction, Leukocyte transendothelial migration, Regulation of actin cytoskeleton, Systemic lupus erythematosus, Arrhythmogenic right ventricular cardiomyopathy (ARVC)
Hs.270291	**actinin, alpha 4**
Related Pathways	Focal adhesion, Adherens junction, Tight junction, Leukocyte transendothelial migration, Regulation of actin cytoskeleton, Systemic lupus erythematosus, Arrhythmogenic right ventricular cardiomyopathy (ARVC)
Hs.459538	**aldehyde dehydrogenase 1 family, member A3**
Related Pathways	Glycolysis / Gluconeogenesis, Histidine metabolism, Tyrosine metabolism, Phenylalanine metabolism, Metabolism of xenobiotics by cytochrome P450, Drug metabolism
Hs.531682	**aldehyde dehydrogenase 3 family, memberA1**
Related Pathways	Glycolysis / Gluconeogenesis, Histidine metabolism, Tyrosine metabolism, Phenylalanine metabolism, Metabolism of xenobiotics by cytochrome P450, Drug metabolism
Hs.513490	**aldolase A, fructose-bisphosphate**
Related Pathways	Glycolysis / Gluconeogenesis, Pentose phosphate pathway, Fructose and mannose metabolism
Hs.515162	**calreticulin**
Related Pathways	Antigen processing and presentation
Hs.519873	**desmoplakin**
Related Pathways	Arrhythmogenic right ventricular cardiomyopathy (ARVC)
Hs.517145	**enolase 1, (alpha)**
Related Pathways	Glycolysis / Gluconeogenesis, RNA degradation
Hs.511915	**enolase 2 (gamma, neuronal)**
Related Pathways	Glycolysis / Gluconeogenesis, RNA degradation
Hs.224171	**enolase 3 (beta, muscle)**
Related Pathways	Glycolysis / Gluconeogenesis, RNA degradation
Hs.595071	**glucosidase, alpha; neutral AB**
Related Pathways	N-Glycan biosynthesis
Hs.592355	**glyceraldehyde-3-phosphate dehydrogenase-like 6; hypothetical protein LOC100133042; glyceraldehyde-3-phosphate dehydrogenase**
Related Pathways	Glycolysis / Gluconeogenesis, Alzheimer's disease

Hs.520973	**heat shock 27kDa protein-like 2 pseudogene; heat shock 27kDa protein 1**
Related Pathways	MAPK signaling pathway, VEGF signaling pathway
Hs.690634	**heat shock 70kDa protein 1-like**
Related Pathways	Spliceosome, MAPK signaling pathway, Endocytosis, Antigen processing and presentation
Hs.719966	**heat shock 70kDa protein 1A; heat shock 70kDa protein 1B**
Related Pathways	Spliceosome, MAPK signaling pathway, Endocytosis, Antigen processing and presentation, Prion diseases
Hs.654614	**heat shock 70kDa protein 7 (HSP70B); heat shock 70kDa protein 6 (HSP70B')**
Related Pathways	Spliceosome, MAPK signaling pathway, Endocytosis, Antigen processing and presentation
Hs.180414	**heat shock 70kDa protein 8**
Related Pathways	Spliceosome, MAPK signaling pathway, Endocytosis, Antigen processing and presentation
Hs.184233	**heat shock 70kDa protein 9 (mortalin)**
Related Pathways	RNA degradation
Hs.525600	**heat shock protein 90kDa alpha (cytosolic), class A member 2; heat shock protein 90kDa alpha (cytosolic), class A member 1**
Related Pathways	Antigen processing and presentation, NOD-like receptor signaling pathway, Progesterone-mediated oocyte maturation,Pathways in cancer, Prostate cancer
Hs.701787	**heat shock protein 90kDa alpha (cytosolic), class B member 1**
Related Pathways	Antigen processing and presentation, NOD-like receptor signaling pathway, Progesterone-mediated oocyte maturation,Pathways in cancer, Prostate cancer
Hs.710890, Hs.605502	**hypothetical gene supported by AF216292; NM_005347; heat shock 70kDa protein 5 (glucose-regulated protein, 78kDa)**
Related Pathways	Antigen processing and presentation, Prion diseases
Hs.487027	**hypothetical protein LOC100129652; ezrin**
Related Pathways	Leukocyte transendothelial migration, Regulation of actin cytoskeleton, Pathogenic Escherichia coli infection
Hs.514174	**junction plakoglobin**
Related Pathways	Pathways in cancer, Acute myeloid leukemia, Arrhythmogenic right ventricular cardiomyopathy (ARVC)
Hs.87752	**Moesin**
Related Pathways	Leukocyte transendothelial migration, Regulation of actin cytoskeleton
Hs.449621	**netrin 3**
Related Pathways	Axon guidance
Hs.632828	**ribosomal protein L36a pseudogene 51; ribosomal protein L36a pseudogene 37; ribosomal protein L36a pseudogene 49; heterogeneous nuclear ribonucleoprotein H2 (H'); ribosomal protein L36a**
Related Pathways	Ribosome
Hs.546292	**ribosomal protein S27a pseudogene 12; ribosomal protein S27a; ribosomal protein S27a pseudogene 11; ribosomal protein S27a pseudogene 16**
Related Pathways	Ribosome
Hs.55279	**serpin peptidase inhibitor, clade B (ovalbumin), member 5**
Related Pathways	p53 signaling pathway
Hs.89643	**Transketolase**
Related Pathways	Pentose phosphate pathway
Hs.654422, Hs.713158	**tubulin, alpha 1a**

Related Pathways	Gap junction, Pathogenic Escherichia coli infection
Hs.349695, Hs.503749	**tubulin, alpha 3d; tubulin, alpha 3c**
Related Pathways	Gap junction, Pathogenic Escherichia coli infection
Hs.75318	**tubulin, alpha 4a**
Related Pathways	Gap junction, Pathogenic Escherichia coli infection
Hs.303023	**tubulin, beta 1**
Related Pathways	Gap junction, Pathogenic Escherichia coli infection
Hs.654543	**tubulin, beta 2A**
Related Pathways	Gap junction, Pathogenic Escherichia coli infection
Hs.433615	**tubulin, beta 2C**
Related Pathways	Gap junction, Pathogenic Escherichia coli infection
Hs.513829	**tubulin, beta 3; melanocortin 1 receptor (alpha melanocyte stimulating hormone receptor)**
Related Pathways	Neuroactive ligand-receptor interaction, Gap junction, Melanogenesis, Pathogenic Escherichia coli infection
Hs.110837	**tubulin, beta 4**
Related Pathways	Gap junction, Pathogenic Escherichia coli infection
Hs.720070, Hs.706875	**tubulin, beta 6**
Related Pathways	Gap junction, Pathogenic Escherichia coli infection
Hs.532659	**tubulin, beta 8**
Related Pathways	Gap junction, Pathogenic Escherichia coli infection
Hs.636480	**tubulin, beta; similar to tubulin, beta 5; tubulin, beta pseudogene 2; tubulin, beta pseudogene 1**
Related Pathways	Gap junction, Pathogenic Escherichia coli infection
Hs.5308	**ubiquitin A-52 residue ribosomal protein fusion product 1**
Related Pathways	Ribosome
Hs.719097, Hs.356190	**ubiquitin B**
Related Pathways	Parkinson's disease
Hs.520348	**ubiquitin C**
Related Pathways	PPAR signaling pathway

Table. 3-10. Related Pathways of ^{13}C Labeled Proteins in Human MIA PaCa-2 Cells

Hs.652267	**ATP-binding cassette, sub-family C (CFTR/MRP), member 11**
Related Pathways	ABC transporters,
Hs.555902	**ArfGAP with SH3 domain, ankyrin repeat and PH domain 2**
Related Pathways	Endocytosis, Fc gamma R-mediated phagocytosis,
Hs.480085	**TNNI3 interacting kinase; fucose-1-phosphate guanylyltransferase**
Related Pathways	Fructose and mannose metabolism, Amino sugar and nucleotide sugar metabolism,
Hs.500483	**actin, alpha 2, smooth muscle, aorta**
Related Pathways	Vascular smooth muscle contraction,
Hs.520640	**actin, beta**
Related Pathways	Focal adhesion, Adherens junction, Tight junction, Leukocyte transendothelial migration, Regulation of actin cytoskeleton, Vibrio cholerae infection, Pathogenic Escherichia coli infection, Hypertrophic cardiomyopathy (HCM),Arrhythmogenic right ventricular cardiomyopathy (ARVC), Dilated cardiomyopathy, Viral myocarditis,
Hs.76392	**aldehyde dehydrogenase 1 family, member A1**
Related Pathways	Retinol metabolism,
Hs.7101	**anaphase promoting complex subunit 5**
Related Pathways	Cell cycle, Oocyte meiosis, Ubiquitin mediated proteolysis, Progesterone-mediated oocyte maturation,
Hs.517830	**biotinidase**
Related Pathways	Biotin metabolism,
Hs.532491	**cryptochrome 2 (photolyase-like)**
Related Pathways	Circadian rhythm,
Hs.594952	**desmin**
Related Pathways	Hypertrophic cardiomyopathy (HCM), Arrhythmogenic right ventricular cardiomyopathy (ARVC), Dilated cardiomyopathy,
Hs.519873	**desmoplakin**
Related Pathways	Arrhythmogenic right ventricular cardiomyopathy (ARVC),
Hs.655469	**dynein, axonemal, heavy chain 1**
Related Pathways	Huntington's disease,
Hs.517145	**enolase 1, (alpha)**
Related Pathways	Glycolysis / Gluconeogenesis, RNA degradation,
Hs.511915	**enolase 2 (gamma, neuronal)**
Related Pathways	Glycolysis / Gluconeogenesis, RNA degradation,
Hs.592355, Hs.544577, Hs.598320	**glyceraldehyde-3-phosphate dehydrogenase-like 6; hypothetical protein LOC100133042; glyceraldehyde-3-phosphate dehydrogenase**
Related Pathways	Glycolysis / Gluconeogenesis, Alzheimer's disease,
Hs.595053, Hs.723164	**heat shock 60kDa protein 1 (chaperonin) pseudogene 5; heat shock 60kDa protein 1 (chaperonin) pseudogene 6; heat shock 60kDa protein 1 (chaperonin) pseudogene 1; heat shock 60kDa protein 1 (chaperonin) pseudogene 4; heat shock 60kDa protein 1 (chaperonin)**
Related Pathways	RNA degradation, Type I diabetes mellitus,
Hs.690634	**heat shock 70kDa protein 1-like**
Related Pathways	Spliceosome, MAPK signaling pathway, Endocytosis, Antigen processing and presentation,

Hs.702139, Hs.274402, Hs.719966	**heat shock 70kDa protein 1A; heat shock 70kDa protein 1B**
Related Pathways	Spliceosome, MAPK signaling pathway, Endocytosis, Antigen processing and presentation, Prion diseases,
Hs.722086, Hs.432648	**heat shock 70kDa protein 2**
Related Pathways	Spliceosome, MAPK signaling pathway, Endocytosis, Antigen processing and presentation,
Hs.654614	**heat shock 70kDa protein 7 (HSP70B); heat shock 70kDa protein 6 (HSP70B')**
Related Pathways	Spliceosome, MAPK signaling pathway, Endocytosis, Antigen processing and presentation,
Hs.180414	**heat shock 70kDa protein 8**
Related Pathways	Spliceosome, MAPK signaling pathway, Endocytosis, Antigen processing and presentation,
Hs.184233	**heat shock 70kDa protein 9 (mortalin)**
Related Pathways	RNA degradation,
Hs.515848	**hydroxyacyl-Coenzyme A dehydrogenase/3-ketoacyl-Coenzyme A thiolase/enoyl-Coenzyme A hydratase (trifunctional protein), beta subunit**
Related Pathways	Fatty acid elongation in mitochondria, Fatty acid metabolism, Valine, leucine and isoleucine degradation,
Hs.710890, Hs.605502	**hypothetical gene supported by AF216292; NM_005347; heat shock 70kDa protein 5 (glucose-regulated protein, 78kDa)**
Related Pathways	Antigen processing and presentation, Prion diseases,
Hs.487027	**hypothetical protein LOC100129652; ezrin**
Related Pathways	Leukocyte transendothelial migration, Regulation of actin cytoskeleton, Pathogenic Escherichia coli infection,
Hs.406013	**keratin 18; keratin 18 pseudogene 26; keratin 18 pseudogene 19**
Related Pathways	Pathogenic Escherichia coli infection,
Hs.87752	**moesin**
Related Pathways	Leukocyte transendothelial migration, Regulation of actin cytoskeleton,
Hs.225968	**myosin, heavy chain 15**
Related Pathways	Tight junction, Viral myocarditis,
Hs.678918	**myosin, heavy chain 7, cardiac muscle, beta**
Related Pathways	Cardiac muscle contraction, Tight junction, Hypertrophic cardiomyopathy (HCM), Dilated cardiomyopathy, Viral myocarditis,
Hs.474751	**myosin, heavy chain 9, non-muscle**
Related Pathways	Tight junction, Regulation of actin cytoskeleton, Viral myocarditis,
Hs.113577	**neurofibromin 1**
Related Pathways	MAPK signaling pathway,
Hs.198760	**neurofilament, heavy polypeptide**
Related Pathways	Amyotrophic lateral sclerosis (ALS),
Hs.521461	**neurofilament, light polypeptide**
Related Pathways	Amyotrophic lateral sclerosis (ALS),
Hs.723633, Hs.458657	**neurofilament, medium polypeptide**
Related Pathways	Amyotrophic lateral sclerosis (ALS),
Hs.37044	**peripherin**
Related Pathways	Amyotrophic lateral sclerosis (ALS),
Hs.584830	**phosphodiesterase 8B**

Related Pathways	Purine metabolism,
Hs.78771	**phosphoglycerate kinase 1**
Related Pathways	Glycolysis / Gluconeogenesis,
Hs.95990	**pyruvate kinase, liver and RBC**
Related Pathways	Glycolysis / Gluconeogenesis, Purine metabolism, Pyruvate metabolism, Insulin signaling pathway, Type II diabetes mellitus, Maturity onset diabetes of the young,
Hs.282260	**rcRPE; ribulose-5-phosphate-3-epimerase**
Related Pathways	Pentose phosphate pathway, Pentose and glucuronate interconversions,
Hs.591239, Hs.513851	**similar to 14-3-3 protein epsilon (14-3-3E) (Mitochondrial import stimulation factor L subunit) (MSF L); tyrosine 3-monooxygenase/tryptophan 5-monooxygenase activation protein, epsilon polypeptide**
Related Pathways	Cell cycle, Oocyte meiosis, Neurotrophin signaling pathway,
Hs.708726, Hs.614974	**similar to Afadin (Protein AF-6); myeloid/lymphoid or mixed-lineage leukemia (trithorax homolog, Drosophila); translocated to, 4**
Related Pathways	Adherens junction, Tight junction, Leukocyte transendothelial migration,
Hs.534770	**similar to Pyruvate kinase, isozymes M1/M2 (Pyruvate kinase muscle isozyme) (Cytosolic thyroid hormone-binding protein) (CTHBP) (THBP1); pyruvate kinase, muscle**
Related Pathways	Glycolysis / Gluconeogenesis, Purine metabolism, Pyruvate metabolism, Type II diabetes mellitus,
Hs.491682	**similar to protein kinase, DNA-activated, catalytic polypeptide; protein kinase, DNA-activated, catalytic polypeptide**
Related Pathways	Non-homologous end-joining, Cell cycle,
Hs.567794, Hs.644919	**similar to sucb; succinate-CoA ligase, GDP-forming, beta subunit**
Related Pathways	Citrate cycle (TCA cycle), Propanoate metabolism,
Hs.703487, Hs.485195	**sortilin 1**
Related Pathways	Lysosome, Neurotrophin signaling pathway,
Hs.406277	**splicing factor 3a, subunit 1, 120kDa**
Related Pathways	Spliceosome,
Hs.523718	**stratifin**
Related Pathways	Cell cycle, p53 signaling pathway, Aldosterone-regulated sodium reabsorption,
Hs.436439	**toll-like receptor 9**
Related Pathways	Toll-like receptor signaling pathway,
Hs.713158, Hs.654422	**tubulin, alpha 1a**
Related Pathways	Gap junction, Pathogenic Escherichia coli infection,
Hs.503749, Hs.349695	**tubulin, alpha 3d; tubulin, alpha 3c**
Related Pathways	Gap junction, Pathogenic Escherichia coli infection,
Hs.433336	**tubulin, alpha 3e**
Related Pathways	Gap junction, Pathogenic Escherichia coli infection,
Hs.75318	**tubulin, alpha 4a**
Related Pathways	Gap junction, Pathogenic Escherichia coli infection,
Hs.137400	**tubulin, alpha 8**
Related Pathways	Gap junction, Pathogenic Escherichia coli infection,
Hs.303023	**tubulin, beta 1**
Related Pathways	Gap junction, Pathogenic Escherichia coli infection,
Hs.511743, Hs.513829	**tubulin, beta 3; melanocortin 1 receptor (alpha melanocyte stimulating hormone**

	receptor)
Related Pathways	Neuroactive ligand-receptor interaction, Gap junction, Melanogenesis, Pathogenic Escherichia coli infection,
Hs.110837	**tubulin, beta 4**
Related Pathways	Gap junction, Pathogenic Escherichia coli infection,
Hs.720070, Hs.706875	**tubulin, beta 6**
Related Pathways	Gap junction, Pathogenic Escherichia coli infection,
Hs.706246, Hs.720412, Hs.636480	**tubulin, beta; similar to tubulin, beta 5; tubulin, beta pseudogene 2; tubulin, beta pseudogene 1**
Related Pathways	Gap junction, Pathogenic Escherichia coli infection,
Hs.643544	**tyrosine 3-monooxygenase/tryptophan 5-monooxygenase activation protein, beta polypeptide**
Related Pathways	Cell cycle, Oocyte meiosis, Neurotrophin signaling pathway,
Hs.226755	**tyrosine 3-monooxygenase/tryptophan 5-monooxygenase activation protein, eta polypeptide**
Related Pathways	Cell cycle, Oocyte meiosis, Neurotrophin signaling pathway,
Hs.520974	**tyrosine 3-monooxygenase/tryptophan 5-monooxygenase activation protein, gamma polypeptide**
Related Pathways	Cell cycle, Oocyte meiosis, Neurotrophin signaling pathway,
Hs.74405	**tyrosine 3-monooxygenase/tryptophan 5-monooxygenase activation protein, theta polypeptide**
Related Pathways	Cell cycle, Oocyte meiosis, Neurotrophin signaling pathway, Pathogenic Escherichia coli infection,
Hs.492407	**tyrosine 3-monooxygenase/tryptophan 5-monooxygenase activation protein, zeta polypeptide**
Related Pathways	Cell cycle, Oocyte meiosis, Neurotrophin signaling pathway, Pathogenic Escherichia coli infection,

Table. 3-11. Related Pathways of ^{13}C Labeled Proteins in HPDE Cells

Hs.555902	**ArfGAP with SH3 domain, ankyrin repeat and PH domain 2**
Related Pathways	Endocytosis, Fc gamma R-mediated phagocytosis,
Hs.655835	**RAD50 homolog (S. cerevisiae)**
Related Pathways	Homologous recombination, Non-homologous end-joining,
Hs.500483	**actin, alpha 2, smooth muscle, aorta**
Related Pathways	Vascular smooth muscle contraction,
Hs.520640	**actin, beta**
Related Pathways	Focal adhesion, Adherens junction, Tight junction, Leukocyte transendothelial migration, Regulation of actin cytoskeleton, Vibrio cholerae infection, Pathogenic Escherichia coli infection, Hypertrophic cardiomyopathy (HCM), Arrhythmogenic right ventricular cardiomyopathy (ARVC), Dilated cardiomyopathy, Viral myocarditis,
Hs.654432	**actinin, alpha 3**
Related Pathways	Focal adhesion, Adherens junction, Tight junction, Leukocyte transendothelial migration, Regulation of actin cytoskeleton, Systemic lupus erythematosus, Arrhythmogenic right ventricular cardiomyopathy (ARVC),
Hs.594952	**desmin**
Related Pathways	Hypertrophic cardiomyopathy (HCM), Arrhythmogenic right ventricular cardiomyopathy (ARVC), Dilated cardiomyopathy,
Hs.519873	**desmoplakin**
Related Pathways	Arrhythmogenic right ventricular cardiomyopathy (ARVC),
Hs.655469	**dynein, axonemal, heavy chain 1**
Related Pathways	Huntington's disease,
Hs.598320, Hs.544577, Hs.592355	**glyceraldehyde-3-phosphate dehydrogenase-like 6; hypothetical protein LOC100133042; glyceraldehyde-3-phosphate dehydrogenase**
Related Pathways	Glycolysis / Gluconeogenesis, Alzheimer's disease,
Hs.595053, Hs.723164	**heat shock 60kDa protein 1 (chaperonin) pseudogene 5; heat shock 60kDa protein 1 (chaperonin) pseudogene 6; heat shock 60kDa protein 1 (chaperonin) pseudogene 1; heat shock 60kDa protein 1 (chaperonin) pseudogene 4; heat shock 60kDa protein 1 (chaperonin)**
Related Pathways	RNA degradation, Type I diabetes mellitus,
Hs.719966, Hs.274402, Hs.702139	**heat shock 70kDa protein 1A; heat shock 70kDa protein 1B**
Related Pathways	Spliceosome, MAPK signaling pathway, Endocytosis, Antigen processing and presentation, Prion diseases,
Hs.432648, Hs.722086	**heat shock 70kDa protein 2**
Related Pathways	Spliceosome, MAPK signaling pathway, Endocytosis, Antigen processing and presentation,
Hs.180414	**heat shock 70kDa protein 8**
Related Pathways	Spliceosome, MAPK signaling pathway, Endocytosis, Antigen processing and presentation,
Hs.447506	**heterogeneous nuclear ribonucleoprotein A1-like 2**
Related Pathways	Spliceosome,
Hs.632537, Hs.655424, Hs.546261, Hs.711067, Hs.534822, Hs.631978	**heterogeneous nuclear ribonucleoprotein A1-like 3; similar to heterogeneous nuclear ribonucleoprotein A1; heterogeneous nuclear ribonucleoprotein A1 pseudogene 2; heterogeneous nuclear ribonucleoprotein A1; heterogeneous nuclear ribonucleoprotein A1 pseudogene**
Related Pathways	Spliceosome,

Hs.710890, Hs.605502	**hypothetical gene supported by AF216292; NM_005347; heat shock 70kDa protein 5 (glucose-regulated protein, 78kDa)**
Related Pathways	Antigen processing and presentation, Prion diseases,
Hs.512235	**inositol 1,4,5-triphosphate receptor, type 2**
Related Pathways	Calcium signaling pathway, Phosphatidylinositol signaling system, Oocyte meiosis, Vascular smooth muscle contraction, Gap junction, Long-term potentiation, Long-term depression, GnRH signaling pathway, Alzheimer's disease,
Hs.406013	**keratin 18; keratin 18 pseudogene 26; keratin 18 pseudogene 19**
Related Pathways	Pathogenic Escherichia coli infection,
Hs.2795	**lactate dehydrogenase A**
Related Pathways	Glycolysis / Gluconeogenesis, Cysteine and methionine metabolism, Pyruvate metabolism, Propanoate metabolism,
Hs.668877	**lactate dehydrogenase A-like 6A**
Related Pathways	Glycolysis / Gluconeogenesis, Cysteine and methionine metabolism, Pyruvate metabolism, Propanoate metabolism,
Hs.446149	**lactate dehydrogenase B**
Related Pathways	Glycolysis / Gluconeogenesis, Cysteine and methionine metabolism, Pyruvate metabolism, Propanoate metabolism,
Hs.654377	**lactate dehydrogenase C**
Related Pathways	Glycolysis / Gluconeogenesis, Cysteine and methionine metabolism, Pyruvate metabolism, Propanoate metabolism,
Hs.100299	**ligase III, DNA, ATP-dependent**
Related Pathways	Base excision repair,
Hs.338207	**mechanistic target of rapamycin (serine/threonine kinase)**
Related Pathways	ErbB signaling pathway, mTOR signaling pathway, Insulin signaling pathway, Adipocytokine signaling pathway, Type II diabetes mellitus, Pathways in cancer, Glioma, Prostate cancer, Acute myeloid leukemia,
Hs.689619	**myosin, heavy chain 1, skeletal muscle, adult**
Related Pathways	Tight junction, Viral myocarditis,
Hs.198760	**neurofilament, heavy polypeptide**
Related Pathways	Amyotrophic lateral sclerosis (ALS),
Hs.37044	**peripherin**
Related Pathways	Amyotrophic lateral sclerosis (ALS),
Hs.23111	**phenylalanyl-tRNA synthetase, alpha subunit**
Related Pathways	Aminoacyl-tRNA biosynthesis,
Hs.584830	**phosphodiesterase 8B**
Related Pathways	Purine metabolism,
Hs.433701	**ribosomal protein L37a**
Related Pathways	Ribosome,
Hs.614974, Hs.708726	**similar to Afadin (Protein AF-6); myeloid/lymphoid or mixed-lineage leukemia (trithorax homolog, Drosophila); translocated to, 4**
Related Pathways	Adherens junction, Tight junction, Leukocyte transendothelial migration,
Hs.534770	**similar to Pyruvate kinase, isozymes M1/M2 (Pyruvate kinase muscle isozyme) (Cytosolic thyroid hormone-binding protein) (CTHBP) (THBP1); pyruvate kinase, muscle**
Related Pathways	Glycolysis / Gluconeogenesis, Purine metabolism, Pyruvate metabolism, Type II diabetes mellitus,
Hs.133892	**tropomyosin 1 (alpha)**

Related Pathways	Cardiac muscle contraction, Hypertrophic cardiomyopathy (HCM), Dilated cardiomyopathy,
Hs.535581, Hs.654421, Hs.644306	**tropomyosin 3**
Related Pathways	Cardiac muscle contraction, Pathways in cancer, Thyroid cancer, Hypertrophic cardiomyopathy (HCM), Dilated cardiomyopathy,

Table. 3-12. Related Pathways of ^{13}C Labeled Proteins in MIA PaCa-2 Mouse Tumor Tissue

Mm.238973	**ATP synthase, H+ transporting mitochondrial F1 complex, beta subunit**
Related Pathways	Oxidative phosphorylation, Alzheimer's disease, Parkinson's disease, Huntington's disease,
Mm.261329	**RIKEN cDNA 2900073G15 gene; predicted gene 6517**
Related Pathways	Focal adhesion, Tight junction, Leukocyte transendothelial migration, Regulation of actin cytoskeleton,
Mm.460382, Mm.19892, Mm.332320, Mm.456405	**Wolf-Hirschhorn syndrome candidate 1 (human)**
Related Pathways	Lysine degradation,
Mm.686	**actin, alpha, cardiac muscle 1; similar to alpha-actin (AA 27-375)**
Related Pathways	Cardiac muscle contraction, Hypertrophic cardiomyopathy (HCM), Dilated cardiomyopathy,
Mm.328431, Mm.469717, Mm.391967	**actin, beta**
Related Pathways	Focal adhesion, Adherens junction, Tight junction, Leukocyte transendothelial migration, Regulation of actin cytoskeleton, Hypertrophic cardiomyopathy (HCM), Arrhythmogenic right ventricular cardiomyopathy (ARVC), Dilated cardiomyopathy, Viral myocarditis,
Mm.439729, Mm.331313	**amylase 2a2, pancreatic; amylase 2a3, pancreatic; amylase 2b, pancreatic; amylase 2a1, pancreatic; amylase 2a4, pancreatic; amylase 2a5, pancreatic**
Related Pathways	Starch and sucrose metabolism,
Mm.6712	**desmin**
Related Pathways	Hypertrophic cardiomyopathy (HCM), Arrhythmogenic right ventricular cardiomyopathy (ARVC), Dilated cardiomyopathy,
Mm.29975	**glycine amidinotransferase (L-arginine:glycine amidinotransferase)**
Related Pathways	Glycine, serine and threonine metabolism, Arginine and proline metabolism,
Mm.330160, Mm.470180	**heat shock protein 5**
Related Pathways	Antigen processing and presentation, Prion diseases,
Mm.377878	**histone cluster 1, H2af**
Related Pathways	Systemic lupus erythematosus,
Mm.261642, Mm.478233, Mm.255646, Mm.377875, Mm.14775, Mm.228709, Mm.246720, Mm.260530, Mm.227295, Mm.261664, Mm.158272, Mm.442307, Mm.261662	**histone cluster 1, H4k; histone cluster 1, H4m; histone cluster 4, H4; similar to germinal histone H4 gene; histone cluster 1, H4h; histone cluster 1, H4j; histone cluster 1, H4i; histone cluster 1, H4d; histone cluster 1, H4c; histone cluster 1, H4f; histone cluster 1, H4b; histone cluster 1, H4a; histone cluster 2, H4; similar to histone H4**
Related Pathways	Systemic lupus erythematosus,
Mm.299774	**junction plakoglobin**
Related Pathways	Pathways in cancer, Acute myeloid leukemia, Arrhythmogenic right ventricular cardiomyopathy (ARVC),
Mm.242832, Mm.390700	**neurofilament, medium polypeptide**
Related Pathways	Amyotrophic lateral sclerosis (ALS),
Mm.2477	**peripherin**
Related Pathways	Amyotrophic lateral sclerosis (ALS),
Mm.16775, Mm.312053, Mm.429854	**predicted gene 11878; predicted gene 4832; predicted gene 8942; predicted gene 6030; predicted gene 9320; predicted gene 5271; predicted gene 7363;**

	ribosomal protein S24; similar to ribosomal protein S24; predicted gene 8292; predicted gene 6948
Related Pathways	Ribosome,
Mm.476770, Mm.1777	**predicted gene 12141; heat shock protein 1 (chaperonin)**
Related Pathways	RNA degradation, Type I diabetes mellitus,
Mm.261329	**predicted gene 2805; similar to myosin regulatory light chain-like; predicted gene 6242; myosin, light chain 12B, regulatory**
Related Pathways	Focal adhesion, Tight junction, Leukocyte transendothelial migration, Regulation of actin cytoskeleton,
Mm.392113, Mm.479337, Mm.326103	**predicted gene 3756; tubulin, alpha 1B; predicted gene 5620; similar to alpha-tubulin isotype M-alpha-2; predicted gene 14150; predicted gene 3226**
Related Pathways	Gap junction,
Mm.44482	**predicted gene 5279; stratifin; similar to 14-3-3 protein sigma (Stratifin); predicted gene 7850**
Related Pathways	Cell cycle, p53 signaling pathway, Aldosterone-regulated sodium reabsorption,
Mm.290774, Mm.336743, Mm.351377, Mm.412745	**similar to heat shock protein 8; heat shock protein 8**
Related Pathways	Spliceosome, MAPK signaling pathway, Endocytosis, Antigen processing and presentation,
Mm.298283	**similar to neurofilament protein; neurofilament, heavy polypeptide**
Related Pathways	Amyotrophic lateral sclerosis (ALS),
Mm.392113	**tubulin, alpha 1C; predicted gene 6682**
Related Pathways	Gap junction,
Mm.332314	**tyrosine 3-monooxygenase/tryptophan 5-monooxygenase activation protein, eta polypeptide**
Related Pathways	Cell cycle, Oocyte meiosis, Neurotrophin signaling pathway,
Mm.465895, Mm.3360	**tyrosine 3-monooxygenase/tryptophan 5-monooxygenase activation protein, zeta polypeptide; predicted gene 4202**
Related Pathways	Cell cycle, Oocyte meiosis, Neurotrophin signaling pathway,
Mm.238973	**ATP synthase, H+ transporting mitochondrial F1 complex, beta subunit**
Related Pathways	P02721:ATP synthesis,
Mm.330160, Mm.470180	**heat shock protein 5**
Related Pathways	P00006:Apoptosis signaling pathway, P00049:Parkinson disease,
Mm.299774	**junction plakoglobin**
Related Pathways	P00004:Alzheimer disease-presenilin pathway,
Mm.44482	**predicted gene 5279; stratifin; similar to 14-3-3 protein sigma (Stratifin); predicted gene 7850**
Related Pathways	P00018:EGF receptor signaling pathway, P00021:FGF signaling pathway, P00048:PI3 kinase pathway, P00049:Parkinson disease, P00059:p53 pathway,
Mm.290774, Mm.336743, Mm.351377, Mm.412745	**similar to heat shock protein 8; heat shock protein 8**
Related Pathways	P00006:Apoptosis signaling pathway, P00049:Parkinson disease,
Mm.332314	**tyrosine 3-monooxygenase/tryptophan 5-monooxygenase activation protein, eta polypeptide**
Related Pathways	P00018:EGF receptor signaling pathway, P00021:FGF signaling pathway, P00048:PI3 kinase pathway, P00049:Parkinson disease, P00059:p53 pathway,
Mm.465895, Mm.3360	**tyrosine 3-monooxygenase/tryptophan 5-monooxygenase activation protein, zeta polypeptide; predicted gene 4202**
Related Pathways	P00018:EGF receptor signaling pathway, P00021:FGF signaling pathway, P00048:PI3 kinase pathway, P00049:Parkinson disease, P00059:p53 pathway,